

# **Synthesis and Combinatorial Optimization of Novel Star-Shaped Resist Materials for Lithographic Applications**

Dissertation

zur Erlangung des akademischen Grades eines  
Doktors der Naturwissenschaften (Dr. rer. nat.) im Fach Chemie  
der Fakultät für Biologie, Chemie und Geowissenschaften der Universität Bayreuth

vorgelegt von

**Florian Wieberger**

geboren in Scheßlitz

Bayreuth, 2012



Die vorliegende Arbeit wurde in der Zeit von November 2007 bis Mai 2012 am Lehrstuhl *Makromolekulare Chemie I* der Universität Bayreuth unter der Betreuung von Herrn Prof. Dr. Hans-Werner Schmidt angefertigt in enger Kooperation mit dem Lehrstuhl *Materialwissenschaften und Ingenieurwissenschaften* der Cornell Universität, Ithaca, New York, USA von Herrn Prof. Dr. Christopher Kemper Ober.

Datum der Einreichung der Arbeit: 09.Mai 2012

Datum des wissenschaftlichen Kolloquiums: 28.September 2012

Prüfungsausschuss:

Erstgutachter: Prof. Dr. Hans-Werner Schmidt

Zweitgutachter: Prof. Dr. Axel H. E. Müller

Vorsitzender: Prof. Dr. Stephan Förster

Prof. Dr. Carlo Unverzagt



Meiner lieben Familie



Wer nichts als die Chemie versteht, versteht auch die nicht recht.

Georg Christoph Lichtenberg (1742 – 1799)



## Table of contents

Summary	13
Zusammenfassung	17
<b>1 Introduction</b>	<b>21</b>
1.1 Lithography	21
1.1.1 Lithographic patterning process	21
1.1.2 Exposure tools and techniques	24
1.1.3 Resist materials	26
1.2 Atom transfer radical polymerization	29
1.2.1 Controlled radical polymerization	29
1.2.2 The ATRP process and its components	32
1.2.3 Polymer architectures accessible via ATRP	34
1.3 Combinatorial investigations	36
1.3.1 Combinatorics and high-throughput screening	36
1.3.2 Combinatorial investigations of thin films	37
References	39
<b>2 Aim and motivation</b>	<b>45</b>
<b>3 Overview of the thesis</b>	<b>47</b>
3.1 Combinatorial techniques to efficiently investigate and optimize thin film nanopatterning	48
3.2 Tailored Star-Shaped Statistical Teroligomers via ATRP for Lithographic Applications	54
3.3 Tailored Star Block Copolymer Architecture for High Performance Chemically Amplified Resists	58
<b>4 Publications and manuscripts</b>	<b>63</b>
4.1 Individual contributions	63
4.2 Combinatorial techniques to efficiently investigate and optimize thin film nanopatterning	65
4.3 Tailored Star-Shaped Statistical Teroligomers via ATRP for Lithographic Applications	93
4.4 Tailored Star Block Copolymer Architecture for High Performance Chemically Amplified Resists	115
<b>5 Publication list</b>	<b>137</b>
<b>Danksagung</b>	<b>141</b>



## Abbreviations

ATRP	atom transfer radical polymerization
CRP	controlled radical polymerization
DNQ	diazonaphtoquinone
DP <sub>n</sub>	degree of polymerization
DT	degenerative transfer
EBL	electron beam lithography
ESCAP	enviromentally stable chemically amplified photoresist
EUVL	extreme ultra violet lithography
GBLMA	$\alpha$ -gamma butyrolactone methacrylate
GcMcH	teroligomer composition of GBLMA/MAMA/HAMA
GPC	gel permeation chromatography
HAMA	hydroxyl adamantyl methacrylate
HMDS	hexamethyldisilazane
HPLC	high performance liquid chromatography
IC	integrated circuit
ITRS	international technology roadmap for semiconductors
$k_1$	process-dependent coefficient in lithographic pattern transfer
$\lambda$	wave length
LER	line edge roughness
LWR	line width roughness
MALS	multi-angle light scattering
MAMA	methyl adamantyl methacrylate
MG	molecular glass
ML2	maskless lithography
MW	molecular weight
MWD	molecular weight distribution
$n$	refractive index

## Abbreviations

NA	numerical aperture
NIL	nanoimprint lithography
NMP	nitroxide mediated polymerization
PDI	polydispersity index
PAB	post apply bake
PAG	photoacid generator
PEB	post exposure bake
PGMEA	propylene glycol monomethyl ether acetate
PMDETA	N,N,N',N'',N'''- pentamethyldiethylenetriamine
PVD	physical vapor deposition
QCM	quartz crystal microbalance
RAFT	reversible addition-fragmentation chain transfer
rpm	revolutions per minute
SEM	scanning electron microscope
SFRP	stable free radical polymerization
TMAH	tetramethyl ammonium hydroxide
$X_p$	conversion

## Summary

Gordon Earle Moore predicted in the mid-1960s the cost-efficient doubling of transistors' number on integrated circuits every two years – known as Moore's Law. Leading companies orientates by the development of integrated circuits on this Moore's Law and contributed to this prediction to come true up to the present. In so doing, the semiconductor industry drafts every two years aims to fulfill this prediction summarized in the so-called International Technology Roadmap for Semiconductors (ITRS). The ITRS lists guidelines for cost-effective progresses in performance of integrated circuits, e.g. design of integrated circuits, advancements of exposure tools and exposure techniques, and closely correlated resist materials. This thesis deals with the development of new resist materials and their combinatorial investigation concerning the performance in lithographic patterning.

The lithographic patterning procedure is a sequence of multiple processing steps and thus this procedure involves many processing variables interacting strongly with each other. For understanding and comprehensive investigation of such multi-variable dependent systems the development and implementation of combinatorial approaches were in the focus of this thesis. Furthermore this thesis is focused on the synthesis of new tailored resist materials for lithographic patterning. Star topology was the selected polymer architecture of this new resist material realized via the core-first atom transfer radical polymerization (ATRP) technique. The lithographic performance of electron beam lithography patterning was investigated for the resulting randomly distributed star terpolymers and star block copolymers by combinatorial libraries in view of features' quality.

The first chapter deals with developed, adapted, and improved combinatorial techniques for thin film investigations in general and utilized for lithographic patterning investigations in particular. The lithographic patterning procedure of chemically amplified resist systems consists of various steps: *film preparation*, *post apply bake (PAB)* to remove residual solvent, *exposure*, *post exposure bake (PEB)* to activate the catalytic reaction, and *development*. For this rather complex process variable gradients were developed and adapted for each processing step to investigate and optimize the performance of especially new resist systems. For the *film preparation* a method was developed to prepare an internal material composition gradient. This was realized by a gradient extrudate prepared using two individual controllable syringe pumps and subsequent doctor-blading. The material composition gradient was

## Summary

verified by high performance liquid chromatography. The second (*PAB*) and also the fourth (*PEB*) processing step are both annealing processes of the resist film although they serve different purposes. For the investigation of such annealing processes temperature gradients were prepared adjustable in temperature range and temperature slope. This adjustability is ensured by the active heating and the active cooling source and also by the gap and the type of metal plate. For the third step *exposure* methods were developed to realize defined exposure dose gradients in very small areas of the resist film. Different exposure dose gradients were designed for photolithography as well as for electron beam lithography. For the latter case this dose gradient was programmed in the pattern design using the software which controls the electron beam during the exposure process. The dose gradient for photolithography investigations was realized by a special designed shadow mask. For the last processing step *development* a preliminary screening of the dissolubility conditions of the resist film was established utilizing quartz crystal microbalances. Based on this measured dissolubility behavior the time frame was set for development time gradients performed by a stepwise or continuously immersion of the resist films. Lastly two to three variable gradients were combined to binary or ternary combinatorial libraries, respectively. The ternary combinatorial libraries allow the investigation of three variables of the lithographic patterning process in one experiment. Thus it is possible to optimize a resist material system fast and efficiently in respect to resist performance.

In the second chapter a star-shaped teroligomer is reported as new high potential resist type for lithographic patterning purposes. The polymerization was carried out via the core-first ATRP route using a functionalized saccharose with eight initiating sites as core. Four star-shaped teroligomers were synthesized with varying target arm lengths. In addition a saccharose molecule was synthesized with an average number of 3.5 initiating sites and thus a star oligomer was realized with a reduced arm number but an identical core and similar arm length. As reference resist material a linear model oligomer was synthesized using ethyl 2-bromoisobutyrate as initiator. For all polymers narrow monomodal distributions were detected with polydispersity index values of lower than 1.1. Based on calibration polymerizations runs the monomer feed of the three used monomers was adapted to achieve targeted monomer incorporations for all teroligomers. The targeted monomer incorporation was copied from a currently industrially used linear teroligomer. One star oligomer was selected as proof of principle for the utilization of the star architecture for lithographic purposes. This new resist material was combinatorial investigated in a ternary library and thus optimized in one

experiment concerning exposure dose, PEB temperature, and development time. The optimized patterns with a feature size of 100 nm and an excellent line edge roughness (LER) value of 3.1 nm were observed.

The last chapter of this thesis demonstrates the straight forward advancement of the star-shaped resist material reported in chapter two. The statistical monomer incorporation was exchanged by the introduction of the tailored star block copolymer architecture. This architecture was synthesized for the first time via the core-first ATRP route by full conversion of a first polar monomer and in-situ polymerization of additionally added nonpolar monomer. The successful syntheses were indicated by contact angle measurements showing increased hydrophobicity of star block copolymers in contrast to random star copolymers with the same monomer incorporation. The star block copolymers exhibited also enhanced dissolubility behavior characterized by quartz crystal microbalance measurements. Furthermore they demonstrated an up to eight times increased sensitivity at their lithographic application in contrast to the synthesized reference linear copolymer. The most promising star block copolymer was selected to investigate its lithographic performance. The optimization was performed in a ternary combinatorial library based on the gradient variables exposure dose and feature size, PEB temperature, and development time. The optimized pattern of clear lines and a feature size of 66 nm was observed with a LER value of 6 nm.

To conclude, different tailored star-shaped terpolymers were synthesized using the ATRP core-first route and successfully applied in the lithographic patterning process for the first time. In addition the combinatorial optimization offers the absolutely promising potential of utilizing these star shaped resist materials by the demonstrated brilliant LER values, the achieved extremely high sensitivity, and the fast and efficient development of clear 66 nm lines.

Summary

## Zusammenfassung

Gordon Earle Moore prognostizierte Mitte der 1960er Jahre eine kostengünstige Verdopplung der Transistoranzahl von integrierten Schaltkreisen alle zwei Jahre – bekannt geworden als „Moore'sches Gesetz“. Führende Unternehmen orientieren sich bei der Entwicklung von integrierten Schaltkreisen an diesem Mooreschen Gesetz und trugen dazu bei, diese Vorhersage bis heute zu verwirklichen. Dabei formuliert die Halbleiterindustrie zum Erfüllen dieser Voraussage alle zwei Jahre ihre Ziele, welche zusammengefasst in der sogenannten „International Technology Roadmap for Semiconductors“ (ITRS) nachgelesen werden können. Die ITRS ist somit eine Auflistung von Richtlinien, die eine wirtschaftliche Weiterentwicklung der Leistungsmerkmale von integrierten Schaltkreisen ermöglichen soll, wie zum Beispiel die Gestaltung der integrierten Schaltkreise und die Weiterentwicklung von Belichtungsmaschinen und –techniken, sowie – eng damit verbunden – Resistmaterialien. Diese Arbeit behandelt die Entwicklung von neuen Resistmaterialien und ihrer kombinatorischen Untersuchung hinsichtlich der wichtigen Leistungsmerkmale der lithographischen Strukturierung.

Für die lithographische Strukturierung ist eine Abfolge von zahlreichen Prozessschritten nötig. Damit beinhaltet dieser Prozess eine große Anzahl von stark miteinander wechselwirkenden Verarbeitungsbedingungen. Zum Verständnis und zur umfassenden Untersuchung von derartigen Systemen, die durch viele Variablen beeinflussbar sind, waren die Entwicklung und Realisierung von kombinatorischen Anwendungen ein Schwerpunkt dieser Arbeit. Des Weiteren konzentrierte sich diese Arbeit auf die Synthese von neuen maßgeschneiderten Resistmaterialien für die lithographische Strukturierung. Die Stern-topologie stellte sich hierbei als die vielversprechendste Polymerarchitektur für neues Resistmaterial heraus und wurde über eine vom Kern ausgehende „Atom Transfer Radical Polymerization“ (ATRP) Syntheseroute realisiert. Das lithographische Potential der neu hergestellten Resistmaterialien auf Basis von statistischen Sternterpolymere und Sternblockcopolymeren wurde mittels Elektronenstrahlithographie in kombinatorischen Bibliotheken systematisch untersucht.

Das erste Kapitel handelt von entwickelten, angepassten und verbesserten kombinatorischen Techniken zur Untersuchung dünner Filme im Allgemeinen und deren Anwendung auf die lithographische Strukturierung im Speziellen. Der lithographische

## Zusammenfassung

Strukturierungsablauf von chemisch verstärkten Resisten beinhaltet die folgenden Schritte: *Filmherstellung*, einem *Temperierungsprozess* zur Entfernung des Lösungsmittel („*post apply bake*“; PAB), *Belichtung*, einem *Temperierungsprozess* zur Aktivierung der katalytischen Reaktion („*post exposure bake*“; PEB) und *Entwicklung*. Für diesen komplexen Gesamtprozess wurden Variablengradienten für jeden Verarbeitungsschritt entwickelt und angepasst, um das Potential neuer Resistsysteme zu untersuchen und zu optimieren. Für die *Filmherstellung* wurde eine Methode entwickelt um einen Zusammensetzungsgradienten zu präparieren. Dieser wurde verwirklicht durch ein Gradientenextrudat – hergestellt durch zwei individuell ansteuerbare Spritzenpumpen – das anschließend gerakelt wurde. Zum Nachweis der Umsetzung des Zusammensetzungsgradienten wurde Hochleistungsflüssigkeitschromatographie genutzt. Der zweite (PAB) sowie der vierte (PEB) lithographische Verarbeitungsschritt sind jeweils *Temperierungsschritte* des Resistfilms, obgleich sie unterschiedlichen Zwecken dienen. Zur Untersuchung solcher Temperierungsprozesse wurden Temperaturgradienten erzeugt, die auf definierte Temperaturbereiche und -steigungen einstellbar sind. Die Einstellung erfolgt dabei durch aktives Heizen und Kühlen sowie den gewählten Abstand und der Art der verwendeten dazwischen liegenden Metallplatte. Zum dritten Schritt – *Belichtung* – wurden Methoden entwickelt um definierte Belichtungs dosisgradienten in sehr kleinen Flächen des Resistfilms zu realisieren. Unterschiedliche Belichtungs dosisgradienten wurden entworfen für Fotolithographie sowie für Elektronenstrahl lithographie. Für den Dosisgradient vom letztgenannten wurde ein Belichtungsdesign an dem Computer programmiert, welcher den Elektronenstrahl während des Belichtungsprozesses steuert. Der Dosisgradient für die fotolithographischen Untersuchungen wurde durch eine speziell entworfene Schattenmaske realisiert. Für den letzten Verarbeitungsschritt, der *Entwicklung*, wurde eine Voruntersuchung der Löslichkeitsbedingungen des Resistfilms mit Hilfe der Schwingquarzmikrowaagentechnologie eingeführt. Basierend auf den gemessenen Löslichkeitsverhalten wurde das Zeitfenster für Entwicklungszeitgradienten gesetzt, der durch stufenweises oder kontinuierliches Eintauchen der Resistfilme in der Entwicklerlösung realisiert wurde. Schließlich wurden zwei bis drei Variablengradienten zu binären, beziehungsweise ternären kombinatorischen Bibliotheken vereinigt. Diese ternären kombinatorischen Bibliotheken erlauben die zeitgleiche Untersuchung von drei Variablen eines lithographischen Strukturierungsprozesses und ermöglichen so die schnelle und effiziente Optimierung eines Resistsystems in Bezug auf die Güte des Resists.

Das zweite Kapitel handelt von der Synthese von sternförmigen Teroligomeren als potentiell neue Resistarchitektur für lithographische Strukturierungen. Die Polymerisation erfolgte vom Kern weg mittels ATRP. Den Kern bildete dabei ein mit acht Initiatoren funktionalisiertes Saccharose-Molekül. Nach dieser Route wurden vier sternförmige Teroligomere mit unterschiedlichen Armlängen synthetisiert. Des Weiteren wurde ein Saccharose-Molekül mit einer mittleren Initiatoranzahl von 3,5 synthetisiert und ausgehend von diesem zweiten Kern ein Sternteroligomer mit reduzierter Armanzahl, jedoch identischen Kern und ähnlicher Armlänge hergestellt. Weiterhin wurde ein lineares Teroligomer als Referenz-Resistmaterial mit dem Initiator Ethyl-2-brombutyrat synthetisiert. Alle hergestellten Polymere wiesen eine enge und monomodale Molekulargewichtsverteilung mit Polydispersitäten von kleiner 1,1 auf. Basierend auf zuvor ermittelten Monomereinwaagen wurden alle synthetisierten Teroligomere mit den geplanten Monomerverhältnissen erhalten. Dieses angestrebte Monomerverhältnis orientierte sich an dem eines derzeit industriell genutzten linearen Teroligomers. Von den synthetisierten Sternoligomeren wurde eines ausgewählt und im Hinblick auf die grundsätzliche Eignung der Sternarchitektur für lithographisches Strukturieren untersucht. Dieses neue Resistmaterial wurde kombinatorisch in einer ternären Bibliothek mit den Variablen Belichtungs dosis, PEB Temperatur und Entwicklungszeit in einem Optimierungsexperiment untersucht. Hierbei wurden optimierte Strukturen von 100 nm Breite mit einer exzellenten Kantenrauigkeit von 3,1 nm erhalten.

Das letzte Kapitel dieser Arbeit zeigt die zielstrebige Weiterentwicklung des sternförmigen Resistmaterials von Kapitel zwei. Der statistische Monomereinbau wurde hierbei ersetzt durch die Einführung der maßgeschneiderten Sternblockcopolymer-Architektur. Diese Architektur wurde zum ersten Mal über die vom Kern ausgehende ATRP-Route nach vollständigen Umsatz eines ersten Monomers und der in situ Polymerisation des danach hinzugefügten Monomers realisiert. Die erfolgreiche Synthese wurde durch Kontaktwinkelmessungen bekräftigt. Diese zeigte eine erhöhte Hydrophobizität für Sternblockcopolymere im Vergleich zu den statistischen Sterncopolymeren mit gleichem Monomereinbau. Des Weiteren wiesen die Sternblockcopolymere eine erhöhte Löslichkeit im Entwickler auf, welche durch Messungen mit der Schwingquarzmikrowaage ermittelt wurde. Zusätzlich zeigten sie eine bis zu achtfach höhere lithographische Empfindlichkeit im Gegensatz zu dem synthetisierten linearen Referenz-Copolymer. Das vielversprechendste Sternblockcopolymer wurde für die anschließende lithographische Untersuchung in einer ternären kombinatorischen Bibliothek hinsichtlich Belichtungs dosis, Strukturgröße, PEB

## Zusammenfassung

Temperatur und Entwicklungszeit ausgewählt. Mit diesem Resistsystem konnten klare Linien mit einer Breite von 66 nm und einer Kantenrauigkeit von 6 nm realisiert werden.

Zusammenfassend lässt sich feststellen, dass in dieser Arbeit unterschiedliche sternförmige Terpolymere über die vom Kern ausgehende ATRP-Route synthetisiert und erfolgreich zum ersten Mal im lithographischen Strukturierungsprozess eingesetzt wurden. Zusätzlich demonstrierte die kombinatorische Optimierung das durchweg vielversprechende Potential dieser sternförmigen Resistarchitektur. Die wesentlichen Verbesserungen stellen dabei die gezeigte hervorragende Kantenrauigkeit, die erzielte überaus hohe Empfindlichkeit und allgemein der etablierte schnelle und effiziente kombinatorische Optimierungsprozess der zu klaren 66 nm Linien führte.

# 1 Introduction

## 1.1 Lithography

The invention and development of computers and their steady advancements simplified and changed our life to as we know it today. This development was mainly contributed from the miniaturization process of integrated circuits in microprocessors driven by new advancements in lithography over the years.

### 1.1.1 Lithographic patterning process

In the summer of 1958 Jack Kilby made an important breakthrough in the advancement of transistors and invented the first integrated circuit (IC).<sup>1</sup> This can be seen as the beginning of the modern computer age. Only seven years later the development of the performance of ICs grew so rapidly, Gordon Moore made the prediction that the number of transistors on one IC doubles every two years with decreasing costs per single transistor. This describes the so-called “Moore’s Law” (Figure 1).<sup>2</sup>

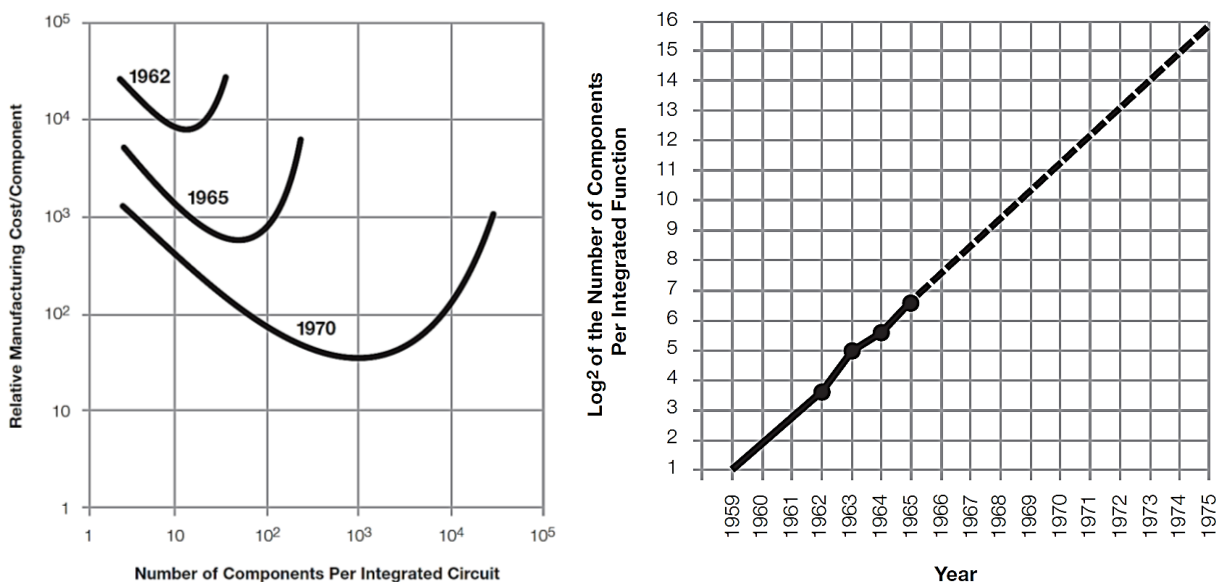


Figure 1: Left: The minimum cost of a single component (transistor) is decreasing with evolution of ICs. Right: The number of components per IC is predicted to be doubled every two years.

Moore was proved right and the development of ICs proceeded as he expected in the following decades. This advancement was mainly attributed to the steady reduction in component’s size. For semiconductor industry his prediction became more and more a kind of

## Introduction

business model but also a challenge. As a result companies of semiconductor industry incorporated national and soon international to state their technological needs and to coordinate developments of ICs. This trade association meets every year and reports overall 17 scopes on research directions and suggests their realization timelines up to 15 years summarized in the so-called “International Technology Roadmap for Semiconductors” (ITRS).<sup>3</sup> Such research directions are for instance further miniaturization or the design of transistors, reduced power consumption, and increase in performance. Recently Intel Corporation presented the first demonstration of a 22 nm microprocessor in 2011.<sup>4</sup> This microprocessor – code-named Ivy Bridge – is the first chip uses 3-D Tri-Gate transistors, which represents a breakthrough in transistor performance and energy efficiency. The realization of such microprocessors is a very complex process and consists of about 500 processing steps.<sup>5</sup> This large number comes from repeating lithography and etch pattern transfer processes up to forty times. In Figure 2 a simplified pattern transfer process is illustrated.

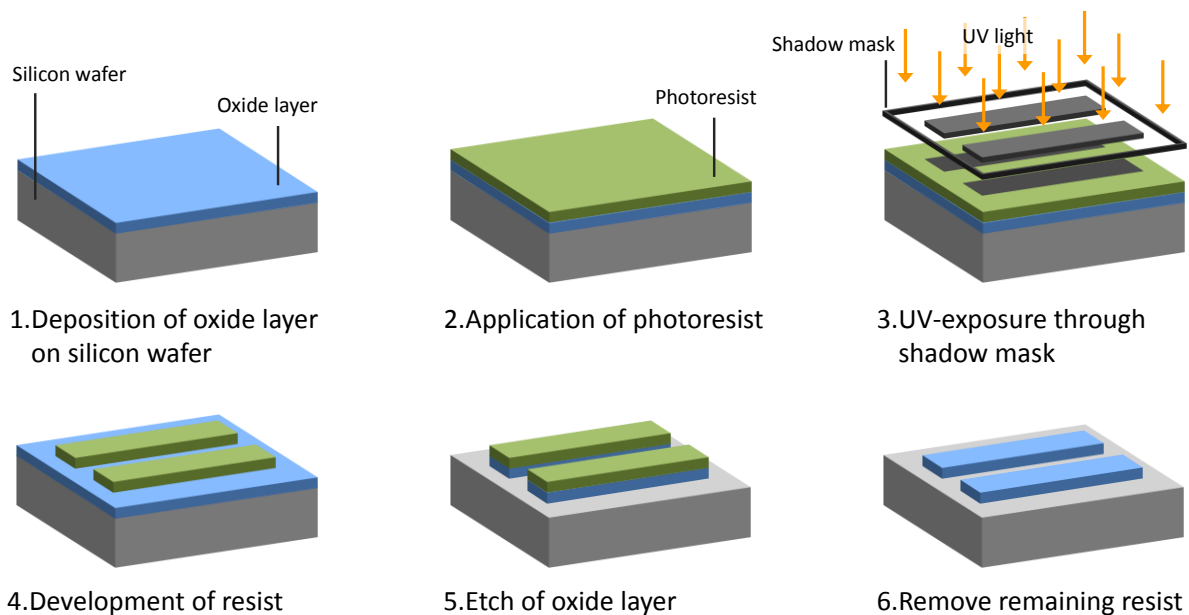


Figure 2: A simplified illustration of the lithographic and etch pattern transfer process.

At the beginning of this lithographic process the substrate has to be deeply cleaned to remove contaminations and annealed to remove water.<sup>6</sup> In the following step (1) a silicon oxide layer is created on the silicon wafer. This can be conducted, e.g., by the oxidation of silicon at very high temperatures in the presence of oxygen or by plasma etching. Ongoing an adhesion promoter solution is spin cast on the substrate. The most common used adhesion

promoter is hexamethyl disilazane (HMDS) which reacts chemically with the surface hydroxy groups. In the second step (2) a photoresist solution is spin cast on the substrate for film application. The film thickness must not exceed the aspect ratio of 3:1 in respect to the targeted line width due to certain pattern collapse. The thickness is adjustable out of the concentration of the solution, the photoresist material itself, and the acceleration and the final revolutions per minute (rpm) of the spin casting process. Subsequently the film is annealed for post apply bake (PAB) to remove most of the remaining solvent in the resist film and to stabilize the film. The basic principle of the following exposure step (3) is to generate a change in dissolubility of the resist film for the ongoing development step (4). This is the actual lithographic pattern transfer as the resist film is exposed through a shadow mask. As already mentioned, the whole process is conducted many times in the production of ICs and thus a precise alignment of mask in every exposure step to substrate is required. In the case of high performance resist systems the exposure alone creates no change in solubility. For these systems a subsequent annealing step is necessary, the so-called post exposure bake (PEB). In the exposed areas a photoactive compound is activated and a catalytic reaction takes place during the PEB. For the following development step (4) an aqueous base (usually tetramethyl ammonium hydroxide: TMAH) is used. In this step the base-soluble resist material is dissolved and the pattern – the image of the shadow mask – is left on the substrate. These patterns are annealed in a following postbake to remove residual water or gas, to improve the adhesion, and to harden for withstanding the upcoming harsh etching step (5). In this step the actual purpose of the resist material becomes important: The resist material ‘resists’ the etchant and protects the oxide areas covered by the resist and thus only the unprotected areas are etched. Such etchants are either acid solution or more commonly dry plasma. The last step in this process contains the stripping of the remaining resist material (6). One option to remove the organic material is to use wet chemical as inorganic acid-based systems or phenol-based strippers. Another method – standard in semiconductor processing – is the use of oxygen plasma which can even strip the etched resist material but leaves the inorganic surface untouched. Further steps are, e.g., ion implanting for altering conduct electricity (doping), applying multiple layers of metal (copper) for electrical connections, and implementation of low- $\kappa$  materials, supplementing the actual patterning transfer process. At the end of all processing steps the finished microprocessor is coated with a so-called passivation layer. This insulating layer increases electrical stability but also protects the IC from contaminations.

Each of these processing steps contains process variables like time, concentration, material, temperature, dose, to name but a few. A variation of one variable at the beginning of this multi-variable process often affects negatively the following steps in this extreme sensitive and thus automated procedure. This sensitivity to process conditions and utilized resist material increases with the further miniaturization of ICs and requires the further development and time-consuming optimization of exposure tools, resist materials, additives, and process set-ups.

### 1.1.2 Exposure tools and techniques

The functional purpose of an exposure tool is the lithographic pattern transfer. A shadow mask is exposed by a light source and the passed light is focused through a lens system to a substrate coated with photosensitive material. Since the development of ICs in the end of the fifties the predominated patterning process for the production of microelectronics is based on optical lithography.<sup>7</sup> The exposure tools and techniques of this patterning process evolved down to the present day. The main driving force for this evolution was to decrease fabrication costs of ICs which was partially done by constant advancements in productivity and throughput of ICs. But improved resolution contributed the most to reduce costs due to more ICs could be fabricated on one single wafer. The theoretically maximum resolution of an exposure tool can be calculated using Equation 1.<sup>8</sup>

$$LW = k_1 * \lambda / NA \quad \text{Equation 1}$$

where LW represents linewidth (resolution),  $k_1$  process-dependent coefficient,  $\lambda$  exposure wavelength, and NA numerical aperture. For the improvement of resolution  $k_1$  and the utilized wavelength  $\lambda$  must decrease, while NA must increase. The  $k_1$  factor combines different effects for instance of the photoresist (reflection and standing waves) or defects in the imaging system (stray light, lens aberrations, and vibrations).<sup>9</sup> Theoretically the lower limit of  $k_1$  is about 0.25. To come close to this value certain techniques can be utilized e.g. so-called phase shift masks, optical proximity correction, or off-axis illumination.<sup>10,11</sup> NA is defined “as the sine of the maximum half-angle of diffracted light that can enter the lens times the index of refraction of the surrounding medium,  $n$ ” (see Equation 2).<sup>6</sup>

$$NA = n \sin\theta_{max} \quad \text{Equation 2}$$

This means to increase NA the acceptance angle of the lens has to be increased and the medium the light passes after the lens system has to be changed to higher  $n$ . With a high  $n$  ( $n=1.44$  of water at 193 nm), due to advancements in lens materials, and increasing of the portion captured light by the objective lens a high value of 1.3 for NA was reported.<sup>12</sup> A very important part of resolution reduction contributes the exposure wavelength  $\lambda$  as can be seen in Equation 1. High-pressure Hg discharge lamps were used till the late 1980s with operating wave lengths of 436 nm (g-line), 365 nm (i-line) and 250 nm whereby the resolution improved from 5  $\mu\text{m}$  down to 0.25  $\mu\text{m}$ .<sup>7,13</sup> The invention of excimer lasers based on Krypton-Fluoride (KrF; 248 nm) and Argon-Fluoride (ArF; 193 nm) in the 1990s ended the utilization of Hg discharge lamps.<sup>14</sup> The steadily advancements of these lasers in power and bandwidth led to higher productivity, larger depth-of-focus and higher resolutions from 250 nm down to 82 nm. Even though an operating light source existed with the  $\text{F}_2$  laser (157 nm), the market leader Intel Corporation never advanced 157 nm lithography beyond the prototype stage due to a lower power in comparison to KrF and ArF lasers and immature lens materials and photoresist materials.<sup>15,16</sup> Instead a huge progress happened with establishing water-based immersion lithography resulting in an improvement in resolution of 30 – 40 %.<sup>8</sup> Afterwards efforts were focused on lowering  $k_1$  e.g. increase of uniformity in imaging and image placement, uniformity in illumination, high purity optical elements.<sup>7</sup> The introduction of exposure techniques like double exposure, double patterning, and spacer double patterning contributed also enormously to the reduction of the process constant  $k_1$ .<sup>17</sup> With the help of all these advancements, optimized techniques and methods Intel Corporation recently realized a full-scale high-volume fabrication of 22 nm resolution.<sup>4</sup>

As mentioned above reducing the wave length further improves resolution but also other non-optical patterning techniques are conceivable to achieve this goal. Extreme ultra-violet lithography (EUVL; 13.5 nm), maskless lithography (ML2) techniques, nanoimprint lithography (NIL), and directed self-assembly are possible prospects.<sup>3,13</sup> In contrast to the established 193 nm lithography these new methods are by now immature and too expensive. But for the realization of the next higher resolution steps which the ITRS aims, the possibilities for 193 nm lithography draw to a close. Directed self-assembly of block copolymers and their possible utilization for ICs fabrication are beyond the beginnings and a cheaper alternative but yet not applicable.<sup>18</sup> NIL is a mechanical replication of a relief pattern by deforming a resist layer under pressure of this pattern. Indeed this pattern transfer offers high throughput in fabrication of replicas but due to defect and overlay issues of the relief

pattern this technique will not be used soon.<sup>19</sup> The most promising candidate to replace 193 nm lithography is EUVL because this technique offers potential of resolutions below 10 nm.<sup>20</sup> But the exposure has to be carried out in high vacuum and instead of lenses ultra-flat mirrors have to be installed as at this wavelength all matters absorbs. Furthermore outgassing of resist material in vacuum causes contaminations of the optical components and due to the harsh EUVL radiation the lifetime of the expensive masks are very short. The investigation in EUVL is meanwhile in a progressed stage but by now it is a very cost-intensive technique. Besides direct laser writing, focused ion beam, and probe tip contact the most promising technique of ML2 methods is electron beam lithography (EBL). EBL is also conducted in high vacuum, similar resolutions can be achieved as EUVL but for exposure EUV is substantially more efficient.<sup>21,22</sup> In contrast to optical lithography which flood exposes the mask and thus the resist material, EBL is a direct write method and exposes with a single beam, pixel by pixel, and thus no mask is needed.<sup>23</sup> This makes this method preferred for the realization of complex pattern as masks for other lithography techniques. But on the other hand this point by point exposure is time-consuming and thus offers just a low throughput and is also cost intensive. Recently three companies developed electron beam tools which operate with many thousands of beams simultaneously, possible up to 256,000.<sup>24-27</sup> The complicated micro-machined assembly enables high-throughput in patterning and combines it with the capability of high-resolution fabrication.<sup>28</sup> This new development of multiple electron beam lithography makes it more interesting for the industrial application. However, the race of getting the next generation of exposure tool is still open, while the favorites are EUVL and EBL are in line with each other up to now.

### 1.1.3 Resist materials

The successful implementation of a new resist material in semiconductor industry demands certain requirements. The three most important requirements are summarized in the so-called “triangle of death” with its corners: resolution, line edge roughness (LER), and sensitivity.<sup>29</sup> At least two of these parameters have to be improved to warrant the implementation of new techniques, tools, or resists. Higher resolutions of resists contribute the most to save costs for ICs fabrication and increase the performance of microprocessors. LER is defined as the deviation of a feature edge after the lithographic pattern transfer from an ideal shape. Low LER values are crucial for low defects and the succeeded etch pattern

transfer. The sensitivity describes the exposure dose required for the lithographic pattern transfer. High sensitivity or low exposure dose, respectively, save time and thus costs for the fabrication of ICs.

The miniaturization of ICs is contributed to exposure tools and techniques, but mainly to the utilized wave length.<sup>30</sup> Since the industrial fabrication of ICs began the exposure wave length decreased from 436 nm to 365 nm to 248 nm to 193 nm and thus the resists evolved as can be seen in Figure 3.

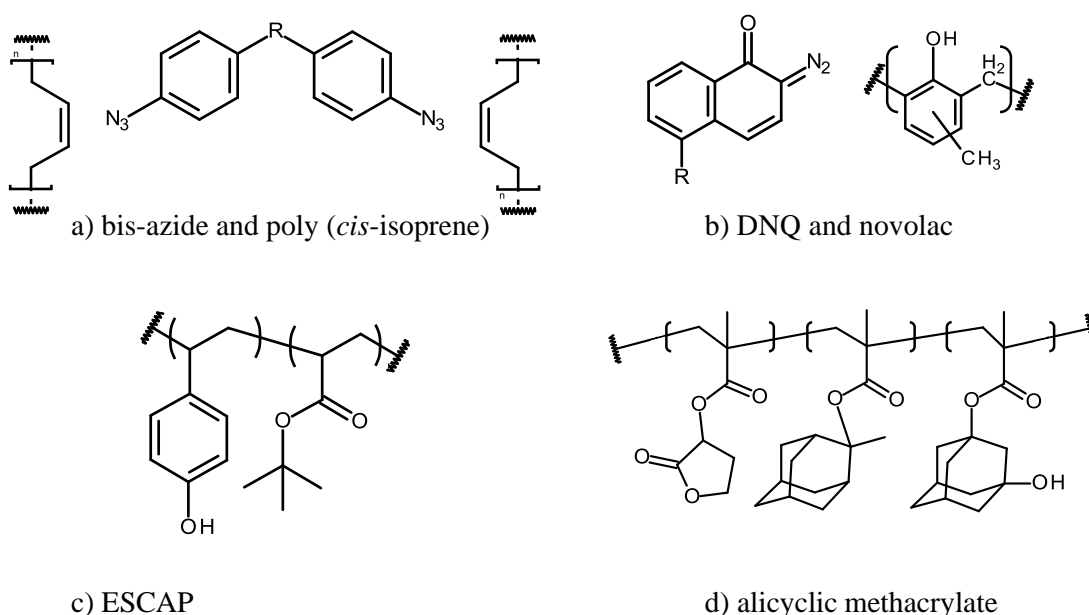


Figure 3: Main developed resist systems used from the beginnings of integrated circuits fabrication. a) bis-azids and poly (*cis*-isoprene) (~1957-1972); b) Diazonaphthoquinone (DNQ) and novolac (phenol formaldehyde resin) (~1972-1990); c) poly (4-hydroxy styrene co *t*-butyl acrylate); Environmentally Stable Chemical Amplification Photoresist (ESCAP) for 248 nm lithography (~1990-2001); alicyclic methacrylate resist for 193 nm lithography (~2001-).

The first working horse for semiconductor industry was bis-azide plus cyclized poly (*cis*-isoprene) of about 150,000 g/mol from Kodak.<sup>31</sup> This resist was used from the beginnings of microdevice fabrication until it reached its resolution limit of 2  $\mu\text{m}$  in about 1972. The subsequent used resist material consists of diazonaphthoquinone (DNQ) and novolac (phenol formaldehyde resin) showing higher contrast and an absence of swelling during the development step. As developer 0.26 N tetramethylammonium hydroxide (TMAH) was used and interestingly, the industry retained this developer optimized for DNQ/novolac up to nowadays.<sup>32</sup> This resist showed a final resolution of 0.5  $\mu\text{m}$  for 365 nm lithography and was

## Introduction

used for integrated circuit fabrication up to about 1990. At the beginning of the 1980s a new “chemical amplified” resist type was developed containing acid-sensitive polymer films and photoacid generators (PAGs).<sup>33</sup> The most successful representative was a copolymer based on p-hydroxystyrene and t-butyl acrylate and was named Environmentally Stable Chemically Amplified Photoresist (ESCAP).<sup>34</sup> This new resist type was also more transparent to the introduced 248 nm lithography than its predecessor. The highest realized resolution with this resist system was about 200 nm and it was utilized until the semiconductor industry introduced 193 nm lithography.<sup>35</sup> Here an exchange of the resist material was necessary because of the high absorption of the benzene building blocks in ESCAPs at a wave length of 193 nm. Acrylic polymers were suitable as chemical amplified resist for 193 nm lithography. However for ensuring a comparable etch resistance carbon-rich alicyclic groups were identified.<sup>36</sup> These chemical amplified polymer resists consist of two to three lactone and adamantene-based monomers and achieved up to now resolutions of 22 nm, to be continued.

Recently Mike Mayberry, director of components research and vice president of technology and manufacturing of Intel Corporation, announced a resist type known as molecular glass resist taking in consideration.<sup>37</sup> Lithographic investigation led to sub-50 nm patterns and makes this resist type to a potential next-generation resist material.<sup>38,39</sup> But the era of polymeric resists is not over yet. Different polymers with adamantene and lactone monomers were investigated for the lithographic performance improvement for 193 nm lithography but also for the next-generation lithographic techniques EUV and EBL.<sup>40</sup> Lately the research focus was broaden to different polymer architectures besides the linear polymers used for industrial applications. Thus hyperbranched topology was investigated using the same monomers leading to a higher performance than a commercial available linear resist applied for 193 nm lithography.<sup>41</sup> An promising architecture for recent research in resist material based on star-shaped polymer.<sup>42,43</sup> The investigated star resist is built of partially protected poly (p-hydroxystyrene) with an acid labile core and thus the core is decomposable during EUVL patterning process. Using this star resists sub-30 nm patterns were achieved with low sensitivities and LERs.

## 1.2 Atom transfer radical polymerization

Tailoring novel resist materials for industrial interest demand besides requirements for 193 nm immersion, EUV, or ebeam exposure also controlled synthesis techniques. The availability of suitable monomers and the numerous simple synthesizable initiators make atomic transfer radical polymerization a versatile method for the design of new resist material.

### 1.2.1 Controlled radical polymerization

In 1956 Michael Szwarc, Moshe Levy, and Ralph Milkovich coined, for the first time, the term “living” polymer while describing anionic polymerization.<sup>44</sup> Szwarc defined the term living polymerization as a chain growth process in which termination or transfer reactions are absent (or negligible).<sup>45</sup> Such an innovative technique allowed the polymerization of monomers sequentially giving access to block copolymers due to their "living" chain ends. This mechanistic insight marked the beginning of the development of numerous polymerization techniques just as well as the preparation of novel nanostructured materials.<sup>46</sup> Although free radical polymerization was known for a long time, it took about forty years before radical polymerizations became “living”. However, "living" is not synonymous with the "control" over molecular weight (MW) or the realization of narrow molecular weight distributions (MWD).<sup>47</sup> For radical polymerization techniques which can provide these characteristics and offer "living" end-groups the term “controlled” was established.<sup>48</sup> Controlled radical polymerizations (CRPs) must provide a fast initiation and a fast exchange between the reactive species in comparison to propagation.<sup>49</sup> Although termination reactions are present for CRP techniques, they are negligible and do not affect the control over molecular properties. Beyond comparable control over polymerization, comprehensive studies over the last two decades clearly demonstrated that CRPs are much less susceptible to impurities and especially the simple handling of its components makes CRPs the more versatile polymerization technique.

There are three major CRP methods that are used the most nowadays: the on degenerative transfer (DT) based reversible addition-fragmentation chain transfer (RAFT) polymerization, the stable free radical polymerization (SFRP) with its best known representative nitroxide mediated polymerization (NMP), and the atom transfer radical polymerization (ATRP).<sup>50</sup> All three techniques have an established dynamic equilibrium in

## Introduction

common between the propagating radicals ( $P^*$ ) and the dormant species ( $P-X$ ).<sup>51</sup> The radicals are either involved in a degenerative exchange process (Figure 4a) or are trapped in a reversible activation/deactivation process (Figure 4b/c). For all CRPs fast exchange among the active and the deactivated state is necessary to control MW and polydispersity as well as architecture.<sup>52</sup> In an ideal situation the propagating radical reacts only with a few monomers before it is deactivated again. This is only realized when the rate of deactivation ( $k_{\text{deact}}$ ) is much faster than the rate of activation ( $k_{\text{act}}$ ). Hence, the active state only exists in a split second whereas the deactivated state exists a thousand times longer. The monomer consumption occurs several hundred times and although the overall active lifetime of this radical is similar to the one of a conventional radical polymerization the permanent deactivation allows for all propagating chains the same chance of reaching equal degrees of polymerization. But as the polymerization for a CRP method takes several hours and the chain end is still “living” there is the opportunity to functionalize the end-group for a further synthetic processing.

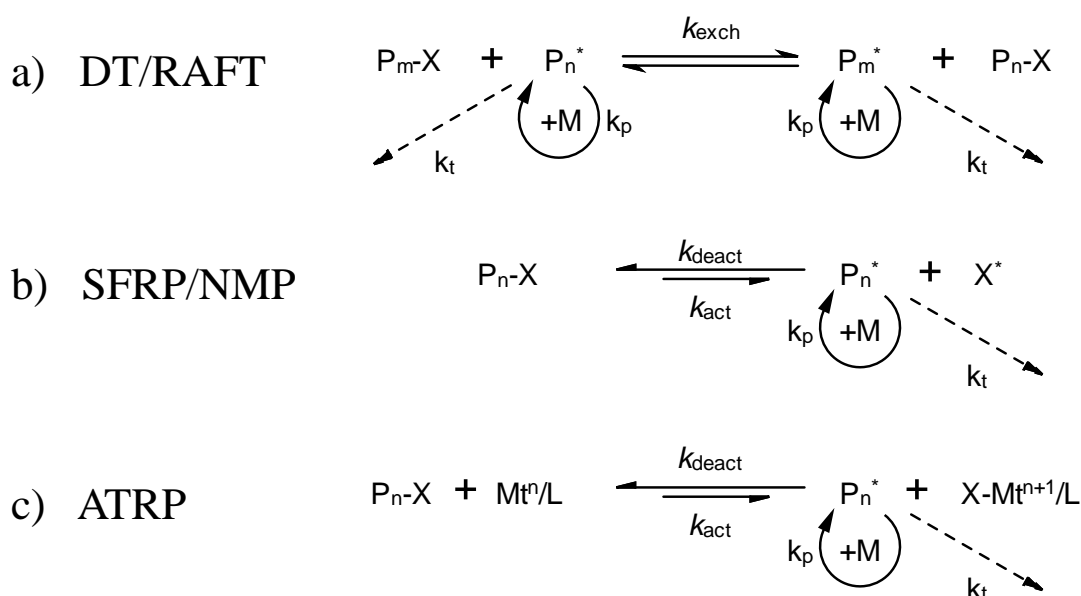


Figure 4: Activation/deactivation mechanisms of the three dominant controlled radical polymerization methods. a) Degenerative transfer (DT) or reversible addition-fragmentation chain transfer (RAFT), b) Stable free radical polymerization (SFRP) or nitroxide mediated polymerization (NMP), and c) Atom transfer radical polymerization (ATRP).

In detail the DT process exhibits a slow initiation and a fast termination and thus follows typical radical polymerization kinetics. The concentration of the transfer agent ( $X$ ) is higher compared to the initiator concentration and acts as the dormant species. While active,

only a small amount of radicals can undergo propagation, i.e., consumption of monomer (M) with a polymerization rate ( $k_p$ ), or are able to terminate via disproportionation or recombination reactions (termination rate ( $k_t$ )). The active radicals, however, are transferred faster into the dormant state ( $k_{exch}$ ) via the degenerative transfer before side reactions can occur.

For the two mechanisms of the reversible activation/deactivation process the radicals are rapidly deactivated by a species X and thus transferred into the dormant state. This dormant state can be activated into the monomer consuming radical and propagate either thermally/spontaneously (SFRP) or with a redox active catalyst (ATRP) soluble due to a certain ligand ( $Mt^n/L$ ). Although these active radicals are transferred into the dormant species very fast, a negligible amount will also terminate via disproportionation or recombination reactions.

In 2002 a comparison of these three CRP methods RAFT, NMP, and ATRP was made and updated in 2006 (Figure 5).<sup>51,53</sup> Here the authors try to compare some crucial aspects for the applicability of successful CRP which are: monomer range that can be polymerized and control over molecular weight (LMW/HMW) therein, feasibility of end-group functionalization (end funct), block copolymer (blocks) and hybrid materials synthesis (hybrids), and handling/working in aqueous media (water) or under environmental sustainability (env) in general.

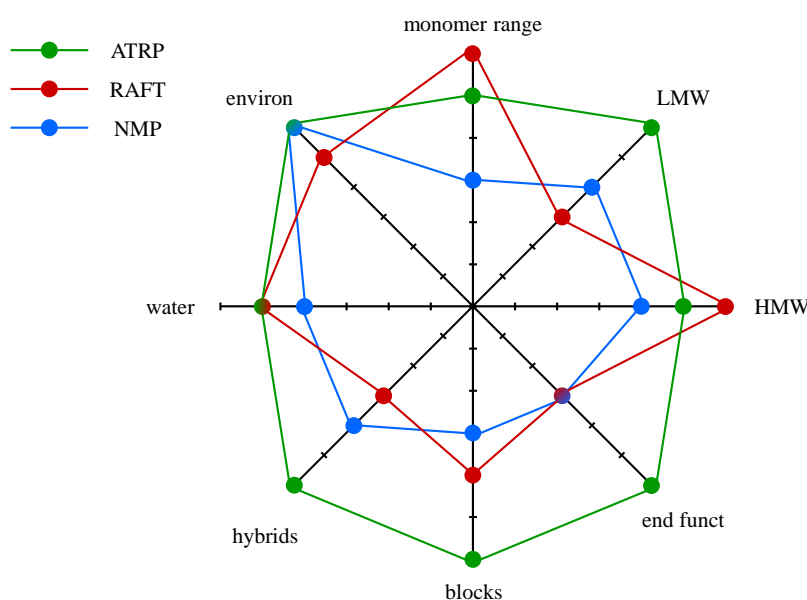


Figure 5: Comparison of crucial aspects for applicability of the CRP methods: ATRP (green), RAFT (red), and NMP (blue)

## Introduction

An absolute determination of capability and efficiency is difficult as all of them have their advantages and limitations. So, for instance, nearly all monomers are polymerizable using RAFT and in the last decade more and more monomers were accessible for ATRP, even vinyl acetate.<sup>49,54,55</sup> Although there is some progress in making the NMP process more adaptive to functional monomers, this polymerization technique exhibits the most restrictions on this matter.<sup>56</sup> The expense for polymerization is mainly dependent on monomer's choice but in combination with applicable initiators ATRP is the most favorable technique. From an economic point of view the differences between these three techniques are marginal. But lastly it is fair to say ATRP is a very versatile and robust technique and for many studies and applications more suitable than the RAFT or NMP.

### 1.2.2 The ATRP process and its components

ATRP is one of the most powerful CRP techniques, especially because it is a very versatile process and the components to conduct a successful polymerization are easily available. Besides monomer, the polymerization process usually requires a transition metal ( $Mt^n$ ; where  $n$  is the oxidation state) and a ligand (solubilizing the metal in organic solvents) together serving as the catalyst system. Combined with an initiator carrying an active group it can be transferred between the metal center and the chain end and thus reversibly activating/deactivating the reactive chain. Various metals like titan, iron, molybdenum, nickel can be used as catalyst whereas copper (Matyjaszewski et al.) and ruthenium (Sawamoto et al.) are by far the most frequently reported.<sup>57</sup> Usually the initiator is an alkyl halide (chlorine, bromine, or rarer iodine), but the usage of others, e.g. pseudohalogen molecules, or hexafluorophosphate was also demonstrated.<sup>58</sup> Ligands, influenced by the structure and type of ligand, are used to stabilize the catalyst and thus the atom transfer equilibrium. Very often amines, pyridines and pyridineimines are used as ligands that are exemplified in Figure 6a. The ligands show different activation rates depending on topology (cyclic, linear or branched), nature of N-ligands (aryl amine, alkyl amine, pyridine, etc), number of C-units between N atoms, and also on steric effects.<sup>59</sup> The initiators are alkyl halides activated by  $\alpha$ -carbonyl, phenyl, vinyl, or cyano groups exemplarily shown in Figure 6b.<sup>60</sup> The reactivity depends on the number of substituents at the active carbon atom (primary, secondary, tertiary), groups able to stabilize (delocalize) the radical (phenyl, ester, allyl, cyano), and the

halogen atom (bromine, chlorine, iodine). For polymerizations nearly all monomers with activated double bond can be utilized for the ATRP process.

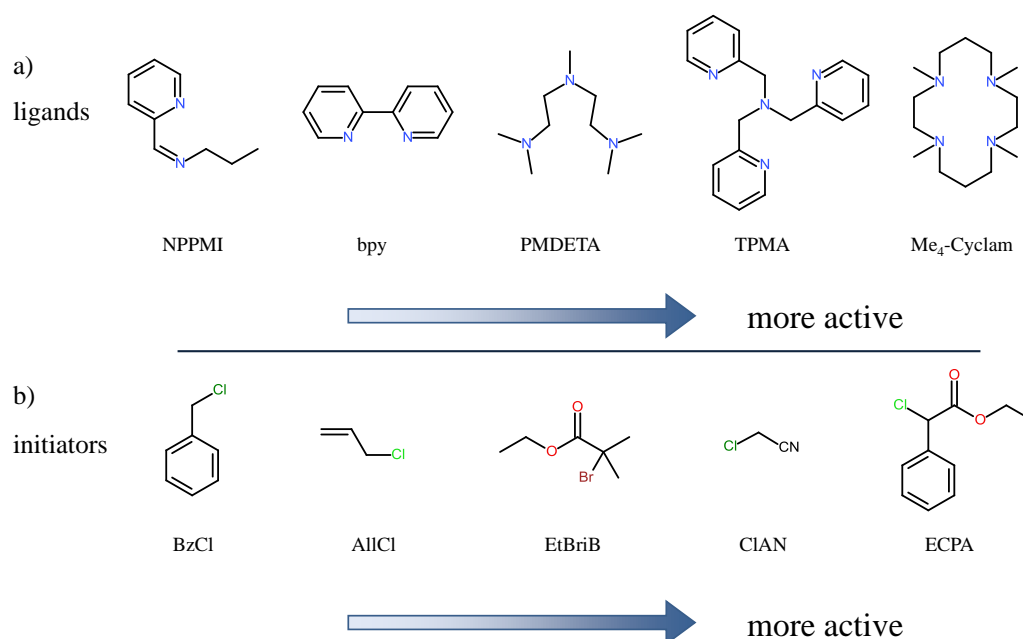


Figure 6: Ligands and initiators frequently used in ATRP. a) Ligands for copper based catalysts for ATRP with an increasing catalytic activity from left to right. Figure 6b) ATRP initiators with increasing initiator reactivity from left to right.

The basic ATRP process starts with an equivalent concentration of initiator to transition metal ( $Mt^n$ ) and ligand.<sup>61</sup> In the last 15 years various modifications of this standard process were created. An oxidatively stable ATRP was conducted using a transition metal with a higher oxidation state ( $Mt^{n+1}$ ).<sup>62</sup> The catalyst was converted to an active catalyst ( $Mt^n$ ) by a standard free radical initiator *in situ*. But here side effects occur as polymerization starts with a small amount of the free radical initiator as well as only homopolymers could be achieved. A substitution of the free radical initiator with a reducing agent forming no initiating species solves this issue of side polymerizations. Such reducing agents are for instance ascorbic acid, glucose, phenol, hydrazine, and tin (II) 2-ethylhexanoate.<sup>63</sup> The reducing agent can also be used to eliminate oxygen in the reaction solution. The amount of catalyst (activator) can here be as low as in the ppm region as the activator is regenerated by electron transfer (ARGET). This process provides another advantage as it suppresses side reactions caused by the catalyst itself due to the small amount used.<sup>64</sup> This advantage allows synthesizing HMW copolymers. Lately  $Fe^0$ ,  $Mg^0$ , and  $Zn^0$  were used as reducing agents.<sup>65</sup> These zerovalent metals showed different reactivities and proceeded in a well-controlled fashion. Recently ATRP made a leap

in evolution: the reducing agent was replaced by an electrical current, so-called electrochemically mediated ATRP (eATRP).<sup>66</sup> In doing so, the ratio of activator to deactivator is controlled by current, potential, and total charge passed and thus the polymerization can be switched on and off reversibly. This process was studied on methacrylates demonstrating low polydispersities even for HMW polymers. In environmentally friendly point of view electrodeposition of copper from an ATRP is conceivable to remove the catalyst.<sup>67</sup> Recently, another ATRP process was developed avoiding metallic catalysts entirely, replacing the metal by the enzyme horseradish peroxidase.<sup>68</sup> Furthermore progresses were made using water as an inexpensive and environmentally friendly medium and thus examples of polymerizations in emulsions, suspensions, or dispersions in aqueous systems were shown.<sup>69</sup> These new developments in ATRP utilizing less catalyst and water as the reaction medium are pushing this polymerization method towards green and sustainable polymer chemistry.

### 1.2.3 Polymer architectures accessible via ATRP

The multitude of commercially available reagents and monomers as well as the versatility are the prominent reasons for the widespread application of ATRP. Besides homopolymers other polymer compositions can be realized such as block, random, alternating, and even gradient copolymers (Figure 7a). As discussed above nearly all monomers with a radical stabilizing group have been homopolymerized yet. These homopolymers can be used as macroinitiator for a subsequent polymerization of another monomer leading to block copolymers. Recently it was exemplified on different methacrylates that a successive polymerization can be repeated several times yielding, in this case, well-controlled decablock copolymers.<sup>70</sup> For a random copolymerization the same terms as for a homopolymerization are applicable but here also less reactive monomers are polymerizable demonstrated for 1-octene with *n*-butylacrylate.<sup>71</sup> For the preparation of alternating copolymers two monomers with strongly different polarities/reactivities have to be polymerized. The monomers styrene and *N*-phenyl maleimide for example show such a strong tendency to alternate.<sup>72</sup> A new class of copolymers is represented by gradient copolymers, where the composition along the polymer chain changes continuously. Such a gradient polymer can be yielded by changing the monomer feeds as the copolymerization proceeds. For instance such a gradient copolymer was realized by continuous addition of *tert*-butylacrylate to a miniemulsion polymerization of *n*-butylacrylate.<sup>73</sup>

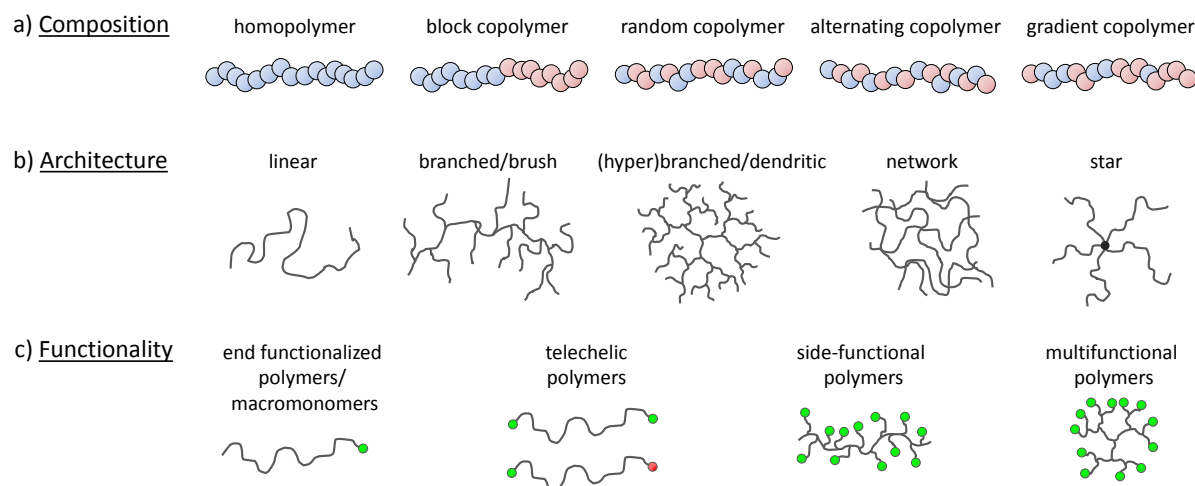


Figure 7: a) Copolymers with controlled compositions prepared by ATRP. b) Examples of polymer architectures prepared by ATRP. c) End-functionalization for different polymer architectures.

ATRP allows the realization of homopolymers and copolymers with control over molecular architecture, e.g. linear, brush, network, hyperbranched or dendritic, and star-shaped architecture, too (Figure 7b). Especially the star architecture impresses with the resulting physical and mechanical properties. Thus star polymers found its way into industry to improve engine oils,<sup>74</sup> coatings,<sup>75</sup> and contact lenses,<sup>76</sup> to name a few. Even for such more sophisticated architectures it is possible to anticipate molecular weight and to achieve narrow molecular weight distributions for linear and even for some more sophisticated architectures.<sup>77</sup> Branched polymers or brushes can be realized by polymerizations using multifunctional initiators,<sup>78</sup> initiator monomers (“inimers”),<sup>79</sup> or branching agents.<sup>80</sup> Increasing the branching sites will lead to hyperbranched polymers. Polymers with well-arranged branching points are called dendrimers. This topology is given, e.g., by a multifunctional initiator from which polymerization starts. The ends of the chains are functionalized with two or more initiating sites and the polymerization starts over.<sup>81</sup> Several topologies result from the copolymerization with divinyl monomers, which depend on the concentration and on the time of addition. Higher concentrations at the beginning and early addition after initiation leads to network/gels. Is the concentration low at the beginning or the divinyl monomer is added some time before the polymerizations ends the resulting architecture is a star or nanogel.<sup>82</sup> Often these architectures are combined with a random or a block monomer composition or even with other architectures. A wide range of different topology compositions are shown for hyperbranched polymers<sup>83</sup> or polymer brushes<sup>84</sup> as well as different types of dendrimer-like polymers<sup>85</sup>, miktoarm star polymers,<sup>86</sup> star-linear block

polymers<sup>87</sup> and star block copolymers.<sup>88</sup> The realization of star block copolymers is a good illustration of the combination of architectures and polymerization techniques. One method describes the preparation of a macroinitiator via a core-first polymerization from a star-shaped initiator.<sup>89</sup> Another method fabricates a macroinitiator with multiple initiating sites by an arms-first approach via crosslinking of linear homopolymers anionically polymerized.<sup>90</sup> In both cases the generated macroinitiator was used for a second polymerization step to design a star block copolymer. The preparation of such architecture was also demonstrated by cross-linking of micelles formed by block copolymers.<sup>91</sup>

In Figure 7c polymer end-functionalization of different architectures is shown. These functional groups can be incorporated via nucleophilic substitution of the alkyl halide on the end chain.<sup>92</sup> In this way vinyl, azide, ester, or hydroxy groups and so on can be introduced for further processing. However, these functional groups can also be introduced by initiators. Besides the alkyl halide the initiator can contain azides, epoxide, alkene, hydroxyl, and ester groups to name but a few. At last monomers providing functional groups can also be copolymerized regulated by monomer feed.

### 1.3 Combinatorial investigations

New developed and improved materials and their multi-step processing are well-known challenges in lithography. For a fast and effective implementation combinatorial approaches are a particularly suitable strategy.

#### 1.3.1 Combinatorics and high-throughput screening

Business rivalry force companies to look on profitability of new products as the development of new and the improvement of existing materials is always a time-consuming and cost-intensive process.<sup>93</sup> Due to mostly complex demands on new material's systems, traditionally a huge amount of single experiments have to be undertaken – meaning also lots of loss of material – to achieve desired material features. But the number of new promising chemicals, material compositions or synthesis routes is too large for such a systematic investigation.<sup>94</sup> Combinatorial scanning produces relief as a fast, cost-efficient, and capable tool for investigation and optimization of materials. Variable gradients, the linear variation of parameters, as well as their perpendicular combination to so-called combinatorial libraries

yields in a high amount of results in a single experiment. The characterization of these results and the identification of trends in these combinatorial libraries provides besides material's development also fundamental knowledge of investigated systems. The first attempts of combinatorial approaches were done by Edison and Ciamician at the end and beginning of the nineteenth century, respectively.<sup>95,96</sup> In 1970 Hanak implemented the "multi-sample concept" and thus firstly reported combinatorics using combinatorial libraries by automated sample preparation for material's optimization.<sup>97</sup> These new thinking in investigating was successfully adapted by the pharmaceutical industry and revolutionized this research field.<sup>98</sup> This evolution in drug research led to a tremendously increased number of compounds which were synthesized and analyzed.<sup>99,100</sup> The success of combinatorics is also closely related to developments in standard binding assays for the identification of bioactive materials and in analyzing methods like liquid chromatography and mass spectrometry.<sup>101</sup> Thus due to these methods synthesized compounds can be screened efficiently.<sup>102</sup> But this high-throughput screening technique was also adopted by the field of materials research in the last decades.<sup>103,104</sup> Combinatorial material research targets the combination of related experiments in one experiment for investigation of interacting parameter systems and for optimization of materials and processes.<sup>105</sup> Important material research fields are biomaterials for drug delivery,<sup>106</sup> sensing materials,<sup>107</sup> polymeric coatings,<sup>108</sup> electronic and functional materials,<sup>109</sup> and catalysis<sup>110</sup> to name a few. Recently, material research made a great leap forward in fast and efficient investigation of material compositions. On a silicon substrate 24 combinatorial libraries consisting of titan, nickel, and silver were prepared and tested on etch behavior.<sup>111</sup>

### 1.3.2 Combinatorial investigations of thin films

An interesting research field represents property investigations of thin film in terms of certain variable gradients.<sup>112</sup> For film applications in general the film thickness is a crucial parameter. The preparation of continuous film thickness gradients were successfully demonstrated via doctor blading depending on concentration, application solvent, gap size of the doctor blade and acceleration of the doctor blade.<sup>113</sup> A 2-D combinatorial library consisting of a film thickness gradient versus a temperature gradient was made to investigate dewetting behavior of a polystyrene film by Amis et al.<sup>114</sup> His group also prepared a 2-D library consisting of a thin film with an internal polymer blend gradient out of polystyrene and poly (vinyl methyl ether) in combination with a temperature gradient and investigated phase

## Introduction

separation.<sup>115</sup> For the polymer blend gradient a gradient extrudate was realized with the help of syringe pumps and a custom built set-up. This extrudate was applied on a substrate and subsequently doctor bladed. Such gradient film preparations and also thickness gradients can also be conducted utilizing physical vapor deposition. Recently combinatorial optimizations regarding film thickness and composition was reported for the investigation of electro-optical devices.<sup>116</sup> For adhesion investigations in particular the chemical surface treatment of films is an important parameter and for this gradients of surface characteristics were developed. Surface modifications can be obtained via electron beam treatment and were demonstrated on a poly (2-vinylpyridine) coated surface resulting in a hydrophilicity gradient.<sup>117</sup> Another method for a surface hydrophilization gradient was shown utilizing a poly (vinyl carbonate) film continuously immersed in an aqueous NaOH solution.<sup>118</sup>

Lithography is a special field of research regarding thin film investigations as the whole lithographic pattern transfer procedure is based on treating thin resist films. Thus, this procedure consists of a large amount of variables, e.g. resist composition, film thickness, annealing temperature, exposure dose, or development time to name a few. The fact that these variables interact strongly with each other makes lithography an interesting research area. Thus combinatorial approaches find its way into lithography in the last decade. An important variable in general for thin films but especially in the lithographic context is the bake (annealing) temperature and of course the time. A combinatorial library of these two variables was created for degradation investigations of poly (*tert*-butoxy-carbonyloxy-styrene).<sup>119</sup> Such annealing steps are conducted for the nowadays utilized chemically amplified resist systems in the lithographic patterning process at least two times. Hence, for performance optimizations of a resist system two bake steps were investigated orthogonally to each other in a 2-D library.<sup>120</sup> Another important variable is the material composition as utilized resist systems consist of more than two components. For this reason a combinatorial library out of different compositions of a molecular glass photoresist system prepared via PVD was investigated in regard to exposure dose.<sup>121</sup> Recently a synergistic effect was found for resist composition and the post exposure bake.<sup>122</sup> This was identified due to the investigation in a ternary combinatorial library. This ternary library was realized out of a composition gradient perpendicular to a temperature gradient resulting in a 2-D library and an exposure dose gradient matrix-like on top of this 2-D library.

## References

- 1 J. C. St. Kilby, *ChemPhysChem* **2001**, 2, 482.
- 2 G. E. Moore, *Electronics* **1965**, 38, 114.
- 3 <http://www.itrs.net/> (April **2012**)
- 4 <http://www.intel.com/> (April **2012**)
- 5 B. J. Lin, *Optical Lithography*, SPIE, 1000 20th Street, Bellingham, WA USA **2010**.
- 6 C. A. Mack, *Fundamental principles of optical lithography: The science of microfabrication*, Wiley, Chichester, West Sussex, England; Hoboken, NJ, USA **2007**.
- 7 J. H. Bruning, *Proceedings of SPIE*, 6520, **2007**, 652004.
- 8 M. Rothschild, *Materials Today* **2005**, 8, 18.
- 9 B. Fay, *Microelectronic Engineering* **2002**, 61-62, 11.
- 10 C. Cork, F. Amoroso, A. Poonawala, S. Jang, K. Lucas **2010**, 76401C, 1.
- 11 S. Mangan, E. Byers, D. Rost, M. Garrett, M. Carlson, C. Hickman, J. Finders, P. Luehrmann, R. Kazinczi, I. Minnaert-Janssen, F. Duray, B. Wisse, N. Schoumans, L. Reijnen, T. Theeuwes, M. Ben-Yishai, R. Ren, R. Gibson, L. Shoval, Y. Cohen, Y. Elblinger, I. Englard, *Proceedings of SPIE*, 7272, **2009**, 72722B.
- 12 E. Jeong, J. Kim, K. Choi, M. Lee, D. Lee, M. Kim, C. Park, *Proceedings of SPIE*, 6924, **2008**, 692424.
- 13 R. Pease, S. Chou, *Proc. IEEE* **2008**, 96, 248.
- 14 B. LaFontaine, *SPIE Professional* **2010**.
- 15 D. Basting, G. Marowsky, *Excimer Laser Technology*, Springer-Verlag, Berlin, Heidelberg **2005**.
- 16 <http://www.eetimes.com/electronics-news/4092441/Intel-drops-157-nm-tools-from-lithography-roadmap> (April **2012**)
- 17 <http://www.itrs.net/Links/2011ITRS/2011Chapters/2011Lithography.pdf> (April **2012**)
- 18 R. R. Dammel, *J. Photopol. Sci. Technol.* **2011**, 24, 33.
- 19 K. Kincade, *Laser Focus World* **2007**, 43, 97.
- 20 C. Wagner, N. Harned, *Nature Photon* **2010**, 4, 24.
- 21 J. Cameron, J. Thackeray, J. W. Sung, S. M. Coley, V. Jain, O. Ongayi, M. D. Wagner, P. LaBeaume, A. Kwok, D. Valeri, M. Hellion, B. Icard, B. Dal'zotto, C. Sourd, L. Pain *Proceedings of SPIE*, 8322, **2012**, 83222F-1.

- 22 L. D. Bozano, P. J. Brock, H. D. Truong, M. I. Sanchez, G. M. Wallraff, W. D. Hinsberg, R. D. Allen, M. Fujiwara, K. Maeda, *Proceedings of SPIE*, 7972, **2011**, 797218
- 23 A. Broers, A. Hoole, J. Ryan, *Microelectronic Engineering* **1996**, 32, 131.
- 24 <http://www.mapperlithography.com/> (April **2012**)
- 25 <http://www.multibeamcorp.com/> (April **2012**)
- 26 <http://www.ims.co.at/> (April **2012**)
- 27 E. Platzgummer, S. Cernusca, C. Klein, S. Kvasnica, B. Sonalkar, H. Loeschner, *Proceedings of SPIE*, 7748, **2010**, 77480H.
- 28 M. Slodowski, H.-J. Döring, I. A. Stolberg, W. Dorl, *Proceedings of SPIE*, 7823, **2010**, 78231J.
- 29 <http://www.life.lithoguru.com/> (April **2012**)
- 30 J. H. Bruning, *Proceedings of SPIE*, 3051, **1997**, 14.
- 31 C. G. Willson, *Proceedings of SPIE*, 3050, **1997**, 38.
- 32 A. de Silva, L. K. Sundberg, H. Ito, R. Sooriyakumaran, R. D. Allen, C. K. Ober, *Chem. Mater* **2008**, 20, 7292.
- 33 H. Ito, C. G. Willson, *Polym. Eng. Sci.* **1983**, 23, 1012.
- 34 W. Conley, G. Breyta, B. Brunsvold, R. DePietro, D. Hofer, S. Holmes, H. Ito, R. Nunes, G. Fichtl, *Proceedings of SPIE*, 2724, **1996**, 34.
- 35 H. Ito, *Proceedings of SPIE*, 6923, **2008**, 692302.
- 36 D. P. Sanders, *Chem. Rev* **2010**, 110, 321.
- 37 M. Mayberry, TECHCON, Austin TX, USA, September **2010**
- 38 A. de Silva, J.-K. Lee, X. André, N. M. Felix, H. B. Cao, H. Deng, C. K. Ober, *Chem. Mater* **2008**, 20, 1606.
- 39 J. Sha, J.-K. Lee, C. K. Ober, *Proceedings of SPIE*, 7273, **2009**, 72732T.
- 40 K. Furukawa, S. Seki, T. Kozawa, S. Tagawa, *Proceedings of SPIE*, 6923, **2008**, 692334.
- 41 C. L. Chochos, E. Ismailova, C. Brochon, N. Leclerc, R. Tiron, C. Sourd, P. Bandelier, J. Foucher, H. Ridaoui, A. Dirani, O. Soppera, D. Perret, C. Brault, C. A. Serra, G. Hadziioannou, *Adv. Mater* **2009**, 21, 1121.
- 42 J. Iwashita, T. Mimura, T. Hirayama, T. Iwai, *Proceedings of SPIE*, 7273, **2009**, 72733O.
- 43 T. Hirayama, J. Iwashita, S. Yoshizawa, K. Konno, T. Iwai, *Proceedings of SPIE*, 7639, **2010**, 76390Q.
- 44 M. Szwarc, M. Levy, R. Milkovich, *J. Am. Chem. Soc.* **1956**, 78, 2656.

- 45 M. Szwarc, *Nature* **1956**, 178, 1168.
- 46 K. Matyjaszewski, A. H. Müller, *Progress in Polymer Science* **2006**, 31, 1039.
- 47 K. Matyjaszewski, *J. Phys. Org. Chem.* **1995**, 8, 197.
- 48 K. Matyjaszewski, A. H. Müller, *Polym. Prepr.* **1997**, 38, 6.
- 49 K. Matyjaszewski, T. P. Davis, *Handbook of radical polymerization*, Wiley-Interscience, Hoboken **2002**.
- 50 K. Matyjaszewski, J. Spanswick, *Materials Today* **2005**, 8, 26.
- 51 W. A. Braunecker, K. Matyjaszewski, *Progress in Polymer Science* **2007**, 32, 93.
- 52 A. H. E. Müller, K. Matyjaszewski, *Controlled and living polymerizations: Methods and materials*, Wiley-VCH, Weinheim **2009**.
- 53 K. Matyjaszewski, *Controlled/living radical polymerization*, ACS Symp. Ser. 854, 2, American Chemical Society, Washington, DC **2003**.
- 54 M. Wakioka, K.-Y. Baek, T. Ando, M. Kamigaito, M. Sawamoto, *Macromolecules* **2002**, 35, 330.
- 55 V. Percec, A. V. Popov, E. Ramirez-Castillo, M. Monteiro, B. Barboiu, O. Weichold, A. D. Asandei, C. M. Mitchell, *J. Am. Chem. Soc.* **2002**, 124, 4940.
- 56 J. Nicolas, C. Dire, L. Mueller, J. Belleney, B. Charleux, S. R. A. Marque, D. Bertin, S. Magnet, L. Couvreur, *Macromolecules* **2006**, 39, 8274.
- 57 F. Di Lena, K. Matyjaszewski, *Progress in Polymer Science* **2010**, 35, 959.
- 58 K. Davis, K. Matyjaszewski, *J. of Macromolecular Sc., Part A* **2004**, 41, 449.
- 59 W. Tang, K. Matyjaszewski, *Macromolecules* **2006**, 39, 4953.
- 60 W. Tang, K. Matyjaszewski, *Macromolecules* **2007**, 40, 1858.
- 61 J.-S. Wang, K. Matyjaszewski, *Macromolecules* **1995**, 28, 7901.
- 62 J.-S. Wang, K. Matyjaszewski, *Macromolecules* **1995**, 28, 7572.
- 63 K. Min, H. Gao, K. Matyjaszewski, *Macromolecules* **2007**, 40, 1789.
- 64 H. Dong, W. Tang, K. Matyjaszewski, *Macromolecules* **2007**, 40, 2974.
- 65 Y. Zhang, Y. Wang, K. Matyjaszewski, *Macromolecules* **2011**, 44, 683.
- 66 A. J. D. Magenau, N. C. Strandwitz, A. Gennaro, K. Matyjaszewski, *Science* **2011**, 332, 81.
- 67 M. Nasser-Eddine, C. Delaite, P. Dumas, R. Vataj, A. Louati, *Macromol. Mater. Eng.* **2004**, 289, 204.

- 68 S. J. Sigg, F. Seidi, K. Renggli, T. B. Silva, G. Kali, N. Bruns, *Macromol. Rapid Commun.* **2011**, 32, 1710.
- 69 K. Matyjaszewski, *Macromolecules* **2012**, 45, 4015.
- 70 C. Boyer, A. H. Soeriyadi, P. B. Zetterlund, M. R. Whittaker, *Macromolecules* **2011**, 44, 8028.
- 71 K. Tanaka, K. Matyjaszewski, *Macromolecules* **2007**, 40, 5255.
- 72 H. Wenyan, P. Huili, J. Bibiao, R. Qiang, Z. Guangqun, K. Lizhi, Z. Dongliang, C. Jianhai, *J. Appl. Polym. Sci.* **2011**, 119, 977.
- 73 K. Min, J. Kwon Oh, K. Matyjaszewski, *J. Polym. Sci. A Polym. Chem.* **2007**, 45, 1413.
- 74 R. B. Rhodes, D. L. Handlin, C. A. Stevens, US 5460739 (**1995**).
- 75 S. Petrash, C. Xiao, A. Mukherjee, J. S. Thomaides, EP 1086980 A1 20010328 (**2001**).
- 76 H. J. Spinelli, W. L. Anton, L. Seidner, H. D. Coleman, M. I. Ali, L. Weintraub, P. White, US 5314960 A 19940524 (**1994**).
- 77 K. A. Davis, K. Matyjaszewski, *Advances in Polymer Science*, Vol. 159, Springer Berlin, Heidelberg **2002**, p. 1.
- 78 H.-I. Lee, W. Jakubowski, K. Matyjaszewski, S. Yu, S. S. Sheiko, *Macromolecules* **2006**, 39, 4983.
- 79 F. Bally, E. Ismailova, C. Brochon, C. A. Serra, G. Hadziioannou, *Macromolecules* **2011**, 44, 7124.
- 80 Y. Li, S. P. Armes, *Macromolecules* **2005**, 38, 8155.
- 81 B. Lepoittevin, R. Matmour, R. Francis, D. Taton, Y. Gnanou, *Macromolecules* **2005**, 38, 3120.
- 82 H. Gao, K. Matyjaszewski, *Prog. Polym. Sci.* **2009**, 34, 317.
- 83 C. Gao, D. Yan, *Prog. Polym. Sci.* **2004**, 29, 183.
- 84 R. Barbey, L. Lavanant, D. Paripovic, N. Schüwer, C. Sugnaux, S. Tugulu, H.-A. Klok, *Chem. Rev.* **2009**, 109, 5437.
- 85 A. Sunder, R. Haag, R. Mülhaupt, H. Frey, *Adv. Mater.* **2000**, 12, 235.
- 86 H. Gao, K. Matyjaszewski, *Macromolecules* **2008**, 41, 4250.
- 87 A. Hirao, M. Hayashi, S. Loykulnant, K. Sugiyama, S. Ryu, N. Haraguchi, A. Matsuo, T. Higashihara, *Prog. Polym. Sci.* **2005**, 30, 111.
- 88 K. Matyjaszewski, *Polym. Int.* **2003**, 52, 1559.

- 89 J. L. Hedrick, M. Trollsås, C. J. Hawker, B. Atthoff, H. Claesson, A. Heise, R. D. Miller, D. Mecerreyes, R. Jérôme, P. Dubois, *Macromolecules* **1998**, 31, 8691.
- 90 V. Y. Lee, K. Havenstrite, M. Tjio, M. McNeil, H. M. Blau, R. D. Miller, J. Sly, *Adv. Mater.* **2011**, 23, 4509.
- 91 W. Li, K. Matyjaszewski, *J. Am. Chem. Soc.* **2009**, 131, 10378.
- 92 V. Coessens, T. Pintauer, K. Matyjaszewski, *Progress in Polymer Science* **2001**, 26, 337.
- 93 B. Jandeleit, D. J. Schaefer, T. S. Powers, H. W. Turner, W. H. Weinberg, *Angew. Chem. Int Ed.* **1999**, 38, 2494.
- 94 W. Maier, G. Kirsten, M. Orschel, P.-A. Weiß, A. Holzwarth, J. Klein, *Macromol. Symp.* **2001**, 165, 1.
- 95 G. S. Bryan, *Edison, The Man and His Work*, Knopf, London **1930**.
- 96 R. Hoogenboom, M. A. R. Meier, U. S. Schubert, *Macromol. Rapid Commun.* **2003**, 24, 15.
- 97 J. J. Hanak, *J Mater Sci* **1970**, 5, 964.
- 98 S. P. Rohrer, E. T. Birzin, R. T. Mosley, S. C. Berk, S. M. Hutchins, D. M. Shen, Y. S. Xiong, E. C. Hayes, R. M. Parmar, F. Foor, S. W. Mitra, S. J. Degrado, M. Shu, J. M. Klopp, S. J. Cai, A. Blake, W. W. S. Cha, A. Pasternak, L. H. Yang, A. A. Patchett, R. G. Smith, K. T. Chapman, J. M. Schaeffer, *Science* **1998**, 282, 737.
- 99 D. J. Newman, G. M. Cragg, *J. Nat. Prod* **2007**, 70, 461.
- 100 J. P. Kennedy, L. Williams, T. M. Bridges, R. N. Daniels, D. Weaver, C. W. Lindsley, *J. Comb. Chem* **2008**, 10, 345.
- 101 H. E. Tuinstra, C. H. Cummins, *Adv. Mater.* **2000**, 12, 1819.
- 102 J. Burbaum, *Current Opinion in Chemical Biology* **1997**, 1, 72.
- 103 L. A. Thompson, J. A. Ellman, *Chem. Rev.* **1996**, 96, 555.
- 104 B. Jandeleit, D. J. Schaefer, T. S. Powers, H. W. Turner, W. H. Weinberg, *Angew. Chem. Int Ed.* **1999**, 38, 2494.
- 105 R. Potyrailo, K. Rajan, K. Stoewe, I. Takeuchi, B. Chisholm, H. Lam, *ACS Comb. Sci.* **2011**, 13, 579.
- 106 J. C. Meredith, *J. Mater. Chem.* **2008**, 19, 34.
- 107 R. A. Potyrailo, V. M. Mirsky, *Chem. Rev.* **2008**, 108, 770.
- 108 B. J. Chisholm, D. C. Webster, J. C. Bennett, M. Berry, D. Christianson, J. Kim, B. Mayo, N. Gubbins, *Rev. Sci. Instrum.* **2007**, 78, 72213.
- 109 H. Koinuma, I. Takeuchi, *Nat Mater* **2004**, 3, 429.

- 110 W. F. Maier, K. Stöwe, S. Sieg, *Angew. Chem. Int. Ed.* **2007**, 46, 6016.
- 111 P. J. S. Buenconsejo, A. Siegel, A. Savan, S. Thienhaus, A. Ludwig, *ACS Comb. Sci* **2012**, 14, 25.
- 112 Z. H. Barber, M. G. Blamire, *Mats. Sci. Tech* **2008**, 24, 757.
- 113 C. M. Stafford, K. E. Roskov, T. H. Epps, M. J. Fasolka, *Rev. Sci. Instrum.* **2006**, 77, 23908.
- 114 J. C. Meredith, A. P. Smith, A. Karim, E. J. Amis, *Macromolecules* **2000**, 33, 9747.
- 115 J. C. Meredith, A. Karim, E. J. Amis, *Macromolecules* **2000**, 33, 5760.
- 116 C. Neuber, M. Bäte, M. Thelakkat, H.-W. Schmidt, H. Hänsel, H. Zettl, G. Krausch, *Rev. Sci. Instrum.* **2007**, 78, 72216.
- 117 S. Burkert, M. Kuntzsch, C. Bellmann, P. Uhlmann, M. Stamm, *Applied Surface Science* **2009**, 255, 6256.
- 118 T. Ueda-Yukoshi, T. Matsuda, *Langmuir* **1995**, 11, 4135.
- 119 J. L. Lenhart, R. L. Jones, E. K. Lin, C. L. Soles, W.-l. Wu, D. L. Goldfarb, M. Angelopoulos, *J. Vac. Sci. Technol. B* **2002**, 20, 704.
- 120 T. H. Dam, A. Jamieson, M. Lu, K.-H. Baik, *Proceedings of SPIE*, 6349, **2006**, 634906.
- 121 F. Pfeiffer, N. M. Felix, C. Neuber, C. K. Ober, H.-W. Schmidt, *Adv. Funct. Mater.* **2007**, 17, 2336.
- 122 W.-A. C. Bauer, C. Neuber, C. K. Ober, H.-W. Schmidt, *Adv. Mater* **2011**, 23, 5404.

## 2 Aim and motivation

Moore's law describes the cost-efficient doubling of number of transistors placed on an integrated circuit every two years.<sup>1</sup> In the international technology roadmap for semiconductors (ITRS) – refreshed every two years – all requirements necessary to keep in step with this prediction are listed.<sup>2</sup> This list comprises the advancement of exposure tools as well as exposure techniques, integrated circuit's architecture but also the development of new resist materials has to proceed steadily. The aim of this thesis is the synthesis of new resist materials with controlled molecular architecture and the development and adaption of combinatorial methods and strategies for the continuous patterning optimization applied on these new tailored resist materials.

A currently in industry used resist system for the production of integrated circuits is based on a linear terpolymer chemically amplified resist (Figure 2.1).<sup>3</sup> For the development of new polymeric resist systems of industrial interest it is reasonable to utilize the established aliphatic monomers to stay with the currently applied patterning process. To improve existing resist systems one way is the tailoring of polymer architecture. Atomic transfer radical polymerization is an established and versatile controlled polymerization technique which offers numerous examples of demonstrated topologies. Chochos et al. has investigated a hyperbranched architecture and demonstrated an increase in lithographic performance in comparison to a linear reference polymer.<sup>4</sup>

In this thesis new resist systems based on star architecture are in the focus of investigations. The star topology offers a controlled shape in contrast to the aforementioned hyperbranched or linear architecture. These star-shaped terpolymers should be realized with defined monomer incorporations independent on molecular weight orientated on monomer compositions of industrial standard resists. By the utilization of the more sophisticated star block copolymer topology the monomer positioning should be controlled. Due to the core-shell-like structure the new resist system should exhibit an increase in lithographic performance.

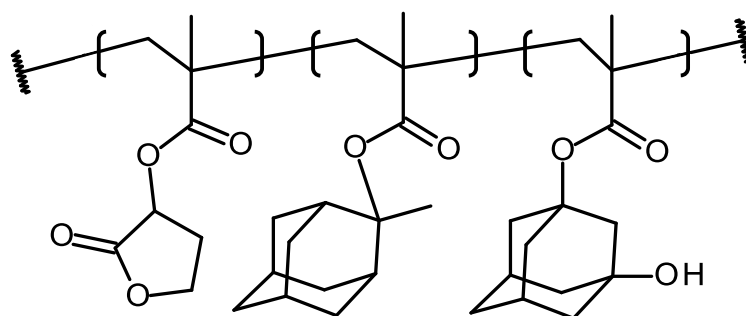


**Figure 2.1:** Currently industrial utilized chemically amplified positive-tone photoresist for 193 nm lithography

The potential and optimized performance of the new resist materials should be investigated in view of lithographic patterning by means of resulting feature's quality. But the lithographic patterning process is a multi-step process and consists of many variables interacting strongly with each other. Thus processing established variable gradients utilizable in combinatorial approaches should be improved and developed further. Furthermore the combination of these variable gradients to combinatorial libraries is targeted for successive investigation and understanding as well as fast optimization of new resist materials in just one experiment.

- 
- 1 G. E. Moore, *Electronics* **1965**, 38, 114.
  - 2 <http://www.itrs.net/> (April 2012)
  - 3 D. P. Sanders, *Chem. Rev.* **2010**, 110, 321.
  - 4 C. L. Chochos, E. Ismailova, C. Brochon, N. Leclerc, R. Tiron, C. Sourd, P. Bandelier, J. Foucher, H. Ridaoui, A. Dirani, O. Soppera, D. Perret, C. Brault, C. A. Serra, G. Hadziioannou, *Adv. Mater.* **2009**, 21, 1121.

### 3 Overview of the thesis

This thesis includes three publications which are presented in chapters 4.2 to 4.5. Two publications have been already published in *Journal of Materials Chemistry* and in *Advanced Materials* and the third one has been submitted to *Molecules*.

This thesis deals with the synthesis and development of new resist material types for lithographic patterning on the one hand and their combinatorial optimization concerning resist performance on the other hand. The lithographic patterning procedure is a succession of several processing steps involves many processing parameters strongly interacting with each other. For their investigation and optimization especially for new resist materials a combinatorial approach is a strong and efficient tool. In the course of the first part of this thesis variable gradients for each lithographic patterning processing step were developed, improved and consequently adapted for respective requirements. These gradients were combined to binary and ternary combinatorial libraries. This allows now to conduct multiple variables variations in one experiment, and thus to investigate the influence of processing conditions of resist systems and finally to optimize feature's quality. These combinatorial approaches were applied to new resist types synthesized and developed in this work representing the second part of this thesis. For the development of new polymeric resist systems of industrial interest it is important to develop these systems compatible to current respectively future patterning processes but advanced in performance. Thus in this thesis the advanced topology of star architecture was selected due to its controlled spherical shape to generate a new resist material generation. For the polymerization the established and versatile method atomic transfer radical polymerization was taken. In this way random terpolymers and block star copolymers were tailored in monomer incorporation and molecular weight. These polymers were combinatorial investigated in view of lithographic patterning and the so-called "triangle of death" with its corners: resolution, line edge roughness, and sensitivity.<sup>1</sup>

The standard exposure for lithographic patterning was conducted using the scanning electron microscope Zeiss Leo 1530 FESEM with an acceleration voltage of 20 kV. For a precise beam control the SEM was equipped with the Raith Elphi Plus. This tool was controlled by the software Elphy Plus (v. 5.0 SP 14.0) which defines the areas for exposure – so-called write-fields. The here used write-fields were of a size of  $(100 \mu\text{m})^2$  containing 18

## Overview of the thesis

1:1 line/space patterns with a feature size of 100 nm but differing in the exposure dose representing a dose gradient. The resulting patterns were investigated concerning feature's quality by observing images in the scanning electron microscope mode. Here multiple high-resolution micrographs had to be observed from each pattern of every sector of the combinatorial libraries to calculate and evaluate the line edge roughness using the software SuMMIT (v. 8.0.4).

In the following the key results of the individual publications are summarized. Detailed descriptions of synthesis and process conditions as well as measured values are provided in the respective chapters.

### **3.1 Combinatorial techniques to efficiently investigate and optimize thin film nanopatterning**

*(Submitted to Molecules, see chapter 4.2)*

The first chapter summarizes all developed and implemented combinatorial techniques for a thoroughly investigation of thin film processing and properties and were applied in view to the optimization of the complex *lithographic patterning process*. The motivation of this chapter was to investigate process conditions and to establish techniques for a fast and efficient optimization of especially new resist systems applicable to the multi-step lithographic process. In the following the gradient preparation of material composition, exposure dose, temperature, and development time as well as their combination to combinatorial libraries are presented.

The systems throughout used in this thesis were chemically amplified resists (CARs) systems. These systems may consist of two to four components. To investigate the properties of different component ratios and to evaluate the optimized resist composition concerning feature's quality, a method was developed to realize an internal composition gradient within a thin film. The preparation of such a gradient was conducted in two steps: first a gradient extrudate out of two solutions were applied – via a syringe pump system with two individual controllable syringe pumps and a connected mixing device – which was directly afterwards

doctor bladed for the second step (see Figure 1a) and subsequently annealed to remove residual solvent (post apply bake; PAB). For the characterization of the achieved composition gradient the solid film was sectioned into segments for using fluorescence spectroscopy or cut together with the substrate into pieces which were then rinsed for using high performance liquid chromatography (HPLC). The graph in Figure 1b shows exemplarily the composition gradient of a negative tone photoresist film characterized using HPLC.

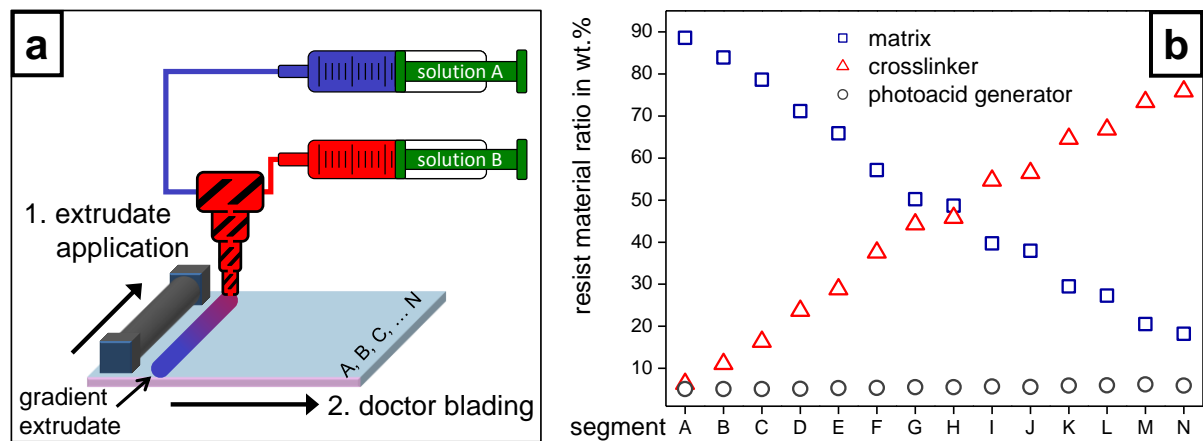


Figure 1a: The gradient extrudate was realized on a substrate via opposite flow rates of two solutions – one contains matrix component and photoacid generator and the other crosslinker component and photoacid generator – in the first step, subsequently doctor bladed and annealed in the following step. The resulting gradient film was sectioned in segments parallel to the application direction, cut into pieces (A-N) and analyzed using high performance liquid chromatography. Figure 1b shows the resist material ratios of each segment and the continuous decrease of the matrix component ( $\square$ ) and the continuous increase of the crosslinker component ( $\triangle$ ) while the photoacid generator stays constant.

The next step in the lithographic process after film application and PAB is the exposure. For CAR systems acids are released during this step which crosslink negative tone resists or deprotect positive tone resists during the subsequent post exposure bake (PEB). The dissolution behavior of reacted to unreacted resist material causes the development contrast of exposed to unexposed areas. The exposure dose is very critical for high-throughput industrial applications and should be as low as possible. It is strongly influenced by the nature of applied materials, differs for every individual resist system, and also is affected by the other applied processing conditions. Thus exposure dose gradients applicable to electron beam lithography and UV-lithography were developed, respectively. For the exposure dose gradient in the latter case a special designed shadow mask was used to realize the dose gradient in a mask-alignment system (Figure 2a). This shadow mask is composed of 4900 sectors with a

## Overview of the thesis

sector's size of 1.2 mm x 1.2 mm. One sector consists of nine subsectors and only one out of nine parts has translucent patterns while the remaining part is coated lightproof. Thus 4900 dose gradients are realizable in one experiment via precise realignment of the substrate between different exposures. This is exemplified by one sector with five doses using a positive tone resist (dark grey) where the subsequent PEB and development was already performed to realize the features (Figure 2b). The dose gradient shows obviously from underexposed to optimized to overexposed features. This is indicated by the features becoming ongoing brighter in grey scale means more and more of the positive tone resist was deprotected and removed during development.

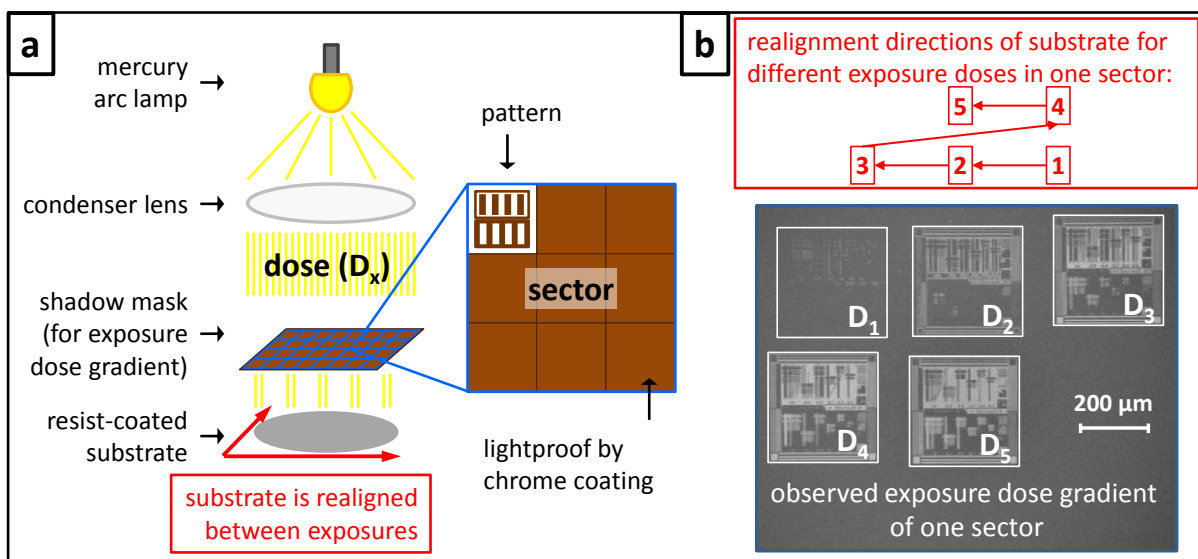


Figure 2a: A schematic illustration shows the main components of a mask-alignment system. One sector of overall 4900 is highlighted in a schematic magnification showing nine subsectors: Only one out of nine subsectors has a translucent pattern while the rest is lightproof coated. Thus the precise micrometer adjustment of the substrate holder allows the realization of dose gradients (Figure 2b). The SEM image shows one sector with an exposure dose gradient of five different subsectors realized with a positive tone resist (dark grey). The increasing dose is indicated by the brighter grey scales means more of the resist was developed and shows the substrate (light grey).

For a realization of a dose gradient with the direct write technique electron beam exposure no mask was needed but with the software Elphy Plus a so-called write-field of a size of 100 μm x 100 μm size was programmed. This write-field consists of multiple features each having a different dose representing the dose gradient. Such writing fields can be exposed similar on several positions of the substrate for example in a matrix-like arrangement resulting in comparable exposed areas for photolithography in our capabilities.

The subsequent PEB step is a for the resulting pattern quality very important step in the case of applying CAR systems. The acid which is generated in the previous exposure step catalyzes deprotection or crosslinking reactions dependent on the resist type and thus results in the development contrast of exposed to non-exposed areas. Especially for the investigation of new resists the optimal PEB temperature is of considerable value which controls the diffusion length of the acid molecules and the reaction rate. At a too low PEB temperature the deprotection/crosslinking is insufficient while at a too high PEB temperature acids diffuse into non-exposed areas and catalyze reactions. For an efficient investigation of the PEB temperature gradients were prepared via self-made set-ups on metal plates with active cooling agents on one side and a heating source on the other side. This set-up is adjustable for particular requirements to different temperatures and temperature slopes. In Figure 3 two temperature profiles with different temperature slopes are exemplarily shown. A flat temperature slope of  $0.55\text{ }^{\circ}\text{C}/\text{mm}$  ( $\circ$ ) was realized on an aluminum plate using ice-water as cooling agent on one side and heated to  $240\text{ }^{\circ}\text{C}$  on the other side. However a steep temperature slope of  $1.85\text{ }^{\circ}\text{C}/\text{mm}$  ( $\Delta$ ) was realized on a steel plate using liquid nitrogen for cooling on one side and heated to  $300\text{ }^{\circ}\text{C}$  on the other side.

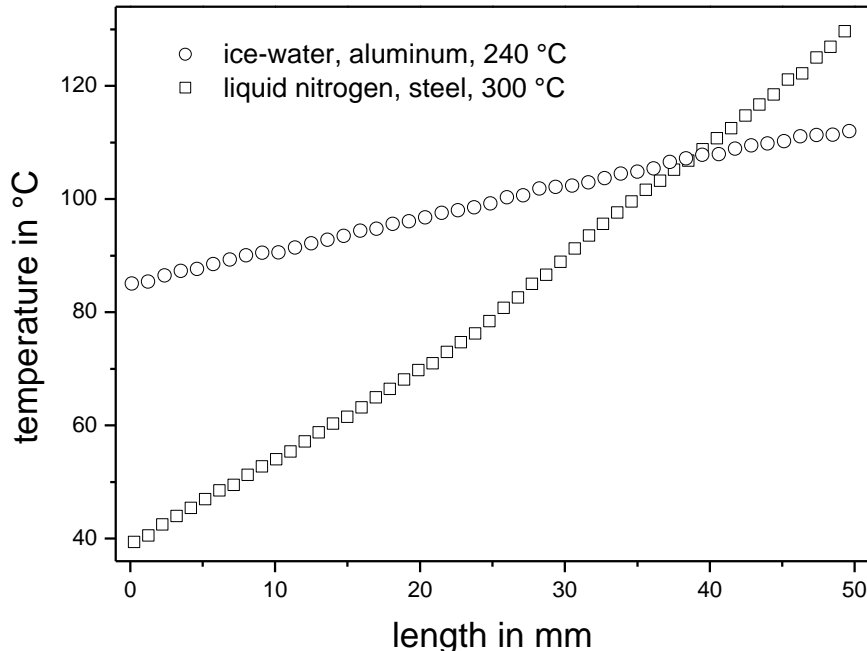


Figure 3: Two temperature profiles are shown for a length of 50 mm using different cooling agents, metal plates, and heating temperatures. A flat temperature slope of  $0.55\text{ }^{\circ}\text{C}/\text{mm}$  ( $\circ$ ) in the range of  $85\text{ }^{\circ}\text{C}$  to  $112\text{ }^{\circ}\text{C}$  was achieved on an aluminum plate using ice-water and  $240\text{ }^{\circ}\text{C}$  for temperature adjustment. A steep temperature slope of  $1.85\text{ }^{\circ}\text{C}/\text{mm}$  in the range of  $39\text{ }^{\circ}\text{C}$  to  $130\text{ }^{\circ}\text{C}$  was achieved on a steel plate using liquid nitrogen and  $300\text{ }^{\circ}\text{C}$  for temperature adjustment.

## Overview of the thesis

The last step of the lithographic patterning process of CAR systems is the development. In this step the non-crosslinked material for negative tone resists and for positive tone resists the deprotected material is dissolved and removed by the developer. For the determination of the dissolution behavior of non-exposed and exposed resist material quartz crystal microbalance (QCM) measurements conducted plunged into the developer solution was established. This method allows an estimation of the applicable developer strength and the right development time period for the respective resist film which plays a chief part for the quality of the resulting patterns. Here a deviation of an optimum development time period, so called underdevelopment or overdevelopment, results in material residues between patterns respectively thinner or even stripped off patterns. Based on these prescreening results of the QCM measurements the time frame of further detailed development investigations on Si-wafers was identified. For this a resist film which already passed the lithographic patterning process pending development was stepwise or continuously immersed into the developer solution using simple set-ups. For the stepwise development of the resist film the substrate was clamped into an inverse pair of tweezers and was then immersed step by step into the developer solution. For the continuous development a wire was attached to the pair of tweezers and connected to an electrical motor drive with adjustable speeds. The immersion time periods were identified by the time frame determined by the QCM measurements resulting in a development time gradient.

For the investigation and optimization of new resist materials combinations of the most important processing parameters were arranged to binary and to ternary combinatorial libraries by the use of the above listed gradients. Thus it is possible to investigate and optimize two respectively three strong interacting parameters in one experiment. For this two linear gradients are arranged orthogonally to each other resulting in a binary library. For the preparation of a ternary library a third variable variation has to be conducted either in the third dimension or in a very small area in which the first and second variable are effectively unchanged and applied matrix-like on the binary library. In Figure 4 such a ternary combinatorial library is exemplarily shown applied on a positive tone resist system. This library is composed of a PEB temperature gradient perpendicular to a development time gradient representing the binary library, while an electron beam exposure dose gradient is applied matrix-like to this binary library. The observation and evaluation of this library shows that for each write-field only one exposure dose fits to the applied PEB temperature and development time. The patterns were evaluated regarding their feature's quality which is

described by the line edge roughness (LER). The clearest lines out of this combinatorial library were observed in sector **B2** determined by a LER value of 5.3 nm. The patterns resulting from a higher and a lower PEB temperature than the identified optimum of 100 °C but with the same development time show clearly increased LER values. Such increase of LER values is also evident at patterns with a longer and shorter development time than the observed optimum of 30 s.

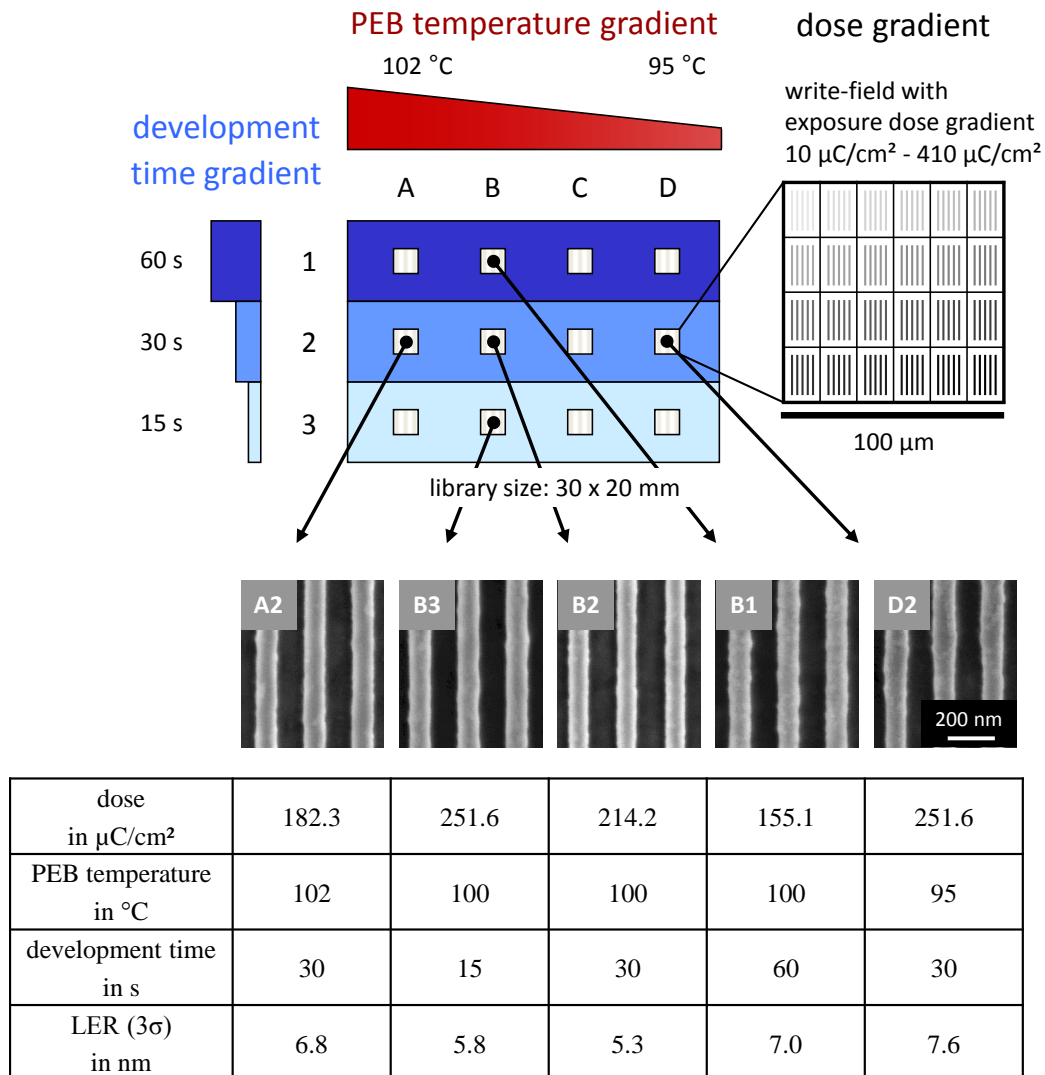


Figure 4: A schematic illustration of a ternary combinatorial library composed a PEB temperature gradient (95 °C – 102 °C) and orthogonally to it a development time step gradient (15 s, 30 s, 60 s) representing the binary library. The exposure dose gradient is conducted in write-fields (10  $\mu\text{C}/\text{cm}^2$  – 410  $\mu\text{C}/\text{cm}^2$ ), provided in 24 arrays of a 100 nm line/space profile and is applied matrix-like on the binary library. Selected SEM images demonstrate the strong influence of the applied variable gradients. The respective conditions (PEB temperature, development time, and dose plus the LER values) of these patterns are listed below the illustration.

In summary, techniques for the preparation of variable gradients regarding thin film investigations and their combination to combinatorial libraries were presented and their powerful and efficient optimization demonstrated. All variable gradients are completely adjustable to the requirements need for investigation and optimization of new resist materials or other complex investigation of multi-variable dependent thin film systems.

### **3.2 Tailored Star-Shaped Statistical Teroligomers via ATRP for Lithographic Applications**

*(Journal of Materials Chemistry, see chapter 4.3)*

The second chapter deals with the presentation of a star-shaped teroligomer as a new resist type. The synthesis of this new material was carried out using atom transfer radical polymerization (ATRP) via the core-first route out of saccharose molecule with eight initiating sites. For comparison reasons a linear model oligomer was synthesized and a saccharose initiator was modified to hold less ATRP initiating sites. Thus star teroligomers were synthesized with a reduced arm number but the identical saccharose core. The resulting teroligomers showed a narrow molecular weight distribution as well as a controlled incorporation ratio of the three monomers and targeted molecular weights were precisely achieved. Finally the most promising synthesized star-shaped teroligomer was investigated in a combinatorial library to its lithographic performance.

In this study the monomers used for the polymerizations are currently industrially used in respect to the potential application of these star oligomers for lithographic patterning:  $\alpha$ -gamma butyrolactone methacrylate (GBLMA), methyl adamantyl methacrylate (MAMA), and hydroxyl adamantyl methacrylate (HAMA) (see Figure 5). A linear model oligomer (**L**) was synthesized using ethyl 2-bromoisobutyrate as initiator. For the realization of the star architecture a saccharose molecule functionalized with eight ATRP initiating sites (**1**) was used and four star-shaped oligomers with varying target arm lengths were synthesized (**S1a-d**). In addition, a saccharose molecule was synthesized with ATRP initiating sites as well as non-reactive sites (**2**). The average number of initiating sites of this core amounts to 3.5 and thus results in a reduced functionality in contrast to **1**. Thus a star-shaped teroligomer (**S2**) was realized as missing link between the linear oligomer and the star teroligomer (**S1**).

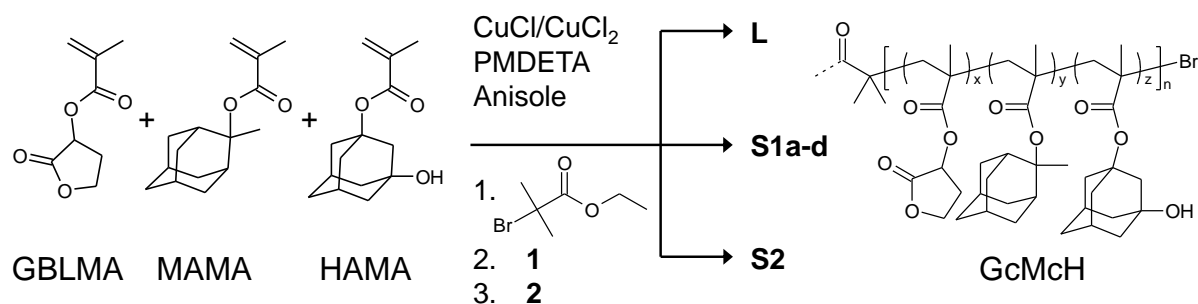


Figure 5: This figure shows the used monomers  $\alpha$ -gamma butyrolactone methacrylate (GBLMA), methyl adamantyl methacrylate (MAMA), and hydroxyl adamantyl methacrylate (HAMA). The polymers **L**, **S1a-d**, and **S2** were realized using the linear initiator ethyl 2-bromoisobutyrate and the saccharose initiators **1** and **2**, respectively. The overall teri-copolymer composition of GBLMA/MAMA/HAMA (GcMcH) was about 50/30/20.

For all polymers narrow monomodal distributions were detected, GPC/ multi-angle light scattering (MALS) traces exhibited symmetrical shapes and polydispersity index values of lower than 1.1 were determined (see Figure 6). The MALS detector revealed recombination shoulders for the traces of **S1c** and **S1d**. As the scattering detector is disproportionally sensitive (intensity  $\sim$  diameter<sup>6</sup>) these recombinations are negligible.

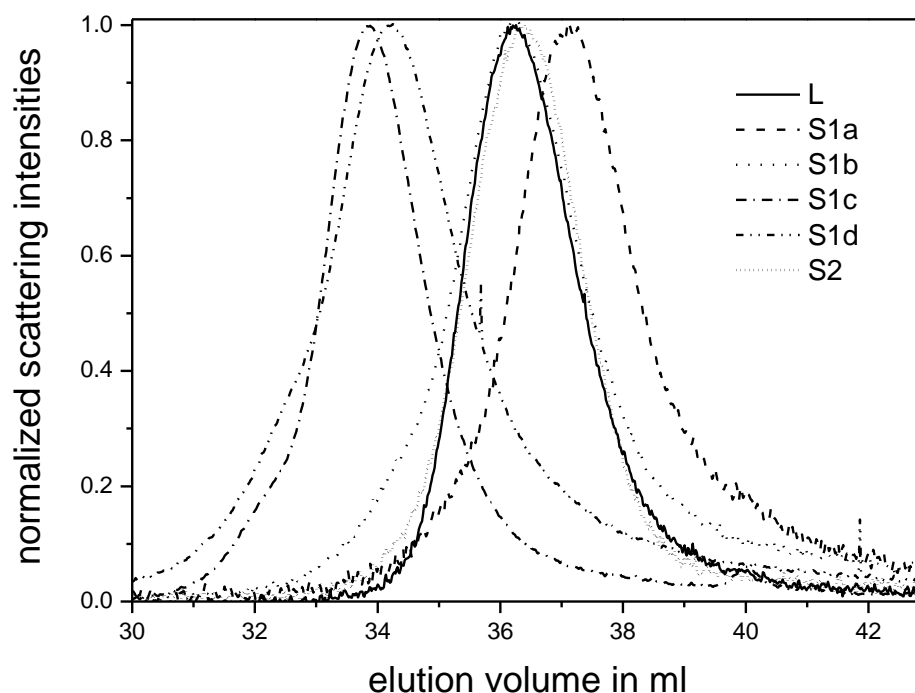


Figure 6: Normalized scattering intensity of GPC traces of **L**, **S1a**, **S1b**, **S1c**, **S1d** and **S2** measured with a multi-angle light scattering detector. Slight recombinations are visible by shoulders for the star-shaped teri-copolymers **S1c** (dash dot) and **S1d** (dash dot dot). Due to the fact that the scattering detector is disproportionally sensitive to the molecular size (intensity  $\sim$  diameter<sup>6</sup>) these recombinations are negligible.

The targeted monomer composition of all teroligomer was 50 % GBLMA, 30 % MAMA and 20 % HAMA due to its potential application as resist material.<sup>2</sup> For the realization of this monomer composition a monomer feed of 41 % GBLMA, 41 % MAMA and 18 % HAMA was identified because of repeated experimentations. The monomer composition was determined via <sup>1</sup>H-NMR measurements of taken aliquots out of the polymerization solution. The shown composition was achieved over a conversion range of  $X_p = 30 - 60 \%$  on the example of **S1d** (see Figure 7).

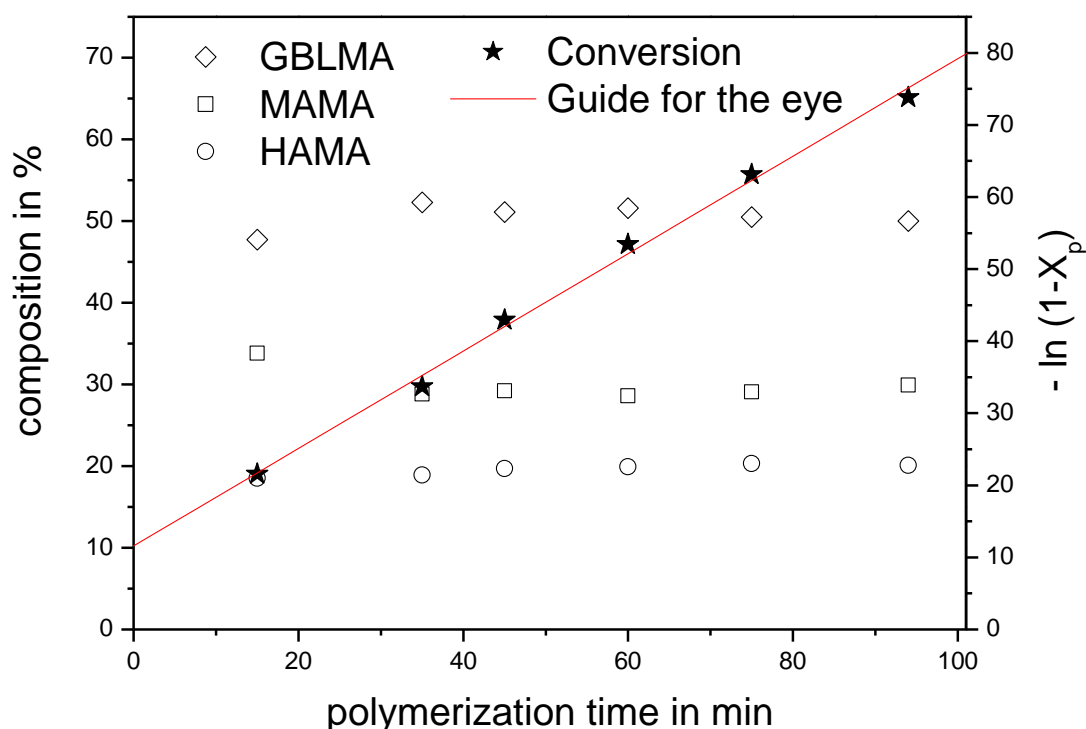


Figure 7: Evolution of monomer incorporation (GBLMA (◇), MAMA (□) and HAMA (○)) and also  $-\ln(1-X_p)$  (★) versus polymerization time of **S1d**.

For a proof of principle the synthesized star resist **S1d** was investigated for lithographic application as this well-defined star oligomer has the most distinct star character, a similar molecular weight and the same monomer composition as the non-controlled architecture of the hyperbranched polymer resist material published by Hadziioannou et al.<sup>3</sup> In this work the new star resist material was directly optimized in one experiment concerning the lithographic variables exposure dose, PEB temperature, and development time. The prepared ternary combinatorial library consisted of a temperature gradient for PEB set perpendicular to a development time gradient and an exposure dose gradient of 1:1 line/space 100 nm patterns applied matrix-like with electron beam lithography (see Figure 8). Low line edge roughness (LER: deviation of feature edge from ideal shape) and also low line width roughness (LWR:

deviation of width) values gave the information on optimized processing conditions. The excellent LER value of 3.1 nm and LWR of 5.9 nm were observed at an electron beam dose of 214.2  $\mu\text{C}/\text{cm}^2$ , a PEB temperature of 98  $^\circ\text{C}$ , and a development time of 60 s.

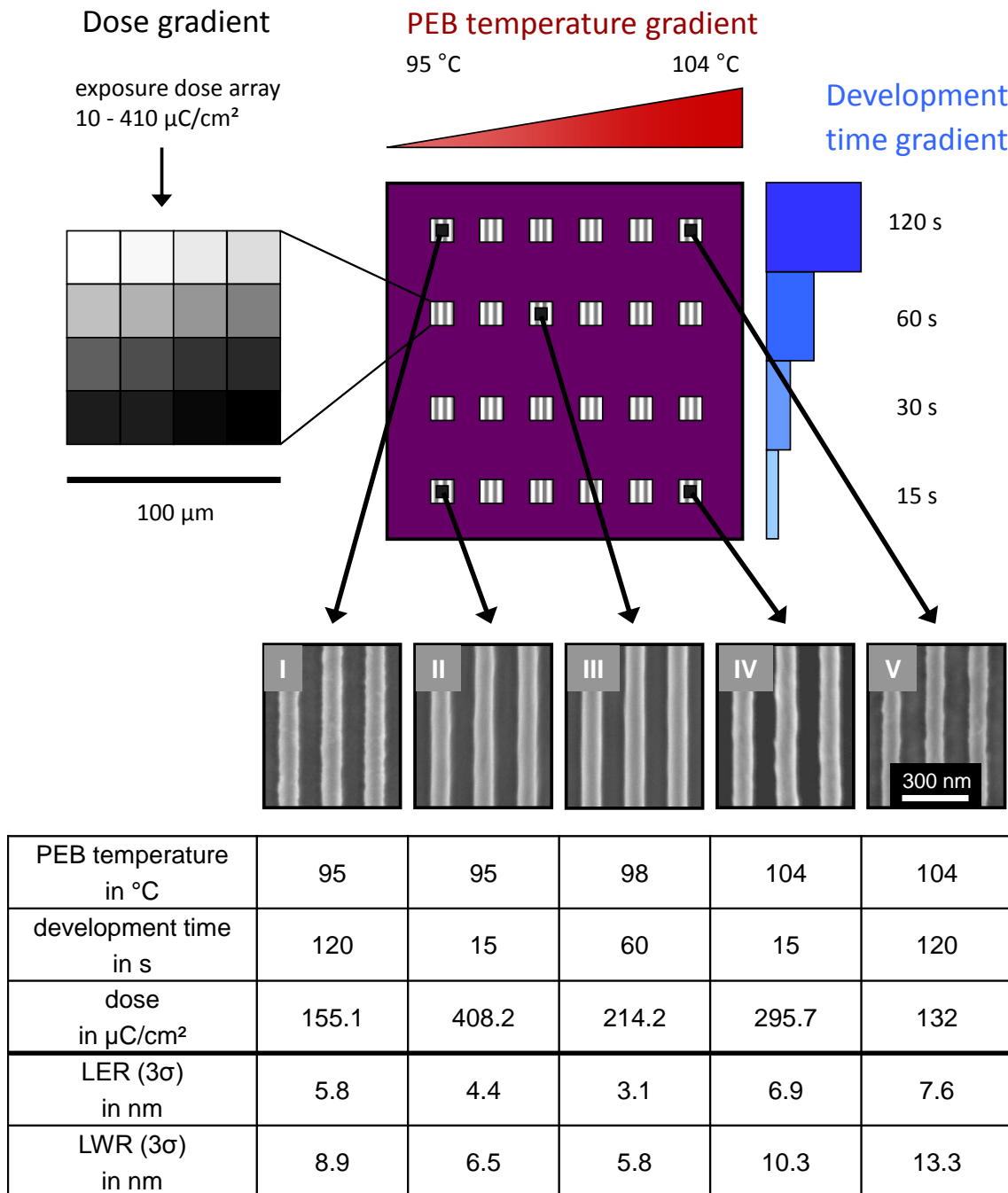


Figure 8: The upper figure shows a schematic illustration of the ternary combinatorial library consisting of the PEB temperature gradient, the development time step gradient, and the electron beam dose gradient. The table exhibits patterns from the four corners of the combinatorial library (I, II, IV, V) and the optimized pattern (III). The respective conditions (PEB temperature, development time, and dose) of these patterns and the calculated LER and LWR are listed.

In summary the precision syntheses of star-shaped oligomers and the capability to study the impact of arm number and short arm length of star-shaped oligomers were presented. Four star teroligomers with varying target arm lengths, a star-shaped teroligomer with identical core but reduced arm number, and a linear model oligomer were synthesized. All oligomers were realized with the identical monomer composition and showed narrow and symmetrical molecular weight distributions with low polydispersity indices (PDIs < 1.1). On the example of one star oligomer the high potential of the star architecture for lithographic purposes were demonstrated preparing a combinatorial library and observing optimized 100 nm line/space patterns with a LER of 3.1 nm and a LWR of 5.8 nm.

### **3.3 Tailored Star Block Copolymer Architecture for High Performance Chemically Amplified Resists**

*(Advanced Materials, see chapter 4.4 and supporting information)*

The third chapter progresses the work based on new polymeric star resist material in chapter two: the random monomer incorporation is here replaced by a controlled core-shell structure of star block copolymers. These tailored copolymers were synthesized via the core-first ATRP route by full conversion of a first monomer and in-situ polymerization of additionally added monomer. This new star resist material impressively improves dissolubility and sensitivity in contrast to randomly distributed star polymers or a reference linear terpolymer. The most promising star block copolymer was combinatorial investigated resulting in well-defined 1:1 line/space patterns down to 66 nm with LER values of about 6 nm.

The monomers used for the ATRP syntheses in this chapter are identical to the currently industrially utilized monomers investigated in chapter two:  $\alpha$ -gamma butyrolactone methacrylate (GBLMA), methyl adamantyl methacrylate (MAMA), and hydroxyl adamantyl methacrylate (HAMA) (see Figure 9). A linear terpolymer ran-L was synthesized as reference material to the star block copolymers. Again the core of the synthesized star polymers is the functionalized saccharose with eight initiating sites. Based on this initiator a random star terpolymer ran-S1 and a random star copolymer ran-S2 (composed of GBLMA/ MAMA) were synthesized. Further three star block copolymers were synthesized via full conversion of

GBLMA for the first block and in-situ polymerization of afterwards added monomers: block-S1 (GBLMA/ MAMA/ HAMA), block-S2a and block-S2b (composed of GBLMA/ MAMA in different ratios). All polymers showed monomodal distributions with symmetrical shape and narrow molecular weight distributions (PDI  $< 1.2$ ).

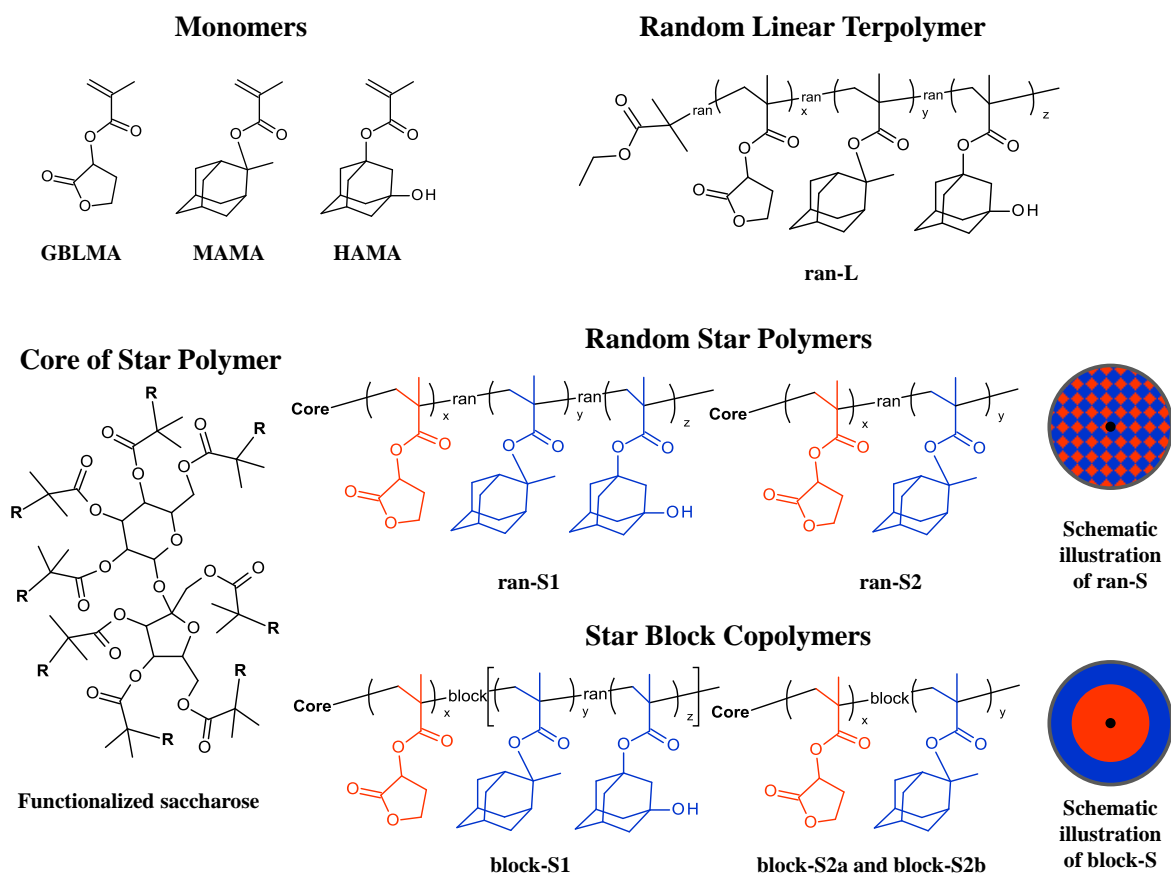


Figure 9: Chemical structures of used monomers GBLMA, MAMA, HAMA, the core for the star polymers (functionalized saccharose), and synthesized reference linear terpolymer (ran-L), random star copolymers (ran-S1, ran-S2) and tailored star block copolymers (block-S1, block-S2a, and block-S2b) are shown.

The core-shell-like structure of the star block copolymers – the hydrophilic lactone monomer units form the inner shell and the more hydrophobic adamantyl monomer units the outer shell – was indicated by the direct comparison to the randomly distributed polymers by contact angle measurements. The polymer architecture and the monomer incorporation also have a tremendous influence on the dissolution behavior. Films of each polymer with added photoacid generator (PAG) were prepared on quartz crystals, flood exposed for PAG activation and annealed for post exposure bake (PEB) to catalyze the deprotection of MAMA units for a dissolubility change. In Figure 10a traces of film thickness variations are shown of the exposed and non-exposed polymer films in an alkaline developer detected by QCM

measurements. In this measurement series the exposed and annealed films of block-S2a and block-S2b (both composed of GBLMA/MAMA) showed a complete development within 5 s and thus the highest solubility contrast compared to untreated films. A similar trend of material properties for the synthesized polymers was demonstrated in sensitivity measurements. Films of all polymers were exposed to an electron beam dose gradient of 25 increasing doses, annealed for PEB and developed in an alkaline solution. The resulting patterns were measured in regard to dose dependent achieved film thickness loss using a mechanical profilometer (see Figure 10b). The highest sensitivity was measured for the star block copolymer block-S2b with a clearing dose of  $21.5 \mu\text{C}/\text{cm}^2$ ; this demonstrates a sensitivity increase up to eight times in comparison to the reference linear polymer ran-L.

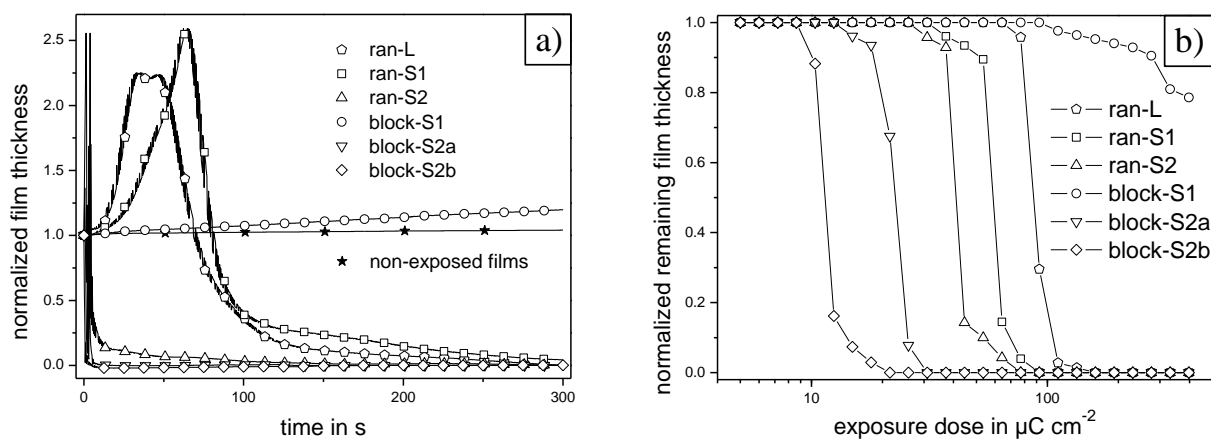


Figure 10: a) Quartz crystal microbalance measurements of non-exposed and flood exposed polymer resist films. All non-exposed films (★) exhibit no significant change in film thickness while the flood exposed films just swell (block-S1 ○), swell and subsequently dissolve (ran-L △ / ran-S1 □), or rapidly swell and dissolve within seconds (ran-S2 △ / block-S2a ▽ / block-S2b ◇).

b) Sensitivity curves of investigated polymer resist films utilizing electron beam exposure. Block-S1 (○) was developed partly even at the highest dose while the other polymers show high development contrasts. The most sensitive polymer is block-S2b (◇) exposed to a clearing dose of  $21.5 \mu\text{C}/\text{cm}^2$ .

Because of this measured high sensitivity of star block copolymer block-S2b, it was investigated in a combinatorial library to its lithographic performance (see Figure 11a). An exposure dose as well as feature size gradient was applied via electron beam lithography and combined with a PEB temperature gradient perpendicular to a development time gradient to a ternary library. In Figure 11b selected scanning electron microscopy images of selected patterns, their corresponding LER and LWR values and their process conditions are tabulated. In sector E3 the optimized pattern was observed with the dose of  $51.6 \mu\text{C}/\text{cm}^2$ , the PEB temperature of  $93 \text{ }^\circ\text{C}$ , the development time of 5 s, and showed the LER of 5.9 nm and the

LWR of 8.7 nm. Further the feature size gradient for this optimized sector E3 from 102 nm to 66 nm 1:1 line/space patterns is shown in Figure 11c. For all feature sizes clear lines with similar LER values of about 6 nm are observed.

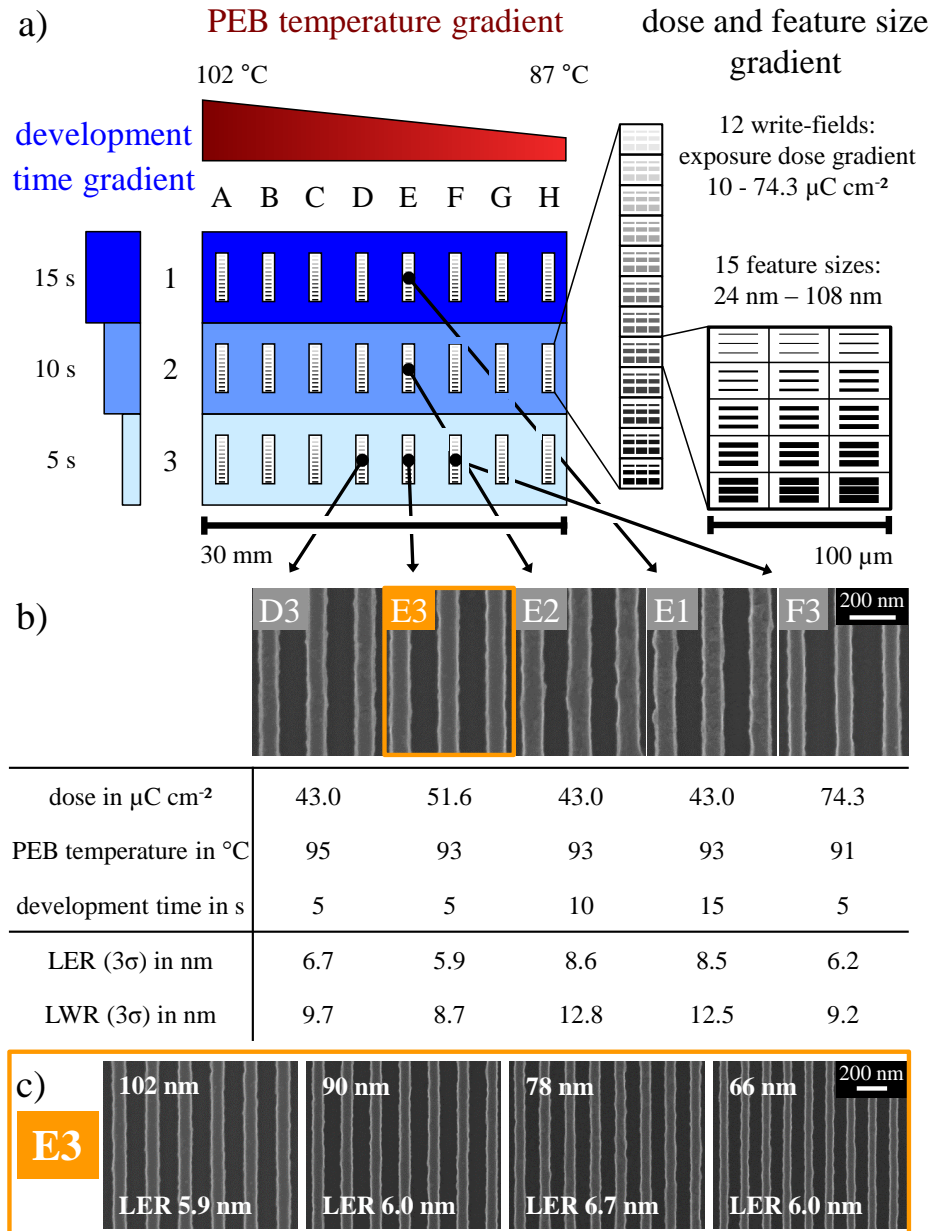


Figure 11: a) Schematic illustration of the investigated ternary combinatorial library consisting of an exposure dose and feature size gradient combined with a PEB temperature gradient and a development gradient.

b) Selected SEM images of the ternary combinatorial library demonstrate the influences of the applied variable gradients. In addition, corresponding process conditions (exposure dose, PEB temperature, and development time) and analyzed LER and LWR values are tabulated.

c) Selected SEM images of e-beam written feature size gradient in sector E3 and corresponding LER values demonstrate the high potential of star block copolymer block-S2b.

## Overview of the thesis

In conclusion, tailoring polymer's architecture towards a core-shell-like star block copolymer leads to a high-sensitivity and high performance resist material. The tailored star block copolymers were synthesized for the first time *in-situ* via a core-first ATRP route under controlled conditions resulting in PDIs below 1.2. These star block copolymers exhibited excellent dissolubility in the exposed state and up to eight times increased sensitivity in comparison to the reference linear polymer. The most promising star block copolymer was combinatorial investigated to its lithographic performance and was optimized to well-defined 66 nm 1:1 line/space patterns with LER values of 6.0 nm.

- 
- 1 <http://www.life.lithoguru.com/> (April 2012)
  - 2 D. P. Sanders, *Chem. Rev.*, 2010, **110**, 321-360.
  - 3 C. L. Chochos, E. Ismailova, C. Brochon, N. Leclerc, R. Tiron, C. Sourd, P. Bandelier, J. Foucher, H. Ridaoui, A. Dirani, O. Soppera, D. Perret, C. Brault, C. A. Serra and G. Hadziioannou, *Adv. Mater.*, 2009, **21**, 1121-1125.

## **4 Publications and manuscripts**

### **4.1 Individual contributions**

This presented work was carried out under the supervision of Prof. Dr. Hans-Werner Schmidt at the chair of Macromolecular Chemistry I and in close cooperation with the chair of Prof. Christopher Kemper Ober (Materials Science and Engineering, Cornell University, Ithaca, NY, USA). In the following individual contributions to the publications of this thesis are presented.

#### **Combinatorial techniques to efficiently investigate and optimize thin film nanopatterning**

Submitted to *Molecules*

F. Wieberger, T. Kolb, C. Neuber, C. K. Ober, and H.-W. Schmidt

The experimental work and the interpretations originated from me, whereas the example experiment for an electron beam exposure dose gradient and one temperature gradient were performed from Tristan Kolb. The composition gradient was conducted by myself in my diploma thesis. The manuscript was written by myself and jointly finalized with the help of all coauthors.

### **Tailored Star-Shaped Statistical Teroligomers via ATRP for Lithographic Applications**

*Journal of Materials Chemistry* **2012**, *22*, 73-79.

F. Wieberger, D. C. Forman, C. Neuber, A. H. Gröschel, M. Böhm, A. H. E. Müller, H.-W. Schmidt and C. K. Ober

The conducted experimental work and most of the synthesized polymer were done on my part. Two polymers were synthesized by Dr. Drew C. Forman (Cornell University). The GPC/MALS measurements were conducted by Dipl.-Ing. Marietta Böhm (University of Bayreuth, Macromolecular Chemistry II). The manuscript was written mainly by myself and jointly finalized with the help of all coauthors.

### **Tailored Star Block Copolymer Architecture for High Performance Chemically Amplified Resists**

*Advanced Materials* **2012**, *24*, 5939-5944.

F. Wieberger, C. Neuber, C. K. Ober, and H.-W. Schmidt

The complete polymer synthesis and all experiments were carried out by me. The manuscript was written by myself and jointly finalized with the help of all coauthors.

## 4.2 Combinatorial techniques to efficiently investigate and optimize thin film processing and properties

*By Florian Wieberger,<sup>1)</sup> Tristan Kolb,<sup>1)</sup> Christian Neuber,<sup>1)</sup>  
Christopher K. Ober,<sup>2)</sup> and Hans-Werner Schmidt<sup>1,a)</sup>*

<sup>1)</sup>*Macromolecular Chemistry I and Bayreuth Institute of Macromolecular Research (BIMF),  
University of Bayreuth, D-95447 Bayreuth, Germany*

<sup>2)</sup>*Materials Science & Engineering, Cornell University, Ithaca, NY 14853*

This paper is submitted to  
*Molecules*

---

<sup>a)</sup> Author to whom correspondence should be addressed.

Electronic mail: hans-werner.schmidt@uni-bayreuth.de.

**Abstract:** In this article we present several developed and improved combinatorial techniques to optimize processing conditions and material properties of thin films. The combinatorial approach allows investigations of multi-variable dependencies and is the perfect tool to investigate thin films regarding their high performance purpose. In this context we develop and establish the reliable preparation of gradients of material composition, temperature, exposure, and immersion time. Furthermore we demonstrate the smart application of combinations of composition and processing gradients to create combinatorial libraries. First a binary combinatorial library is created by applying two gradients perpendicular to each other. A third gradient is carried out in very small areas and arranged matrix-like over the entire binary combinatorial library resulting in a ternary combinatorial library. Ternary combinatorial libraries allow identifying precise trends for the optimization of multi-variable dependent processes which is demonstrated on the lithographic patterning process. Here we verify conclusively the strong interaction and thus the interdependency of variables in the preparation and properties of complex thin film systems. The established gradient preparation techniques are not limited to lithographic patterning. It is possible to utilize and transfer the reported combinatorial techniques to other multi-variable dependent processes and to investigate and optimize thin film layers and devices, for optical, electro-optical, and electronic applications.

### 1. Introduction

Combinatorial optimization methods are widely used above all in pharmaceutical research to screen new molecules for their potential application as drugs [1-4]. Especially in this field of research the method of “high-throughput screening” was developed [5]. But the approach of combinatorial investigations has been aggressively adopted by the field of materials research in recent years [6-8]. Combinatorial materials science pursues the objective of preparing a family of related samples in a single experiment, to investigate interacting parameters and, to optimize materials and processes. Due to continuously arising challenges in materials development, the use of variable gradients and the combination of gradients to so called combinatorial libraries, has been driven forward. Important research areas of established combinatorial approaches include sensing materials, catalysis, electronic and functional materials, and biomaterials [9]. In the last decade research has addressed the investigation of properties of thin films in relation to certain variable gradients [10]. In general the film thickness itself is an important variable for film application. Thus to enable a

combinatorial investigation, films of continuous thickness gradients were prepared [11]. Amis et al. have demonstrated the dewetting behavior of a polystyrene film by preparing a film thickness gradient versus a continuous temperature gradient arranged in a 2-D combinatorial library [12]. His group also investigated the phase separation of a thin film prepared of a polymer blend gradient in combination with a temperature gradient [13]. The film preparation of this polymer blend gradient was realized utilizing a custom built set-up. In addition to solution cast composition as well as layer thickness gradients, solvent-free prepared gradients utilizing physical vapor deposition (PVD) are well-known. Here combinatorial optimizations of electro-optical devices were investigated in a 2-D combinatorial library in regard to composition and layer thicknesses [14]. Another important parameter especially for adhesion investigations is the chemical surface treatment of a film, thus gradients of surface characteristics were developed. Such a surface modification was obtained via electron beam treatment of a poly(2-vinylpyridine) coated surface. This electron beam exposure dose gradient applied over a length of 5 cm generates a hydrophilicity gradient on the surface [15]. Matsuda et al. have shown another method for the preparation of a surface hydrophilization gradient with a poly(vinyl carbonate) coated film [16]. This film hydrolyzes gradually via a continuous immersion in an aqueous NaOH solution.

A special field of interest regarding thin films is lithography. In the process of lithographic patterning the resist film has to pass several steps e.g. film preparation, annealing steps, exposure, development, and etching. This multi-step process on the other hand gives a variety of variables which interact strongly with each other, such as resist composition, film thickness, annealing temperature, exposure dose, or development time to name a few. Not least the engineering and manufacturing of new patterning tools [17] and the introduction of new materials [18] leads to a perpetual optimization of the operating process [19]. Thus combinatorial investigations became an interesting approach for lithographic issues in the last decade. For instance, different compositions of a molecular glass photoresist were investigated in combinatorial PVD prepared libraries as a function of exposure dose [20]. Another important variable especially in the lithographic context but also in general for thin polymer films is the annealing (bake) time and temperature. Therefore degradation of poly(*tert*-butoxy-carbonyloxy-styrene) has been investigated with temperature and also bake time gradients [21]. Furthermore the applied bake steps to chemically amplified resist systems in the lithographic patterning process have to be precisely identified for the post exposure and post apply bake steps. Hence, for the optimization of resist performance both bake steps were

performed as temperature gradients in research laboratories and applied in a manner orthogonal to each other [22]. Recently we have identified a synergistic effect for post exposure bake and resist composition. Therefore the composition gradient was applied perpendicular to the temperature gradient of post exposure bake and combined with an exposure dose gradient as ternary gradient [23-25]. These different techniques of gradient preparation for thin film investigations demonstrate impressively the fast and effective variable investigation in one experiment. The presented article summarizes our improved and newly developed combinatorial techniques on thin film investigations, the preparation of binary and ternary combinatorial libraries, and their characterization.

## **2. Results and Discussion**

### *2.1. Combinatorial Techniques*

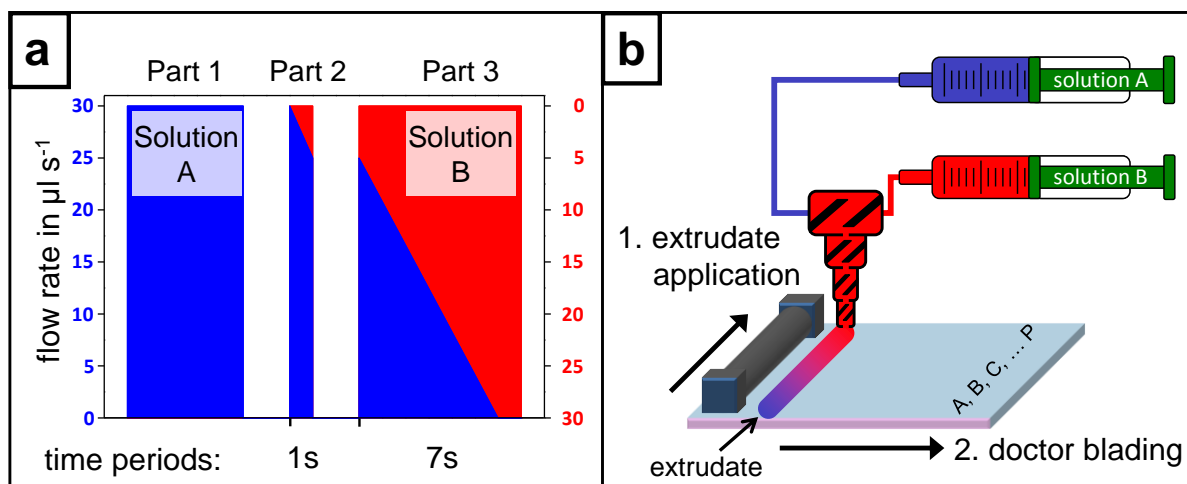
For a combinatorial investigation typically gradients of materials and/or process variables are applied. However for new combinatorial approaches the existing techniques have to be adapted, the setups modified or new techniques developed just to fit a particular set of requirements. In the following sections we show adapted and newly developed combinatorial techniques and the corresponding setups focused on combinatorial approaches for solution-processed thin films.

#### **2.1.1. Internal Material Composition Gradient**

For the preparation of a film including an internal composition gradient two individual controllable syringe pumps were used. The syringe pump system allows the preparation of a gradient extrudate made of solutions A & B, when equipped with two syringes. One syringe is filled with solution A and the other with solution B. The syringes are connected via PTFE tubes to the upper part of a static mixer. Both tubes were filled completely with the respective solutions. The static mixer was rinsed just with solution A to get the static mixer air bubble-free (see the flow rate profile in Figure 1a; part 1). Afterwards the syringe pump system was started for one second (see Figure 1a; part 2) to premix both solutions in the fixed volume of the static mixer. This step is necessary to extrude the rinsing solution A out of the mixing device and to fill it with the solution of the initial gradient extrudate. Subsequently the static mixer was fixed to the movable part of a doctor blade machine to enable the application of the gradient extrudate on a substrate.

**Figure 1a.** Schematic illustration of the flow rate profile controlled by the neMESYS syringe pump system: Part 1 serves as the rinsing step with solution A to get the static mixer air bubble-free; in part 2 the premix inside the static mixer is prepared; part 3 shows the opposite flow rate gradients of the two syringes while the actual extrusion takes place.

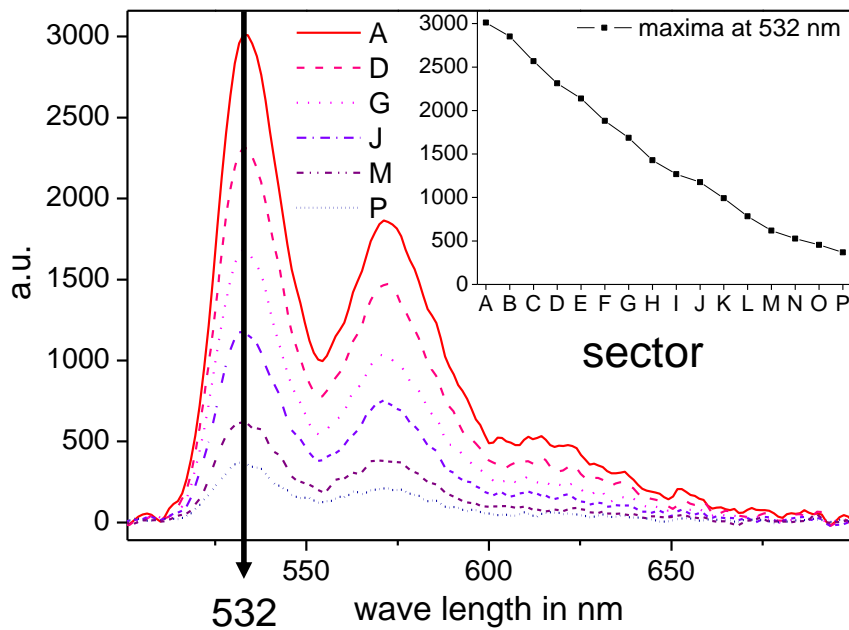
**Figure 1b.** The detailed preparation of a composition gradient film is schematically illustrated. The gradient extrudate of solution A (blue) and solution B (red) (step 1: extrudate application) was realized as described for Figure 1a, part 3. Subsequently the gradient extrudate was doctor bladed perpendicular to the application direction (step 2: doctor blading) and annealed to remove the solvent. For a systematical characterization the yielded film with the internal composition gradient was divided alongside the gradient into the sectors A-P.



The efficiency of this preparation method in view to the constant change of the resulting internal composition gradient film is demonstrated realizing a PMMA film with a gradient of a fluorescence dye. This gradient film was prepared applying two 10 wt.% solutions of PMMA in THF, while in solution A the fluorescent dye *N,N'*-Di(1-heptyloctyl)-perylene-3,4,9,10-bis(dicarboximide) (to exclude concentration quenching: 0.02 mmol in 1 g of solution) was dissolved. The fluorescent dye gradient film was characterized by fluorescence spectroscopy utilizing a fluorescence reader. The acquired fluorescence spectra excited at a wavelength of 455 nm show three maxima at 532 nm, 572 nm and 620 nm (see Figure 2). The observed continuous intensity decrease of the complete spectra demonstrates the prepared internal dye gradient. The intensities of the maximum at 532 nm of all 16 measured spectra of sector A to P along the composition gradient are summarized in the inset verifying the continuous decrease of the fluorescence dye concentration. In conclusion this technique offers a simple and efficient way to make a solvent-based gradient extrudate which withstands

doctor blading as well as an ongoing thermal treatment to realize a solid film with an internal composition gradient over a broad concentration range.

**Figure 2.** The characterization of the fluorescent dye gradient in PMMA via fluorescence spectroscopy: 16 fluorescence spectra (sector A – P) along the application direction with an equal gap were measured (only six spectra are shown over the full measured wave length range for a better overview). The inset of the graph shows the intensities of the maximum at 532 nm of the spectra of all 16 sectors and verifies distinctly the continuous decrease of the fluorescence intensity given by the material gradient.



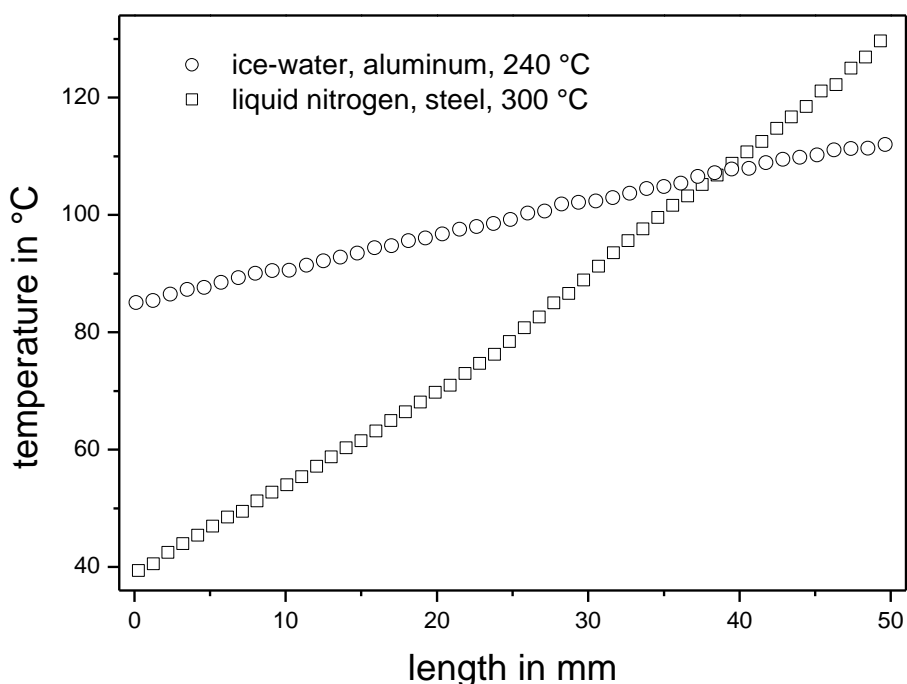
### 2.1.2. Temperature Gradient

Various well defined and long-term stable temperature gradients were engineered in our laboratory on the basis of plates of different metals. On one side of the plate a vessel was welded and filled with, for example, ice-water or liquid nitrogen and represents the cooling source. Here it has to be considered that the vessel must be refilled continuously to ensure constant cooling. The other side was placed planar on a hot plate, serving as an active heating source, and was adjusted to a desired temperature. After a calibration time of one hour the temperature gradient stayed constant and was verified by an infrared camera. For this a reference silicon wafer used for measuring purposes was placed in the center of the setup's metal plate.

In Figure 3 two temperature gradients with different slopes are shown over a length of 50 mm measured using a reference silicon wafer. The gradients demonstrate the ability to

adjust the temperature gradients by defining appropriate conditions: for the more flat temperature gradient (circles) ice-water was used for the active cooling, an aluminum plate served as thermoconductive metal plate and for constant heating the hot plate was adjusted to 240 °C. A steeper gradient (squares) was generated with liquid nitrogen as cooling source, a steel plate and the hot plate adjusted to 300 °C.

**Figure 3.** Two temperature profiles – measured using the reference silicon wafer – are shown utilizing different metal plates prepared over the length of 50 mm. The first temperature gradient (circles) was made on an aluminum plate applying for the left side cooling ice-water and heating on the right side at the temperature of 240 °C. The achieved temperature gradient shows a steady slope of 0.55 °C/mm from 85 °C to 112 °C. The second (squares) was prepared under the conditions liquid nitrogen, steel plate and 300 °C. It shows an overall slope of 1.85 °C/mm from 39 °C to 130 °C.



The flatter temperature gradient (circles) resulted in a steady slope of 0.55 °C/mm from 85 °C to 112 °C. The second temperature gradient (squares) shows a very steep slope of 1.85 °C/mm from 39 °C to 130 °C. Further variations in hot plate temperature, plate material or cooling source allow well-defined temperature slopes in a broad temperature range. The results and customizability demonstrate impressively the applicability of this simple temperature gradient set-up and thus offer a versatile utility for annealing processes e.g. investigations on morphology or thermal crosslinking of polymer films.

### 2.1.3. Exposure Dose Gradient

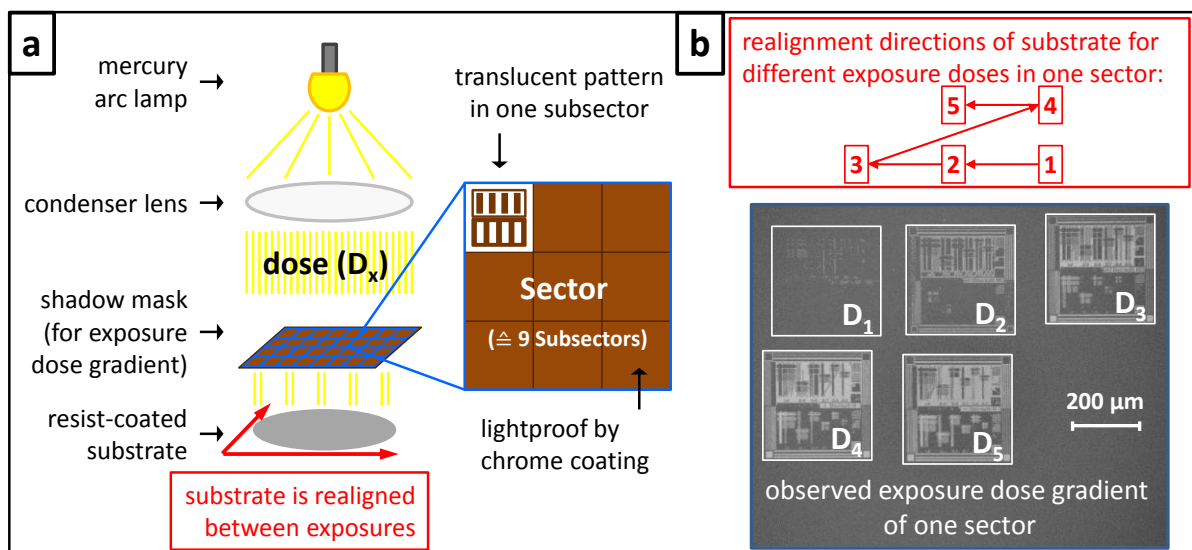
The exposure procedure can be the most time-consuming step in manufacturing processes including a light-induced reaction. Combinatorial investigations are an appropriate approach to identify the optimized exposure conditions to save time and to achieve optimal results. Thus combinatorial exposure optimization methods can be used in a versatile manner and implemented easily in exposure investigations of solid films. Exposure dose gradients are conceivable for photocycloaddition, orientation of chromophores and photopolymerization driven by photo exposure and also evaporation-condensation and polymer degradation investigations caused by electron beam exposure.

An exposure dose gradient for UV exposure was realized for this work with a mask-alignment system and a specially designed quartz glass mask. Figure 4a shows a schematic illustration of such an exposure set-up with a mercury lamp as light source and a condenser lens to generate parallel light thus a film coated substrate is exposed consistently with a dose (**D**) through the shadow mask. This mask consists of 70 x 70 sectors arranged and numbered in an X/Y coordinate system. Each sector has a size of 1.2 mm x 1.2 mm. It is designed with eight out of nine subsectors with a lightproof chrome coating (brown) and one out of nine subsectors of a translucent pattern (white/brown) with an area of 300  $\mu\text{m}$  x 300  $\mu\text{m}$  for each subsector. The mask-alignment system has an alignment stage with micrometer adjustment for the substrate holder. This allows an accurate alignment for subsequent exposures of subsectors in one sector on the same substrate. Therefore the substrate is moved by 400  $\mu\text{m}$  for realignment between two exposures obtaining two subsectors; by this the substrate is moved 100  $\mu\text{m}$  further than the edge length of the translucent pattern which avoids areas of inadvertent double exposure. For the verification of the UV-exposure gradient a positive tone resist was used. The procedure for a dose-gradient exposure was conducted as follows: the film-coated substrate was adjusted to the substrate holder in the mask-alignment system and the exposure of the first subsectors in all sectors was conducted. Subsequently the substrate is realigned by movement of the substrate holder of 400  $\mu\text{m}$  to the left defining the position for the second subsectors' exposure and again 400  $\mu\text{m}$  to the left for the third exposure (see Figure 4b). For the fourth exposure the substrate holder is realigned to the origin (800  $\mu\text{m}$  to the right) and then 400  $\mu\text{m}$  up and for the fifth exposure 400  $\mu\text{m}$  to the left. The dose was increased for every exposure step from 80  $\text{mJ}/\text{cm}^2$  to 160  $\text{mJ}/\text{cm}^2$  and as a result a dose gradient of five different doses on an area of 1.44  $\text{mm}^2$  was created. Subsequently the film-

coated substrate was thermally treated at 105 °C for 30 s for post exposure bake. Afterwards the film is developed in an aqueous 0.26 N tetramethylammonium hydroxide (TMAH) solution for 30 s resulting in the removal of the exposed resist if the dose was sufficiently high. In Figure 4b (SEM image) the exposure dose gradient of a selected sector is shown: Pattern ( $D_1$ ) exposed with the lowest dose is obviously underexposed as the contours of the pattern are just slightly visible and the resist (dark grey) is roughly developed. Increasing the dose results in more clear developed patterns indicated by the stronger contrast (dark - bright) in the corresponding subsectors given by the undeveloped unexposed resist material beside the substrate surface (light grey). At the highest dose ( $D_5$ ) the pattern is overexposed, which is obvious by the beginning of features' stripping off.

**Figure 4a.** The schematic illustration shows a mask-alignment system consisting of the main components: a mercury arc lamp as light source, a condenser lens for the production of parallel light to exposure consistently a film-coated substrate through the shadow mask. One sector of overall 4900 sectors is shown in the schematic magnification of the shadow mask, which are arranged and numbered in an X/Y coordinate system. Each sector consists of eight out of nine subsectors with lightproof chrome coating (brown) and one out of nine subsectors of a translucent pattern (white/brown). The substrate holder is adjustable via micrometer adjustment to allow a precise alignment for subsequent exposures.

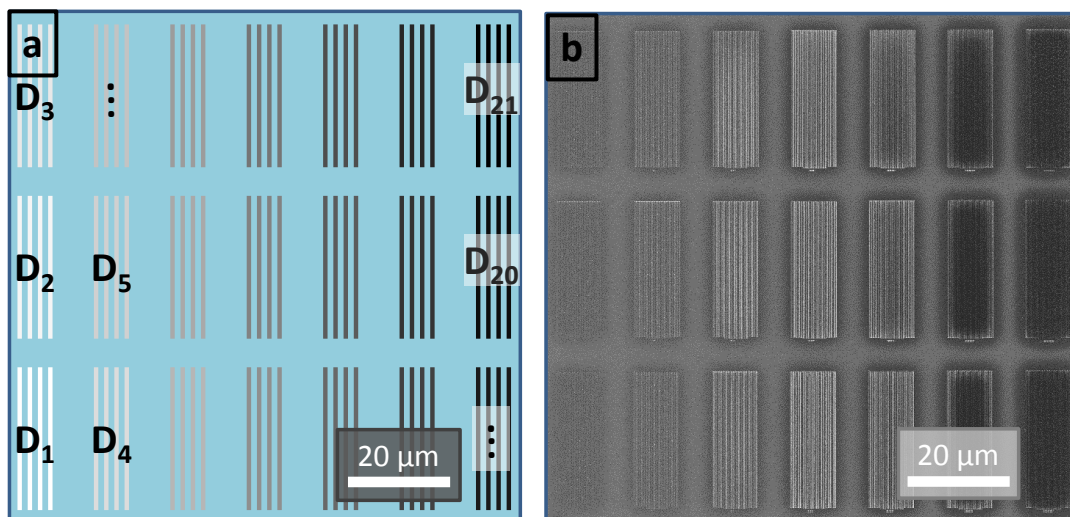
**Figure 4b.** Schematic illustration of the realignment directions of the substrate between different exposures: The SEM image shows a selected sector with an exposure dose gradient of five subsectors realized with a positive tone resist (dark grey). The dose was increased from  $D_1$  to  $D_5$  leading from an under- to an overexposure of the resist shown by the increasing proportion of the bright appearing substrate surface (light grey).



For electron beam exposure a different approach is necessary for realizing an exposure dose gradient. The resist film coated on a substrate is not exposed through a mask in one exposure step, but it is continuously exposed by a controllable electron beam. For this so-called direct write technique the patterns are arranged in write-fields. In Figure 5a an example of a write-field of  $100\ \mu\text{m} \times 100\ \mu\text{m}$  in size is shown, which contains 21 arrays of a  $100\ \text{nm}$  line/space pattern. Each array is written by a defined programmable exposure dose. When beginning with the lowest dose for the first array ( $D_1$ ) and continuing with increasing doses realized by the multiplication with a selected constant, an exposure dose gradient is generated.

**Figure 5a.** The schematic illustration shows a write-field with an area of  $100\ \mu\text{m} \times 100\ \mu\text{m}$  used for electron beam lithography. The write-field consists of 21 arrays of a  $100\ \text{nm}$  line/space pattern with an increasing dose from bottom left ( $D_1$ ) to the upper right ( $D_{21}$ ) indicated by the greyscale gradient.

**Figure 5b.** The SEM image shows the dose gradient of line/space patterns of a developed negative tone resist of a complete write-field.  $D_1$  is underexposed and just shadowy observable on the substrate. The patterns get more visible because of the increasing dose: in the center the pattern are exposed to their optimum dose while at higher doses the patterns get overexposed and even besides the pattern some resist material remains, observable by the darker arrays at these high doses.



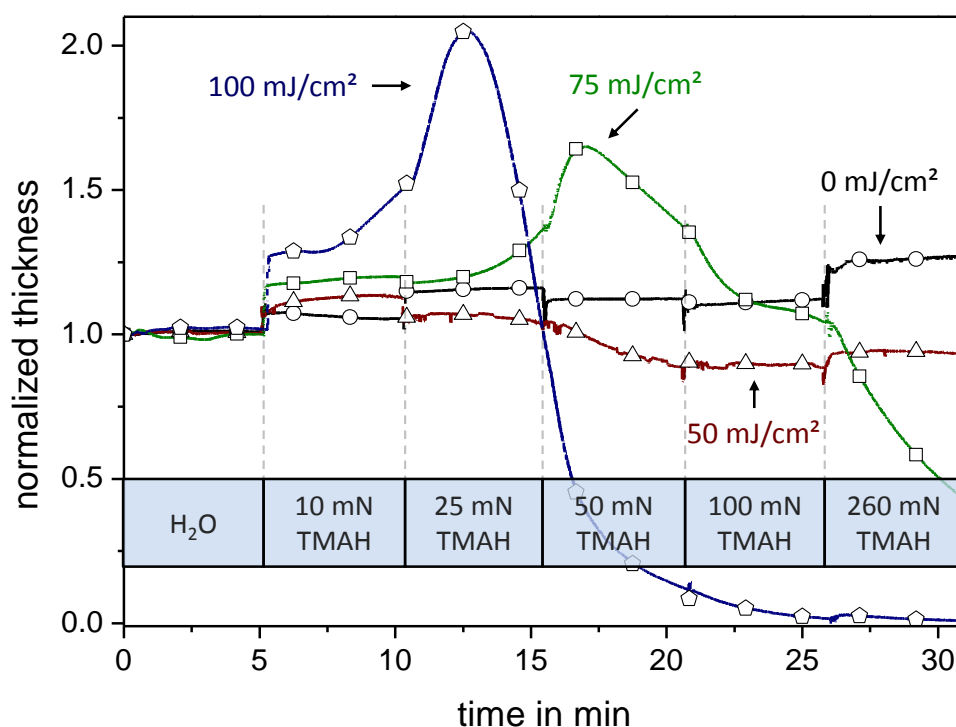
In Figure 5b the SEM image shows a selected section of the resulting exposure dose gradient of a film prepared out of a negative tone resist: The pattern corresponding to the lowest dose ( $D_1$ ) in the bottom left is only shadowy observable and is clearly underexposed. Increasing the dose effects in more distinct patterns and the optimum dose range is observed in the center. A further dose increase results in overexposed patterns (right) indicated by residues surrounding the actual patterns and observable by the darker arrays.

Exposure dose gradients for deep UV and electron beam exposure realized by the combinatorial approaches described above are not limited to the lithographic investigations shown but are also suitable for process optimization of exposure processes.

#### 2.1.4. Dissolution Investigation

The dissolution behavior of organic film systems in distinct organic solvents or aqueous media is for many scientific investigations and technical applications of fundamental and essential interest. Thus we investigated a screening method to measure the impact of solvents or solutions to the film material in view to time resolved swelling and dissolution behavior by quartz crystal microbalances (QCMs). In addition, the influence of mixing ratio or additive concentration of investigated solvents is possible. Here we demonstrate the efficiency of this method in view of the dissolution behavior of a polymer resist film by increasing stepwise the base strength of an aqueous tetramethylammonium hydroxide (TMAH) solution. Therefore films on quartz crystals (QCs) were prepared out of a positive tone resist and a photoacid generator (PAG). Selected QCs were exposed to UV-light to activate the PAG, followed by a PEB step to catalyze the deprotection reaction. Thus, depending on exposure time and consequently the amount of activated PAG, the resist becomes hydrophilic. These selectively exposed QCs were clamped one by one into the QC holder and immersed into water during dissolution measurement. After defined time periods a stepwise increase of the TMAH concentration was achieved from 10 to 25, 50, 100, and 260 mN by adding corresponding amounts of a concentrated TMAH solution (see Figure 6).

**Figure 6.** Quartz crystal microbalance (QCM) measurements of four resist films exposed to different UV exposure doses are shown. The graphs show the corresponding QCM frequencies change – translated to normalized film thickness change [26] – during the periodic titration of a concentrated developer solution observable due to the transient oscillation. The unexposed hydrophobic resist film ( $\circ$ ) stays at a nearly constant film thickness while slight swelling and dissolving of reacted resist material is observable for the resist film exposed to  $50 \text{ mJ/cm}^2$  ( $\triangle$ ). The resist film exposed to  $75 \text{ mJ/cm}^2$  ( $\square$ ) shows a more distinct swelling character. The swelling slightly begins at the first titration and increases markedly until the concentration of  $50 \text{ mN}$  where the dissolving character exceeds. This behavior of swelling and dissolving is also observed for the resist exposed to  $100 \text{ mJ/cm}^2$  ( $\diamond$ ) but the dissolution shifts to a lower concentration of  $25 \text{ mN}$ . The exposed resist film is fully developed at a concentration of  $100 \text{ mN}$  TMAH.



All resist films show no swelling or dissolving character in pure water at the beginning of the measurement. At the first titration a sudden increase of film thickness for all resist films is observable explainable by the deprotonating of the acrylic acid units. Here, the yielded carboxylate anions result in repulsion and in an ambient hydration which dampens the oscillation frequency of the quartz crystal. In addition, this measurement method is so sensitive that the distinct density increase is detected by a general oscillation frequency damp at the last titration step from  $100 \text{ mN}$  to  $260 \text{ mN}$ . The unexposed film ( $0 \text{ mJ/cm}^2$ ) retains a constant film thickness over the complete titration process. Here all titration steps can be

easily identified by the frequency jumps. However the lowest exposed resist film ( $50 \text{ mJ/cm}^2$ ) shows a slight swelling character at the first titration step as well as a slow dissolution occurs at a concentration of 50 mN. The resist film exposed to  $75 \text{ mJ/cm}^2$  shows a more distinct swelling character at the first titration step and shows a swelling maximum at the TMAH concentration of 50 mN followed by the dissolution of the resist material observable by the increasing oscillation frequency. The most exposed resist film ( $100 \text{ mJ/cm}^2$ ) shows a high swelling character already at the first titration step and reaches the maximum at a concentration of 25 mN TMAH. The following fast dissolution of the resist film ends in a fully developed quartz crystal at the concentration of 100 mN TMAH.

The results of the QCM prescreening experiments specify the processing window of the dissolution behavior of investigated materials. Typically the materials' dissolution is influenced by the nature of the solvent as well as the application period. In this context a simple way to study dissolution behavior is an immersion process, which allows also the preparation of gradients controlled by the immersion period. Two options are conceivable to realize an immersion time gradient: stepwise or continuous:

For the stepwise immersion time gradient it is useful to section the substrate into a defined number of segments via marks at the edge of the substrate. The substrate is clamped into an inverse pair of tweezers adjusted above a filled vessel in which it shall be immersed. The substrate can be immersed then into the solution beginning at the lowest segment. In consequence the lowest segment gets the longest immersion time period in contrast to the top segment which gets the shortest one. After the solution treatment the substrate is removed from the vessel all at once. Dependent on the application of this immersion gradient the film on the substrate must be dried, immersed into another solution or the film must be rinsed with an inert solvent.

A continuous immersion gradient was realized with an electrical motor drive which has ten adjustable speeds from  $25 \text{ }\mu\text{m/s}$  to  $25 \text{ mm/s}$ . A wire was attached to the drive roller of the motor drive and connected with the further end to an inverse tweezers which again clamps the substrate. The drive roller was positioned directly above the filled vessel the attached substrate has to be immersed into. Then the substrate was lowered into the vessel at a defined speed. The time intervals of the solution treatment for each position on the substrate are calculated by the length of the immersed substrate and the preset speed of the electrical motor

drive. After complete immersion, the substrate was removed from the solution all at once and treated as described above.

### 2.2. *Combinatorial Libraries*

Synthesis and/or investigation of applicability of new materials are often time-consuming and take a lot of effort. Thus it is a common approach to use combinatorial techniques as a fast way for getting materials and their processing variables optimized. However, the full potential of a new material – be it the synthesis or the properties – is typically affected by the interaction of multi-variables. So the possibility of material optimization of just one variable will result only in a local optimum. To avoid this fact, a combinatorial investigation of at least two interacting variables should be conducted in one investigation, a so-called combinatorial library.

#### 2.2.1. Binary Combinatorial Library

In the following we show an example for the combination of two gradients in one combinatorial library. Therefore a film with an internal composition gradient is applied on a substrate and annealed with a temperature gradient perpendicular to it. These two variables are crucial for lithographic systems, especially as process variables for chemically amplified resists. For the here presented experiment a literature known resist system [27] was used consisting of  $\alpha,\alpha,\alpha'$ -tris(4-hydroxyphenyl)-1-ethyl-4-isopropylbenzene (as matrix component), N,N,N,N-tetra-(methoxymethyl)glycoluril (as crosslinker component), and triphenylsulfonium perfluor-1-butanesulfonate (as photoacid generator; PAG). On this known three component resist system the efficiency of a well-designed combinatorial library is shown.

For the film preparation a silicon wafer of four inch diameter served as substrate. The resist film consisted of an internal composition gradient of matrix component versus crosslinker component with an overall constant concentration of PAG as well as an overall constant film thickness. This film was applied out of solution A (9.5 wt.% of the matrix component + 0.5 wt.% of PAG in 1-methoxy-2-acetoxypropane) and solution B (9.5 wt.% of the crosslinker component + 0.5 wt.% of PAG in 1-methoxy-2-acetoxypropane). The resist material gradient was prepared as described in chapter 2.1.1 followed by a subsequent thermal prebake step of 115 °C for 60 s. For analyzing the material composition of the resulting gradient, high performance liquid chromatography (HPLC) was used. Beforehand the three components were calibrated to determine weight ratios of component mixtures. From the

prepared composition gradient on the silicon substrate a defined stripe was cut off with a length of 70 mm and a width of 10 mm parallel to the application direction. The stripe was divided into 14 pieces (A-N) with a length of 5 mm and each was rinsed off with acetonitrile separately for the HPLC analysis. The measured ratios of the three components are shown graphically in Figure 7 and detailed values listed in Table 1.

The composition gradient received by gradient extrusion and subsequent doctor blading was realized over a broad concentration range with a nearly constant film thickness of 350 nm: the PAG concentration stays nearly constant at 5 - 6 wt.% over the whole length of 70 mm. The matrix content is continuously decreasing from 88.6 wt.% to 18.2 wt.% while the crosslinker content is steadily increasing from 6.4 wt.% to 75.9 wt.%. The gradient covers a huge range of resist component ratios and thus presents a good starting point for a combinatorial investigation of a multicomponent material system.

**Figure 7.** The graph shows the resist material ratios of the 14 wafer pieces of the three components resist gradient film analyzed by high performance liquid chromatography. In the achieved material composition gradient the photo acid generator content (○) stays constant in the desired range of five to six weight percent. The matrix content (□) is constantly decreasing from 88.6 wt.% to 18.2 wt.% while the crosslinker content (△) is steadily increasing from 6.4 wt.% to 75.9 wt.%.

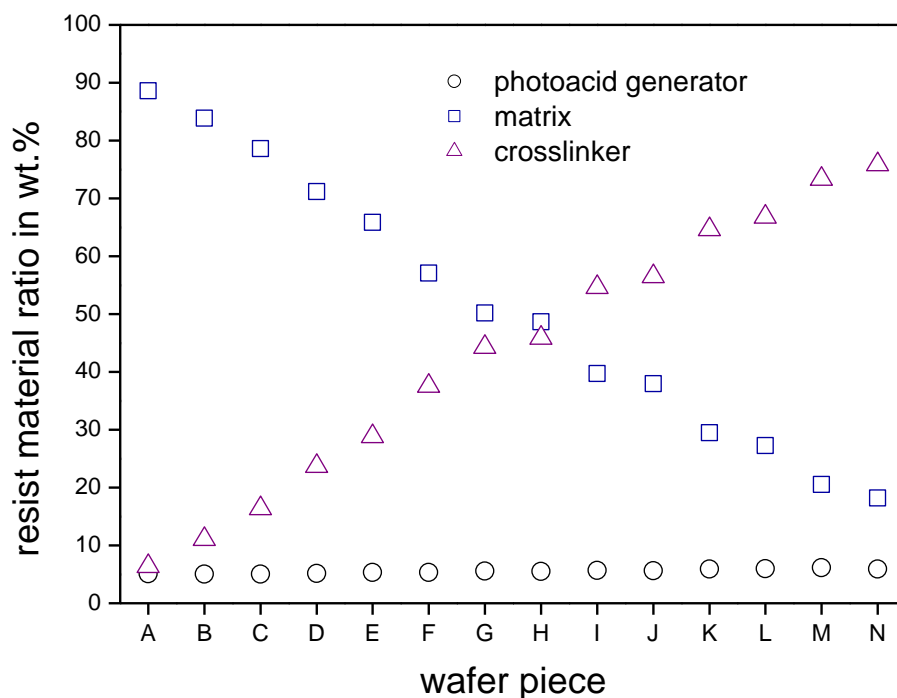
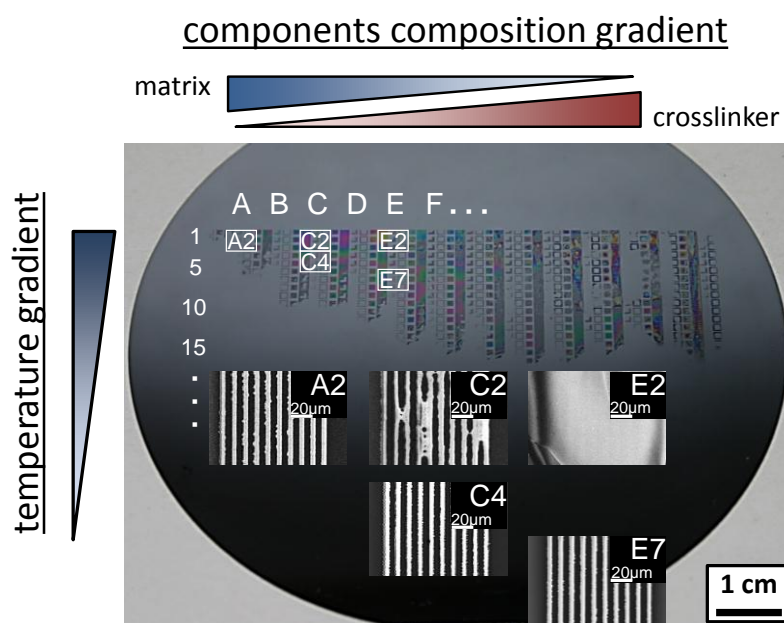


**Table 1.** Material composition ratios of each wafer piece of the three components resist gradient film analyzed by high performance liquid chromatography.

wafer piece	A	B	C	D	E	F	G	H	I	J	K	L	M	N
wafer segment in mm	0-5	5-10	10-15	15-20	20-25	25-30	30-35	35-40	40-45	45-50	50-55	55-60	60-65	65-70
PAG in wt.%	5.0	5.0	5.1	5.1	5.3	5.3	5.5	5.5	5.7	5.6	5.9	5.9	6.2	5.9
matrix in wt.%	88.6	83.9	78.6	71.2	65.9	57.1	50.2	48.7	39.7	37.9	29.5	27.3	20.5	18.2
crosslinker in wt.%	6.4	11.1	16.3	23.7	28.8	37.6	44.3	45.8	54.6	56.5	64.6	66.8	73.3	75.9

The next step in the lithographic process is the exposure, which activates the PAG. This step was conducted with the EVG<sup>®</sup>620 mask-aligner utilizing a shadow mask with a line/space pattern. The dose was adjusted to 60 mJ/cm<sup>2</sup>. Immediately afterwards a PEB was applied to perform the acid catalyzed crosslinking reaction between crosslinker and matrix. For the preparation of a combinatorial library a temperature gradient for PEB was applied perpendicular to the material composition gradient for 30 s. The applied temperature gradient had a constant slope of 1.07 °C/mm within the temperature interval from 85 °C to 20 °C. Subsequently the resist film was developed in a 0.26 N aqueous solution of TMAH for 10 s by dissolving the resist materials of the unexposed areas. In Figure 8 a photograph of the processed film with the remaining patterned resist material and SEM images of the pattern of selected sectors of the combinatorial library are shown.

**Figure 8.** Photograph of the patterned resist film on the silicon wafer after applying the material composition gradient (left to right: column **A** to **N**), post apply bake of 115 °C for 60 s, photo exposure (60 mJ/cm<sup>2</sup>), PEB temperature gradient (top to bottom: row **1** to **40**) and development in a 0.26 N aqueous solution of tetramethylammonium hydroxide for 10 s. Already with the naked eye can be seen that below row **15** (60 °C) all patterns are completely stripped off. The dependence of temperature to material composition is obvious by the SEM insets of column **E**: sector **E7** shows distinct pattern while in sector **E2** all lines are merged. Under the conditions of a steady temperature (row **2**) distinct pattern are obvious at high matrix content (sector **A2**) while with increasing crosslinker content the patterns tend to merge (**C2/E2**). A trend is observable as for higher crosslinker content lower PEB temperatures are needed for distinct patterns (**A2**, **C4**, **E7**).



The composition gradient ranges from a high matrix content (left: column **A**) to a high crosslinker content (right: column **N**) arranged perpendicular to the temperature gradient from a high (top: row **1**) to a low temperature (bottom: row **40**). It can be seen with the naked eye that below row **15** (60 °C) even the exposed resist of each material composition is completely stripped off the substrate during development. This indicates a minimum temperature is necessary to crosslink this resist system at any material composition. Most of patterns right of column **F** (matrix  $\leq 57.1$  wt.% / crosslinker  $\geq 37.6$  wt.% / PAG 5 wt.%) corresponding to high crosslinker contents are stripped off, too. The inset SEM images show clearly the PEB temperature dependence to the resist material composition (column **E**): While sector **E7** (72 °C) shows distinct lines, in sector **E2** (83 °C) the lines of the pattern are merged together.

This is due to the fact that the higher applied temperature results in an increased acid diffusion to this material composition beyond the exposed areas. With a higher matrix component (row **2**) the pattern quality increases from sector **E2** to **C2** until in sector **A2** distinct patterns were observed. These observations reveal a tendency which is confirmed by sector **C4**: Distinct patterns were achieved with decreasing matrix content and concurrent temperature decreases beginning with sector **A2** over sector **C4** and ending with sector **E7**. These results show impressively the strength of combinatorial libraries in recognizing variable dependent trends of interacting multi-variable system and so combinatorial approaches are an excellent technique for optimizing material composition and their processing conditions.

### 2.2.2. Ternary Combinatorial Library

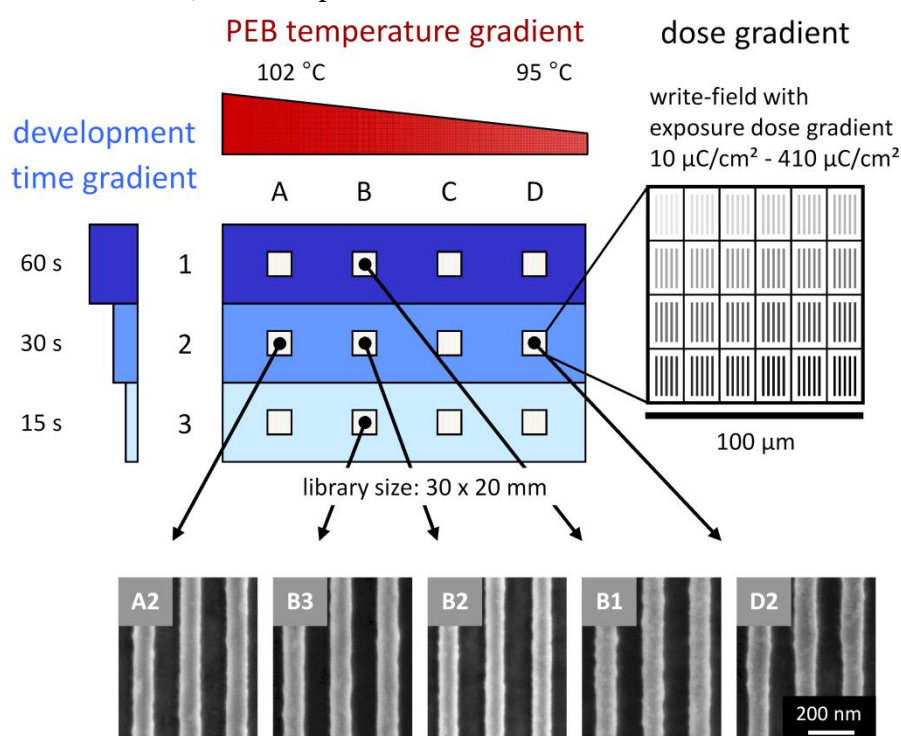
The upgrade of a binary combinatorial library by a third gradient is called ternary combinatorial library. For the preparation of a binary combinatorial library variable gradients are typically arranged orthogonally on two-dimensional areas. Thus for the realization of a ternary library it is required that the third variable gradient is implemented in the third dimension or arranged in a very small area in which the first as well as the second variable are effectively constant within the gradient. To implement the latter case the third variable is applied several times – matrix-like – in one small spot on the binary library. As described above the exposure dose gradients have the ability to fulfill these requirements and hence it is possible to investigate three interacting variables in just one combinatorial library.

In the following we present the developed ternary library for a lithographic investigation as shown schematically in Figure 9.

The ternary library consists of a temperature gradient perpendicular to a development time gradient, which represents the variable gradients of the binary library, while small sectors of electron beam exposure dose gradients are applied matrix-like to this binary combinatorial library. For the shown lithographic combinatorial investigation a star-shaped teroligomer [statistical copolymerized out of  $\alpha$ -gamma butyrolactone methacrylate, methyl adamantyl methacrylate, and hydroxyl adamantyl methacrylate (GBLMA-co-MAMA-co-HAMA)] as positive tone resist plus the PAG triphenylsulfonium perfluoro-1-butanesulfonate was used. The resist material solution was cast via spin coating on a hexamethyldisilazane-primed four inch silicon wafer, resulting in a film thickness of about 90 nm. The film-coated substrate was cut to a rectangle of 30 mm x 20 mm, thermally treated at 125 °C for 150 s, and electron beam exposed by a dose gradient which was conducted in 12 write-fields, applied

matrix-like (see Figure 9). This matrix consists of three rows and four columns while the gap between each row is 10 mm and between each column 5 mm. Each write-field – 100  $\mu\text{m}$  x 100  $\mu\text{m}$  in size – comprises an exposure dose gradient of 24 arrays of 100 nm line/space pattern between 10  $\mu\text{C}/\text{cm}^2$  to 410  $\mu\text{C}/\text{cm}^2$ . Afterwards PEB was applied – parallel to the rows of the exposed matrix – by a temperature gradient for 30 s. This temperature gradient was prepared on an aluminum plate with ice-water as cooling source and a hot plate adjusted to 220  $^{\circ}\text{C}$  as heating source. Thus the temperature gradient applied to the substrate ranged from 95  $^{\circ}\text{C}$  to 102  $^{\circ}\text{C}$  with a slope of 0.47  $^{\circ}\text{C}/\text{mm}$ . After that a development time step gradient was applied alongside the columns of the exposed matrix for 15, 30, 60 s in a 0.26 N tetramethylammonium hydroxide solution. Therefore the substrate was subdivided into three segments whereas each segment contains one row of write-fields. Selected SEM images of line/space patterns and their corresponding processing conditions are shown in Figure 9. Furthermore line edge roughness (LER) values – used as performance criterion – of these selected line/space patterns are also listed. LER is a mathematical calculated value, describing the deviation of pattern edges to an ideal shaped pattern. The LER values of the line/space patterns were calculated over a length of 15  $\mu\text{m}$  by the software SuMMIT<sup>TM</sup> from EUV technology.

**Figure 9.** Schematic illustration of the ternary combinatorial library prepared on a substrate with a size of 30 mm x 20 mm. The PEB temperature gradient (95 °C – 102 °C) is arranged horizontal and perpendicular to it the development time step gradient (15 s, 30 s, 60 s). The 12 write-fields (100µm x 100µm) with the exposure dose gradient (10 µC/cm<sup>2</sup> – 410 µC/cm<sup>2</sup>) are arranged matrix-like in small sectors and provide 24 arrays of 100 nm line/space profiles. The selected SEM images demonstrate the strong influence of the applied three variable gradients. The respective conditions (PEB temperature, development time, and dose plus the LER values) of these patterns are listed below.



dose in µC/cm <sup>2</sup>	182.3	251.6	214.2	155.1	251.6
PEB temperature in °C	102	100	100	100	95
development time in s	30	15	30	60	30
LER (3σ) in nm	6.8	5.8	5.3	7.0	7.6

One interesting observation from the ternary combinatorial library is that for each write-field only one exposure dose fits optimized to the other applied parameter PEB and development and thus only one pattern could be evaluated per sector. For the applied neighboring lower dose in a write-field, much thinner lines than 100 nm or even undeveloped

patterns are observed. This is due to an insufficient deprotection ratio and thus the poor development of the resist in the exposed areas. Consequently the neighboring higher dose resulted in too much removal of resist material so even whole areas are stripped off which indicates to high deprotection occurred. The pattern with the clearest lines (**B2**) was observed at a dose of 214.2  $\mu\text{C}/\text{cm}^2$ , a PEB temperature of 100 °C, and a development time of 30 s resulting in a LER value of 5.3 nm. The patterns prepared at a PEB temperature higher and lower than the observed optimum temperature of 100 °C but with the same development time show clearly increased LER values of 6.8 nm (**A2**) and 7.6 nm (**D2**). Noticeable is the decreasing dose required to achieve pattern for a higher applied PEB temperature (**A2**) at the same development conditions. Less PAG was activated due to a lower dose, but this is compensated by the increased acid diffusion and reaction rate at higher temperatures and vice versa for **D2**. The increase of LER values are also observable for patterns annealed at the same PEB temperature but applied to longer and shorter development times than the observed optimum of 30 s with the LER of 5.3 nm in sector **B2** (**B1**: 60 s, LER 7.0 nm, **B3**: 15 s, LER 5.8 nm). Here the operation with the optimized exposure dose is distinctive and crucial. While the exposure dose for the longest development time **B1** is about 25 % lower than the dose of the optimum **B2**, the dose for the shortest development time **B3** is about 20 % higher than the dose of the optimum pattern in **B2**. This combinatorial investigation demonstrates the strong interdependence and interaction of resist processing variables and shows the high efficiency of a ternary combinatorial library for such a complex investigation of a multi-variable system.

### 3. Experimental Section

#### 3.1. Chemicals and Materials

Unless otherwise stated, all solvents and chemicals were purchased from Sigma-Aldrich and used as received. N,N'-Di(1-heptyloctyl)-perylene-3,4,9,10-bis(dicarboximide) was kindly provided by Dr. André Wicklein, MC I, University of Bayreuth. Poly (methyl methacrylate) ( $M_w = 123.4 \text{ kg/mol}$ ) was purchased from Degussa. 1,1,1-tris(4-hydroxyphenyl)-1-ethyl-4-isopropylbenzene was purchased from ABCR. N,N',N'',N'''-tetra(methoxymethyl)glycoluril was purchased from Worlée-Chemie.

#### 3.2. Internal Material Composition Gradient

The gradient extrudate was prepared using the syringe pump system neMESYS (cetoni GmbH) containing two individual controllable syringe pumps which were connected via

PTFE tubes to a static mixer (Adchem GmbH; MA 3.0-13-S: shortened to a length of 15 mm). The syringe pump system was programmed to start solution A with a flow rate of 30  $\mu\text{l/s}$  but decreasing constantly with time, while solution B starts with a flow rate of 0  $\mu\text{l/s}$  but increasing constantly with time. For the actual extrusion of the homogeneous mixed gradient the flow rates of each syringe pump are tuned regarding a summarized steady flow rate of 30  $\mu\text{l/s}$ , thus a constant variation of the solutions A & B is given for a time period of seven seconds (see Figure 1a; part 3). Simultaneously the doctor blade machine to which the static mixer is fixed has to be activated with a velocity of 10 mm/s for the same time period. Both simultaneously running procedures are described in Figure 1b step 1: extrudate application. The second step takes place after the substrate's rotation through 90 degrees. The extrudate is then doctor bladed with a doctor blade machine (Erichsen Coatmaster 509 MC-1) using a 4-sided bar (BYK: gap: 50, 100, 150, 200  $\mu\text{m}$ ) perpendicular to its application direction with a velocity of 10 mm/s using a doctor blade of corresponding size (see Figure 1b step 2: doctor blading). Afterwards the film was baked to evaporate the application solvent and to fix the composition gradient. The yielded film with the internal composition gradient was divided alongside the gradient into the sectors A to P for a systematical characterization.

The PMMA film with the internal gradient of the fluorescent dye was verified by Fluorescence Reader Flashscan 530 (AnalytikJena AG). The measurement was executed at spots every 5 mm parallel to the gradient. The resist film with the internal composition gradient was verified with high performance liquid chromatography (HPLC) (Agilent 1100 series HPLC, column: ZORBAX Bonus-RP 4.6 x 150 mm, 5  $\mu\text{m}$ ; 1 ml/min of 80 % ACN / 20 % H<sub>2</sub>O; 201 nm / 278 nm).

### 3.3. Temperature Gradient

The temperature gradients were adjusted on metal plates with a length of 35 cm, a width of 20 cm, and a thickness of 0.5 cm. On one side of the plate a vessel was welded with a length of 10 cm, a width of 20 cm, and a height of 10 cm serving as reservoir of the cooling agent. This cooled side of the metal plate was placed on cork for insulation. The other side of the plate was placed planar on a hot plate (Präzitherm PZ 28-2T; Harry Gestigkeit GmbH) with a defined contact area of 6 cm x 20 cm. A reference silicon wafer – 525  $\mu\text{m}$  thickness, polished front side, n-type, highly arsenic doped with a resistance of < 0.01  $\Omega\text{cm}$ , which exhibits less infrared transparency – was placed on the plate after a calibration time of one hour. This wafer was monitored with an infrared camera (ThermaCAM<sup>TM</sup>E300; FLIR

systems), which was adjusted 30 cm directly above the wafer. Before utilizing the infrared camera, the extinction coefficient of the silicon wafer was calibrated with the help of the melting points of stearic acid (69 °C), benzyl (1,2-diphenylethane-1,2-dione) (95 °C) and benzoic acid (122 °C) [28].

### 3.4. Exposure Dose Gradient

The UV-exposure dose gradient using a mask-alignment system (EVG<sup>®</sup> 620; EV Group) and specially designed five inch quartz glass mask (produced by ML&C). For the verification of this UV-exposure gradient a resist film was prepared out of a positive tone star-shaped teroligomer [statistical copolymerized out of  $\alpha$ -gamma butyrolactone methacrylate, methyl adamantyl methacrylate, and hydroxyl adamantyl methacrylate (GBLMA-co-MAMA-co-HAMA)] (95wt.%) and the photoacid generator triphenylsulfonium perfluoro-1-butanefulfonate (5wt.%) and was applied from a 2.5 wt.% solution in 1-methoxy-2-acetoxyp propane on a silicon wafer. After spin coating the resulting film was pre-baked and had a thickness of 90 nm measured by a surface profilometer (Dektak 3030 ST; Veeco). The wavelength range of the mask-alignment system was adapted to 240 nm to 290 nm for the used resist system.

The electron beam exposure was performed using a Zeiss 1530 FESEM equipped with a Raith Elphy Plus at an accelerating voltage of 20 kV and doses were adjusted from 100  $\mu\text{C}/\text{cm}^2$  (**D**<sub>1</sub>) to 2516  $\mu\text{C}/\text{cm}^2$  (**D**<sub>21</sub>). The exposure took place on a new molecular glass negative tone resist utilizing physical vapor deposition for film preparation and consisted of 2-[(methylsulfonyl)oxy]-1H-Benz[de]isoquinoline-1,3(2H)-dione (41%), 1,1'-binaphthyl-2,2'-diamine (40%), and 2-[(methylsulfonyl)oxy]-1H-Benz[f]isoindole-1,3(2H)-dione (19%). Afterwards the film was developed 60 s in stirred cyclohexane.

### 3.5. Dissolution Investigation

For QCM measurements quartz crystal holder (Maxtec CHC-100) and quartz crystals (QCs) (1 inch, 5 MHz, polished gold electrodes; purchased from QT Quarztechnik GmbH) were used. For the resist film preparation on the QCs solutions out of a positive tone star-shaped teroligomer (GBLMA-co-MAMA-co-HAMA) and the photoacid generator (triphenylsulfonium perfluoro-1-butanefulfonate) were spin-coated under equal conditions (3.4. *Exposure Dose Gradient*) on quartz crystals resulting in a film thickness of about 90 nm. The wavelength for UV-exposure was adjusted to 240 nm to 290 nm (F300S; Fusion UV). The PEB was performed at a temperature of 130 °C for 30 s.

#### **4. Conclusions**

This work demonstrates several methods for combinatorial investigations on solution-coated thin films. In this context film preparation of an internal material composition gradient by a syringe pump system and a static mixing device was successfully established for polymeric as well as low molecular weight materials. The characterization by fluorescence spectroscopy as well as HPLC confirmed a linear slope of the achieved material composition gradient. We have also shown the controlled preparation of various temperature gradients here applied for thermal annealing processes whose slope is adjustable to the particular requirement. In addition, we have applied exposure dose gradients for UV light and electron beam exposure on tiny areas allowing a matrix-like application and thus the preparation of a ternary combinatorial library. For dissolution investigations quartz crystal microbalance measurements in combination with a titration process were shown to provide an efficient screening technique. Based on these valuable results further combinatorial investigations on solution-coated films were conducted with either stepwise or continuous immersion gradients. Finally these gradients were combined to a binary and a ternary combinatorial library and applied to lithographic systems. Here the resist material was efficiently prescreened allowing the evaluation of the interdependence of the applied variables. Thus by this method also a fast optimization of the resist material processing was achieved. These results impressively demonstrate the efficiency of combinatorial approaches on thin films applied for complex multi-variable dependent applications.

#### **Acknowledgments**

This work was supported by the Semiconductor Research Corporation's Global Research Collaboration (GRC) Program [Tasks 1675.001 and 1675.002] and the Deutsche Forschungsgemeinschaft (DFG), SFB 481 [Project No. A6]. In addition we thank EUV technology for the roughness evaluation software SuMMIT™. This publication was funded by the German Research Foundation (DFG) and the University of Bayreuth in the funding programme Open Access Publishing.

**References and Notes**

- 1 Drews, J. Drug discovery: A historical perspective. *Science* **2000**, 287, 1960–1964.
- 2 Newman, D.J.; Cragg, G.M. Natural Products as Sources of New Drugs over the Last 25 Years. *J. Nat. Prod.* **2007**, 70, 461–477.
- 3 Kennedy, J.P.; Williams, L.; Bridges, T.M.; Daniels, R.N.; Weaver, D.; Lindsley, C.W. Application of Combinatorial Chemistry Science on Modern Drug Discovery. *J. Comb. Chem.* **2008**, 10, 345–354.
- 4 Jorgensen, W.L. Efficient Drug Lead Discovery and Optimization. *Acc. Chem. Res.* **2009**, 42, 724–733.
- 5 Burbaum, J.; Sigal, N.H. New technologies for high-throughput screening. *Curr. Opin. Chem. Biol.* **1997**, 1, 72–78.
- 6 Thompson, L.A.; Ellman, J.A. Synthesis and Applications of Small Molecule Libraries. *Chem. Rev.* **1996**, 96, 555–600.
- 7 Jandeleit, B.; Schaefer, D.J.; Powers, T.S.; Turner, H.W.; Weinberg, W.H. Combinatorial materials science and catalysis. *Angew. Chem. Int. Ed.* **1999**, 38, 2494–2532.
- 8 Buenconsejo, P.J.S.; Siegel, A.; Savan, A.; Thienhaus, S.; Ludwig, A. Preparation of 24 ternary thin film materials libraries on a single substrate in one experiment for irreversible high-throughput studies. *ACS Comb. Sci.* **2012**, 14, 25–30.
- 9 Potyrailo, R.; Rajan, K.; Stoewe, K.; Takeuchi, I.; Chisholm, B.; Lam, H. Combinatorial and High-Throughput Screening of Materials Libraries: Review of State of the Art. *ACS Comb. Sci.* **2011**, 13, 579–633.
- 10 Barber, Z.H.; Blamire, M.G. High throughput thin film materials science. *Mater. Sci. Technol.* **2008**, 24, 757–770.
- 11 Stafford, C.M.; Roskov, K.E.; Epps, T.H.; Fasolka, M.J. Generating thickness gradients of thin polymer films via flow coating. *Rev. Sci. Instrum.* **2006**, 77, 23908/1-7.
- 12 Meredith, J.C.; Smith, A.P.; Karim, A.; Amis, E.J. Combinatorial Materials Science for Polymer Thin-Film Dewetting. *Macromolecules* **2000**, 33, 9747–9756.
- 13 Meredith, J.C.; Karim, A.; Amis, E.J. High-Throughput Measurement of Polymer Blend Phase Behavior. *Macromolecules* **2000**, 33, 5760–5762.
- 14 Neuber, C.; Bäte, M.; Thelakkat, M.; Schmidt, H.-W.; Hänsel, H.; Zettl, H.; Krausch, G. Combinatorial preparation and characterization of thin-film multilayer electro-optical devices. *Rev. Sci. Instrum.* **2007**, 78, 72216/1-11.

- 15 Burkert, S.; Kuntzsch, M.; Bellmann, C.; Uhlmann, P.; Stamm, M. Tuning of surface properties of thin polymer films by electron beam treatment. *Appl. Surf. Sci.* **2009**, *255*, 6256–6261.
- 16 Ueda-Yukoshi, T.; Matsuda, T. Cellular Responses on a Wettability Gradient Surface with Continuous Variations in Surface Compositions of Carbonate and Hydroxyl Groups. *Langmuir* **1995**, *11*, 4135–4140.
- 17 International Technology Roadmap for Semiconductors, Available online: <http://www.itrs.net/> (accessed on 04 December 2012).
- 18 de Silva, A.; Felix, N.M.; Ober, C.K. Molecular glass resists as high-resolution patterning materials. *Adv. Mater.* **2008**, *20*, 3355–3361.
- 19 Ito, H. Chemical amplification resists: Inception, implementation in device manufacture, and new developments. *J. Polym. Sci., Part A: Polym. Chem.* **2003**, *41*, 3863–3870.
- 20 Pfeiffer, F.; Felix, N.M.; Neuber, C.; Ober, C.K.; Schmidt, H.-W. Physical vapor deposition of molecular glass photoresists: a new route to chemically amplified patterning. *Adv. Funct. Mater.* **2007**, *17*, 2336–2342.
- 21 Lenhart, J.L.; Jones, R.L.; Lin, E.K.; Soles, C.L.; Wu, W.-l.; Goldfarb, D.L.; Angelopoulos, M. Combinatorial methodologies offer potential for rapid research of photoresist materials and formulations. *J. Vac. Sci. Technol., B* **2002**, *20*, 704-709.
- 22 Dam, T.H.; Jamieson, A.; Lu, M.; Baik, K.-H. PAB and PEB temperature gradient methodology for CAR optimization. *Proc. SPIE Int. Soc. Opt. Eng.* **2006**, *6349*, 634906/1-11.
- 23 Bauer, W.-A.C.; Neuber, C.; Ober, C.K.; Schmidt, H.-W. Combinatorial optimization of a molecular glass photoresist system for electron beam lithography. *Adv. Mater.* **2011**, *23*, 5404–5408.
- 24 Wieberger, F.; Forman, D.C.; Neuber, C.; Gröschel, A.H.; Böhm, M.; Müller, A.H.E.; Schmidt, H.-W.; Ober, C.K. Tailored star-shaped statistical teroligomers via ATRP for lithographic applications. *J. Mater. Chem.* **2011**, *22*, 73-76.
- 25 Wieberger, F.; Neuber, C.; Ober, C.K.; Schmidt, H.-W. Tailored Star Block Copolymer Architecture for High Performance Chemically Amplified Resists. *Adv. Mater.* **2012**, *44*, 5939–5944.
- 26 Sauerbrey, G. The use of quartz oscillators for weighing thin layers and for microweighing. *Z.Phys.* **1959**, *155*, 206-222.

- 27 Dai, J.; Chang, S.W.; Hamad, A.; Yang, D.; Felix, N.; Ober, C.K. Molecular Glass Resists for High-Resolution Patterning. *Chem. Mater.* **2006**, *18*, 3404–3411.
- 28 Lide, D.R., Ed. CRC Handbook of Chemistry and Physics, 88th ed.; Taylor & Francis Group: Boca Raton, FL, USA, **2008**; pp. 3-36, 3-38, 3-462.



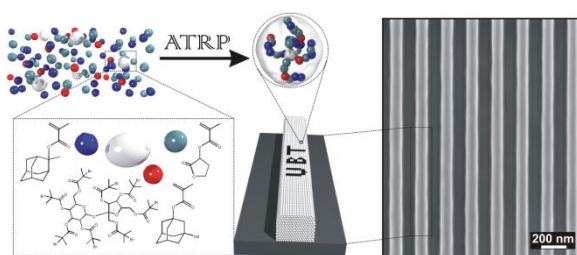
## 4.3 Tailored Star-Shaped Statistical Terpolymers via ATRP for Lithographic Applications

By Florian Wieberger<sup>‡1</sup>, Drew C. Forman<sup>‡2</sup>, Christian Neuber<sup>1</sup>, André H. Gröschel<sup>3</sup>, Marietta Böhm<sup>3</sup>, Axel H. E. Müller<sup>3</sup>, Hans-Werner Schmidt<sup>\*1</sup> and Christopher K. Ober<sup>\*2</sup>

<sup>1</sup>Macromolecular Chemistry I, University of Bayreuth, Universitätstraße 30,  
95440 Bayreuth, Germany,

<sup>2</sup>Materials Science & Engineering, Cornell University, 210 Bard Hall,  
Ithaca, NY 14853

<sup>3</sup>Macromolecular Chemistry II, University of Bayreuth, Universitätstraße 30,  
95540 Bayreuth, Germany



This paper is published in

*Journal of Materials Chemistry* (2012) **22**, 73-79

Reproduced by permission of The Royal Society of Chemistry

DOI: [10.1039/c1jm11922b](https://doi.org/10.1039/c1jm11922b)

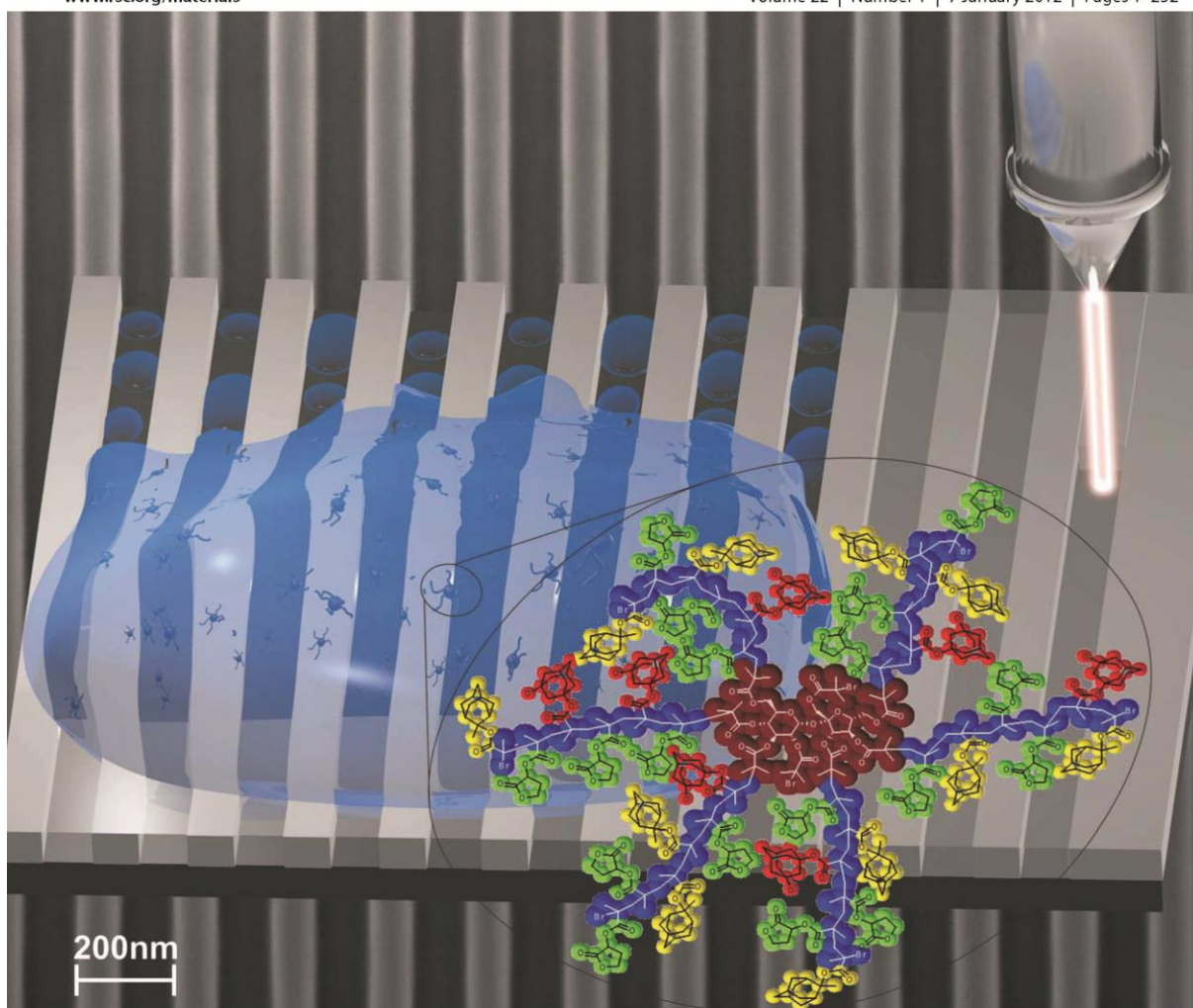
---

<sup>‡</sup> Florian Wieberger and Drew C. Forman contributed equally to this work

# Journal of Materials Chemistry

www.rsc.org/materials

Volume 22 | Number 1 | 7 January 2012 | Pages 1–252



ISSN 0959-9428

RSC Publishing

PAPER

C. Ober *et al.*

Tailored star-shaped statistical teroligomers via ATRP for lithographic applications

Inside front cover

**J. Mater. Chem.**, 2012, **22**, 2-2

DOI: [10.1039/C1JM90185K](https://doi.org/10.1039/C1JM90185K)

*Abstract: A series of five star-shaped teroligomers consisting of a saccharose core and arms composed of  $\alpha$ -gamma butyrolactone methacrylate (GBLMA), methyl adamantyl methacrylate (MAMA) and hydroxyl adamantyl methacrylate (HAMA) with defined arm length and number of arms were prepared via the core-first atom transfer radical polymerization (ATRP) route. The saccharose core was modified with ATRP initiating sites and non-reactive sites, enabling the synthesis of star polymers with a less arm number but identical core. Star teroligomers were synthesized with narrow molecular weight distributions with low polydispersity indices (PDIs < 1.1) showing negligible side reactions only at higher conversions of  $X_p > 50\%$ . The absence of side reaction and the precise achievement of the target molecular weight indicated excellent control over the reaction. A selected star-shaped teroligomer was investigated for the first time as a resist material. The delicate conditions of the lithographic process were optimized by a combinatorial approach. The obtained low line edge and line width roughness of the observed pattern demonstrate the potential of the star architecture for this application.*

## **Introduction**

Star-shaped polymers, which may consist of multiple linear homo-, block, or statistical copolymer arms covalently attached to a central core, have attracted interest in numerous research fields due to properties that can be tuned by varying the number, length and chemical nature of the arms.<sup>1-5</sup> Star-shaped polymers with very few arms behave in a similar fashion to their linear counterparts. However, as the number of arms increases, their ability to interact with neighboring stars decreases, in essence trading intermolecular for intramolecular interactions, leading to their description as “ultrasoft colloids”.<sup>3</sup> In this regime, star-shaped polymers possess properties significantly different from their linear counterparts. As a result stars are used for a range of applications including viscosity index modifiers in oil,<sup>6</sup> oxygen permeability and hardness enhancers in contact lenses,<sup>7</sup> additives in coatings, binder in toner and as an encapsulation material for pharmaceuticals.<sup>8,9</sup> The star-shaped polymer architecture continues to be the focus of both theoretical and experimental studies, which explore the relationship between architecture and thermodynamics, osmotic pressure, molecular size, rheology and polyelectrolyte behavior.<sup>10-15</sup>

There are many areas where the properties of the star-shaped architecture could prove beneficial, such as conjugates for drug delivery,<sup>16</sup> nanoparticle dispersion stabilizers,<sup>17</sup> cosmetic dyes,<sup>18</sup> and *in vivo* sensors.<sup>19</sup> With this work, star-shaped polymers are introduced to

the research field of lithography as new resist materials. Standard resists are still based on linear polymer materials.<sup>20</sup> During the last decade, an additional architecture, molecular glasses (MG), introduced by Shirota et al.,<sup>21</sup> has been studied as a new class of photoresist materials.<sup>22,23</sup> The main advantages of MGs are the formation of transparent films, their monodispersity, the usage of common organic purification methods and the smaller molecule size, which is about the same size as additives such as a photo acid generator and base quencher.<sup>24</sup> The advantages of common polymer materials are stable amorphous film formation, robust processability and the almost unlimited structural flexibility due to monomer choice and architecture.<sup>22</sup> In contrast to MGs, polymers show chain entanglements and have an average coil dimension of 5-10 nm. Chain entanglements and extended coil dimension are considered to be the main reasons for irregularities in high-resolution patterns. The introduction of star-shaped polymer architecture is intended to overcome issues from both the linear polymer and the MG resist materials. Additional research in non-linear polymer architectures has included graft<sup>25</sup> or hyperbranched<sup>26</sup> polymer resists that were designed to improve the resist's dissolution behavior or to enhance the sensitivity of the resist, respectively. These works demonstrate that switching from linear polymers to more complex architectures can yield improved performance.

Anionic polymerization is a well-known and well-established method for the fabrication of tailor made polymers with precise control over molecular weight (MW) and (low) polydispersities.<sup>27</sup> However, this method exhibits major drawbacks in modern material research as it is highly susceptible to impurities (especially oxygen and water) as well as functional groups (electrophilic, polar and protic). Although new synthetic paths like RAFT and NMP overcome some of these obstacles, they involve long and difficult preparative efforts and complicated synthetic paths towards star-shaped polymers.<sup>28</sup> In the past two decades, atom transfer radical polymerization (ATRP) has emerged as one of the most versatile controlled radical polymerization techniques sustaining most functional groups and even small amounts of oxygen.<sup>29</sup> In addition, reaction conditions can be easily tuned by many parameters for accurate polymer synthesis. Another interesting feature is the straightforward preparation of multifunctional, brush- or even star-shaped initiators by simple and inexpensive one-step esterification of oligo- and polyols with halogen bearing moieties.<sup>30,31</sup> The possibility of creating architectures for a wide range of applications is almost infinite as the pool of monomers polymerizable via ATRP is still increasing.<sup>28</sup> When ATRP is used to

prepare copolymers, different conversions yield different compositions except for the case of monomer feeds with the same reactivity.<sup>32</sup>

Based on this knowledge, we address key challenges facing ATRP synthesis of star-shaped statistical teroligomers. While conversion was previously utilized as a process variable, in this study it will be kept in a narrow range, while the reaction rate is controlled by the  $[\text{Cu}^{\text{I}}]/[\text{Cu}^{\text{II}}]$  and  $[\text{M}]:[\text{I}]$  ratios. This allows the synthesis of stars comprised of different cores with different arm lengths to be prepared at similar conversions and hence, identical composition. Introducing specific fractions of non-reactive sites into the saccharose initiator proved successful in controlling the average arm number of synthesized star teroligomers. With reaction conditions and polymerization kinetics resolved, one specific well-defined star architecture was used to investigate its potential in lithographic patterning.

## Experimental Part

### Materials

Ethyl 2-bromoisobutyrate (EBiB) (97 %), 2-bromoisobutyryl bromide (98 %), propionyl bromide (98 %), 4-(dimethylamino)pyridine (99 %), Pyridine, Dichloromethane, Copper(I) chloride (>99 %), Copper(II) chloride (>99 %), and N,N,N',N'',N'''-pentamethyldiethylenetriamine (PMDETA) (98 %), Triphenylsulfonium perfluoro-1-butanefluoroborate (>99%), Propylene glycol monomethyl ether acetate (99%), Tetramethylammonium hydroxide solution (10 wt.%), Hexamethyldisilazane (HMDS) were purchased from Aldrich and D(+)-Saccharose was purchased from Aldi Süd. Methyl adamantyl methacrylate (MAMA) and hydroxyl adamantyl methacrylate (HAMA) were purchased from Idemitsu Chemicals and  $\alpha$ -gamma butyrolactone methacrylate (GBLMA) from Kuraray. MAMA and GBLMA were passed through a basic alumina column to remove the inhibitor. HAMA was used as received. All solvents used were of analytical grade.

### Preparation of Multifunctional Initiators

The core-first<sup>33</sup> approach and ATRP were selected to synthesize star-shaped oligomers. 2,3,4,6,1',3',4',6'-octa-O-(2-bromoisobutyryl)-saccharose (**1**), which has eight initiating sites, was prepared from saccharose as previously published.<sup>34</sup>

A modified multifunctional initiator with fewer initiating sites (**2**) was prepared by substituting the 2-bromoisobutyryl bromide with a 50/50 solution of 2-bromoisobutyryl

bromide and propionyl bromide. 5.0 g (14.6 mmol) D(+)-Saccharose were dehydrated in a vacuum oven at 80 °C for 1 hour prior to being stirred with 4-(Dimethylamino)pyridine in catalytic quantities in a solution of 200 mL chloroform and 90 mL pyridine under nitrogen. After cooling the solution with ice, 26.9 g (116.8 mmol) 2-bromoisobutyryl bromide and 16.0 g (116.8 mmol) propionyl bromide were added from a dropping funnel over a period of 3 hours. The solution was brought to room temperature and stirred overnight before undergoing reflux at 75 °C for three hours. The solution was diluted with diethyl ether and the pyridinium bromide was removed by repeated extraction with water, sodium hydrogen carbonate solution and sodium chloride solution. The solution was concentrated and purified by column chromatography (SiO<sub>2</sub>; Ethyl acetate), the solvent evaporated, then dissolved in hot methanol and precipitated at -20 °C over night. The obtained solid mixture of products corresponding to the saccharose based multifunctional initiator **2** has an average of 3.5 initiating sites. (6.2 g, 5.6 mmol, 38.1 %)

Eight site saccharose-based initiator **1**:  $M (+Li^+) = 1.541 \text{ g}\cdot\text{mol}^{-1}$  by MALDI-TOF MS (DHB:LiCl:initiator 10:1:1).<sup>34</sup> Reduced site Saccharose-based initiator **2**:  $M (+Li^+) = 889$  (5.8 %), 981 (17.6 %), 1.073 (27.6 %), 1.165 (25.8 %), 1.257 (14.5 %), 1.348 (8.7 %)  $\text{g}\cdot\text{mol}^{-1}$  by MALDI-TOF MS (DHB:LiCl:initiator 10:1:1).

### Preparation of Star-shaped Teroligomers

A previous procedure<sup>34</sup> for the preparation of poly(*tert*-butylmethacrylate) stars by ATRP was modified as follows: 0.20 g (0.13 mmol) **1**, 1.76 g (10.4 mmol) GBLMA, 2.43 g (10.4 mmol) MAMA, 1.22 g (5.2 mmol) HAMA, 0.03 g (0.35 mmol) CuCl and 0.93 g (0.69 mmol) CuCl<sub>2</sub> and 20 g anisole were added to a 50 mL round bottom flask sealed with a rubber septum, equipped with a stir bar, and purged with nitrogen for 30 min. The solution was heated in a 65 °C oil bath and 0.18 g (1.04 mmol) PMDETA were added at time  $t=0$ . A characteristic color change to transparent green indicated the start of the reaction.

Aliquots were taken throughout the reaction to follow the conversion of all three monomer with <sup>1</sup>H-NMR simultaneously. Peak integration was performed on the vinyl peaks of GBLMA, MAMA, HAMA at a chemical shift of  $\delta = 6.39$  ppm,  $\delta = 6.27$  ppm and  $\delta = 6.22$  ppm, respectively, and calibrated to the integration of the anisole signal at  $\delta = 3.87$  ppm. The half-logarithmic relationship between conversion and polymerization time was used to determine the end time for 50 % conversion (Equation 1).<sup>35-37</sup>

$$\ln\left(\frac{[M]_0}{[M]_t}\right) = \frac{k_p K_{ATRP} [P_m X] [Cu^I]}{[Cu^{II}]} \cdot t \quad (1)$$

At the calculated end time, a final aliquot was removed to verify the final conversion and the reaction was quenched by rapid cooling to room temperature with liquid nitrogen. The reaction solution was passed through a silica column to remove the copper catalyst, concentrated under reduced pressure while being heated to 80 °C and precipitated in methanol. Following gravity filtration, the resulting powder was taken up in 1,4-dioxane and freeze dried to obtain the star-shaped (GBLMA-co-MAMA-co-HAMA) oligomer (**S1d**) as a white powder (2.75 g, 97 %).

Similar procedures were taken out with reactant ratios and polymerization times modified to achieve samples with different defined arm lengths.

### Gel Permeation Chromatography

GPC with a Wyatt DAWN HELEOS multiangle light scattering (GPC/MALS) detector equipped with a 632.8 nm He-Ne laser and Viscotek Model 250 viscosity detector (GPC/viscosity) were used to determine the absolute molecular weights. THF was used as eluent at a flow rate of 1.0 mL/min: column set, 5  $\mu$ m PSS SDV gel, 10<sup>2</sup>, 10<sup>3</sup>, 10<sup>4</sup>, and 10<sup>5</sup> Å, 30 cm each. For GPC/viscosity, the refractive index increment, dn/dc, was measured on a PSS DnDc-2010/620 differential refractometer in THF at 25 °C.

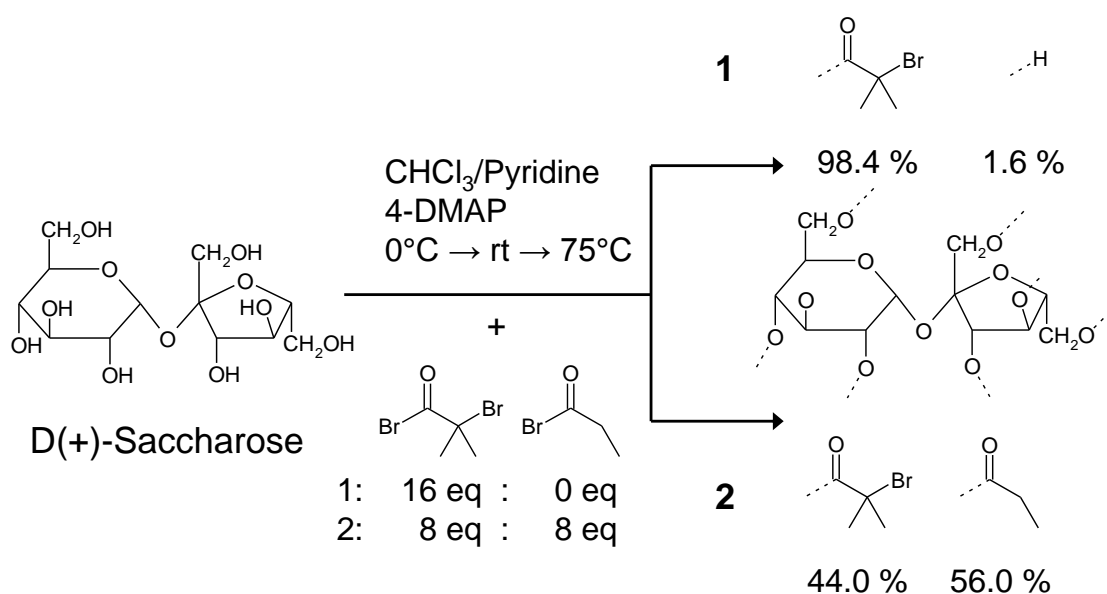
### Lithographic Experiments

For film preparation a 5 wt.-% solution of **S1d** and triphenylsulfonium perfluoro-1-butanoylsulfonate (19:1) in PGMEA was spin coated on a HMDS primed silicon wafer and prebaked at 125 °C for 150 s which corresponded to a 90 nm film thickness. The film was exposed with a 100 nm line/space pattern at doses from 10 to 410  $\mu$ C/cm<sup>2</sup> in 24 steps with a Zeiss 1530 FESEM equipped with a Raith Elphi Plus and an accelerating voltage of 20 kV. The film was annealed for post exposure bake (PEB) with a temperature gradient from 93 °C to 104 °C for 30 s and perpendicular to the temperature gradient developed in 0.26 N TMAH for four time periods of (15, 30, 60, 120) s. A Zeiss 1530 FESEM was used for imaging and the software SuMMIT<sup>TM</sup> was used for evaluation and determination of the line edge roughness (LER) and the line width roughness (LWR) of the line/space pattern.

## Results and Discussion

### Analysis of Initiator Functionality

In order to achieve different functionalities from the same saccharose core, active initiating groups were replaced with a non-reactive propylester resulting in reduced functionality. Scheme 1 shows the reaction pathway toward the nearly complete functionalized saccharose based initiator **1** and the initiator **2** with reduced functionality.



**Scheme 1:** Reaction pathway toward saccharose based initiators **1** and **2**. **1** is the maximum functionalized saccharose based initiator, while **2** has a reduced functionality realized by capping with the non-reactive propylester.

Saccharose contains eight possible reaction sites for 2-bromoisobutyryl bromide and propionyl bromide. The synthetic route to initiator **1** yields the maximum functionalized saccharose based initiator while the synthesized initiator **2** is not a single initiator, but rather a mixture of initiators based on the same saccharose molecule, each of different functionality. The composition of the multifunctional initiators was analyzed by MALDI-TOF mass spectrometry (MS) to determine the numbers of initiating sites and the corresponding content in the mixture of the synthesized initiator **2** (Table 1).

**Table 1:** Absolute numbers of initiating sites and corresponding content for initiator 2 measured by MALDI-TOF MS

$M_w$ (g/mol) <sup>a</sup>	Initiating Sites <sup>b</sup>	Content (%) <sup>c</sup>
<b>889</b>	<b>1</b>	<b>5.8</b>
<b>981</b>	<b>2</b>	<b>17.6</b>
<b>1.073</b>	<b>3</b>	<b>27.6</b>
<b>1.165</b>	<b>4</b>	<b>25.8</b>
<b>1.257</b>	<b>5</b>	<b>14.5</b>
<b>1.348</b>	<b>6</b>	<b>8.7</b>

<sup>a</sup>Molecular weight of MALDI-TOF MS detected initiator + (Li<sup>+</sup>) <sup>b</sup>Number of brominated initiating sites determined by tabulation of molecular weight for possible combinations of sites reacted with 2-bromoisobutyryl bromide, sites reacted with propionyl bromide, and debrominated initiators yielded by the purification procedure. <sup>c</sup>Content of corresponding initiator derivative in the synthesized mixture of initiator **2**. The content is calculated by the integrated strength of the MALDI-TOF MS peaks.

The MALDI-TOF MS measurement shows a Gaussian content distribution with the main content in the mixture of initiator **2** between three (27.6 %) and four (25.8 %) initiating sites. As a result the initiator **2** has the overall average of 3.5 bromine based initiating sites which is given by the endcapping of the saccharose core with propionyl bromide and by the loss of bromides during purification procedure.

The efficiency of the reactive sites to initialize polymerization has to be taken into account, reducing the arm number further. A practical value of 66 % is well-established by numerous reports on methacrylate synthesis with initiating sites of identical reactivity and was also taken into consideration for the initiator efficiency. Thus, a final number of arms of 5.3 for **1** is anticipated and in the same manner, the initiator efficiency of **2** is anticipated to be 2.4. With the initiator **1**, the ethyl 2-bromoisobutyrate initiator and the initiator **2** we are able to synthesize polymers of a star architecture containing more than five arms, linear polymers as well as the corresponding missing links with more than two arms.

### Monomer Feed Ratios

For this study, an average monomer composition of 50 % GBLMA, 30 % MAMA and 20 % HAMA within the product was targeted due to its potential application as a resist material.<sup>30</sup> Through repeated experimentation with a statistical linear copolymer, a feed of 41 % GBLMA, 41 % MAMA and 18 % HAMA was found to achieve the target composition over a conversion range of  $X_p = 30 - 60$  % (Figure 1). For this purpose, the composition was monitored throughout the polymerization by the decrease of the three vinyl signals, which corresponded to each monomer decaying in  $^1\text{H-NMR}$ . Except for the start of the reaction, the composition of the growing polymer remained close to the target composition. Conversion followed first order kinetics without any trace of side reactions like recombination or transfer.

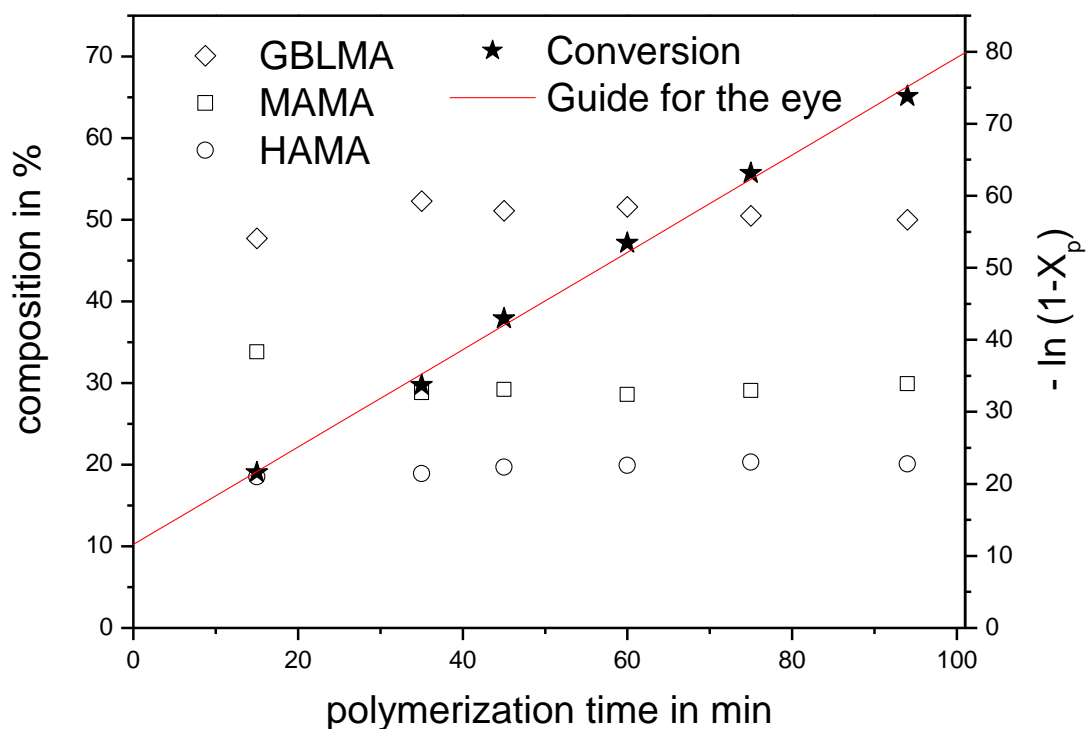
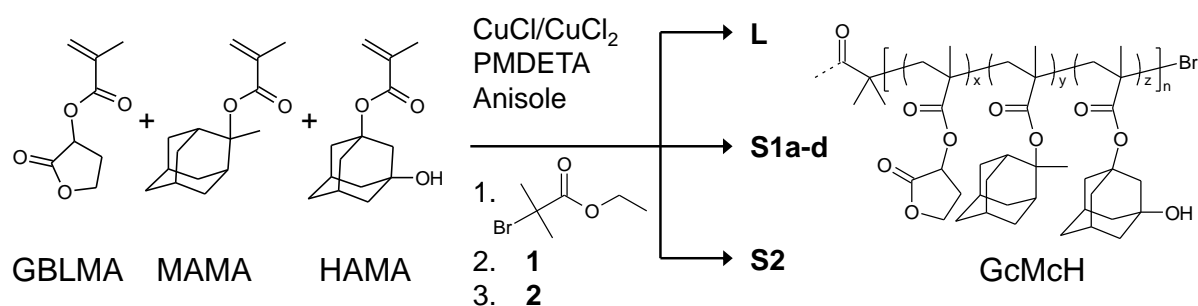


**Figure 1:** Evolution of monomer incorporation (GBLMA (◇), MAMA (□) and HAMA (○)) and also  $-\ln(1-X_p)$  (★) versus polymerization time of **S1d**.

### Synthesis of Star-shaped Teroligomers with Modified Arm Lengths

Four star-shaped oligomers with varying target average arm lengths of 7, 10, 19 and 20 units and identical core **1**, a star with modified core **2** and a linear model oligomer initiated from ethyl 2-bromoisobutyrate were synthesized (Scheme 2; Table 2). For all materials the average monomer composition is 50 % GBLMA, 30 % MAMA and 20 % HAMA, which

demonstrates the effectiveness of the proposed method. **S1c** shows the most distinct star character, a similar molecular weight and the same composition as a hyperbranched polymer published by Hadziioannou et al.<sup>26</sup> Thus **S1d** was synthesized with a focus on the same molecular weight of **S1c** but in a larger scale for lithographic investigations. In addition, as shown in Figure 1 the desired composition is independent on the investigated conversions, this second batch was synthesized up to a higher conversion of 60 % to save monomer.



**Scheme 2:** Synthesis of the linear model teroligomer **L** and the star-shaped teroligomers **1** and **2**. The overall teroligomer composition of GBLMA/MAMA/HAMA (GcMcH) was 50/30/20. **1** is the maximum functionalized saccharose initiator, while **2** has a reduced functionality.

**Table 2:** Synthesis conditions and star teroligomer specifics

Code	Polymer <sup>a,b</sup>	[I] <sub>0</sub> (mmol/L)	[M] <sub>0</sub> <sup>c</sup> : [I] <sub>0</sub> : [L]: [Cu <sup>I</sup> ] <sub>0</sub> : [Cu <sup>II</sup> ] <sub>0</sub>	Time (min)	M <sub>n, theo.</sub> <sup>d</sup> (kg/mol)	M <sub>n, MALS</sub> (kg/mol)	PDI <sup>e</sup>	DP <sub>n</sub> <sup>f</sup>
<b>L</b>	(GcMcH) <sub>41</sub>	27.0	55 : 1.0 : 1.0 : 0.5 : 0.5	200	7.0	8.4	1.05	41
<b>S1a</b>	((GcMcH) <sub>7</sub> ) <sub>5,3</sub>	31.4	70 : 1.0 : 8.0 : 0.5 : 7.5	120	8.4	9.1	1.05	38
<b>S1b</b>	((GcMcH) <sub>10</sub> ) <sub>5,3</sub>	8.9	119 : 1.0 : 8.0 : 1.6 : 6.4	105	12.0	12.5	1.05	55
<b>S1c</b>	((GcMcH) <sub>19</sub> ) <sub>5,3</sub>	4.5	237 : 1.0 : 8.0 : 4.0 : 4.0	124	22.4	20.6	1.03	98
<b>S1d</b>	((GcMcH) <sub>20</sub> ) <sub>5,3</sub>	6.5	200 : 1.0 : 8.0 : 2.7 : 5.3	150	22.4	23.9	1.05	104
<b>S2</b>	((GcMcH) <sub>14</sub> ) <sub>2,4</sub>	25.0	75 : 1.0 : 4.0 : 0.8 : 3.2	45	8.2	8.0	1.08	35

<sup>a</sup> First subscript denotes degree of polymerization per arm; <sup>b</sup> Second subscript denotes arm number; <sup>c</sup> Monomer feed ratio: 41 % GBLMA, 41 % MAMA, 18 % HAMA; <sup>d</sup> theoretical targeted molecular weight; <sup>e</sup> polydispersity index measured by MALS detection; <sup>f</sup> overall degree of polymerization deduced from MALS values.

The ratio of monomer units to initiator plays a crucial role in synthesizing the desired arm length and the average monomer composition of the star. Reaction conditions were adjusted for each polymerization to result in monomer percentages of 50 %, 30 % and 20 %, for GBLMA, MAMA and HAMA, respectively, when conversion approached the predetermined region of 40-60 %. Since the reaction time decreases sharply when synthesizing shorter molecules, the ratio  $[Cu^I]_0/[Cu^{II}]_0$  was decreased to slow down reaction times significantly. The addition of  $[Cu^{II}]$  deactivator allows targeting very short arms without losing control over the reaction. Analysis of the final aliquots yielded an overall composition of (46/32/22), (47/31/22), (50/31/19), (50/30/20), (49/30/21) and (49/31/20) (GBLMA%/MAMA%/HAMA%) for **L**, **S1a**, **S1b**, **S1c**, **S1d** and **S2**. This is very well within the expected range and underlines previously made assumptions.

The conversion index (Equation 1) describes a logarithmic relationship between the conversion of monomer and polymerization time and therefore corresponds to a first order kinetic.<sup>35-37</sup> By normalizing the conversion index with reaction quantities that are proportional to the remaining terms (Equation 2), it can be shown that all four reactions follow the same kinetics (Figure 2) independent of  $[I]_0/[Cu^I]_0$  and  $[Cu^I]_0/[Cu^{II}]_0$  ratios.

$$\ln\left(\frac{[M]_0}{[M]_t}\right) \cdot \left(\frac{[Cu^{II}]_0}{[Cu^I]_0[I]_0}\right) \cdot \left(\frac{[M]_0}{[I]_0}\right) \sim t \quad (2)$$

This information can then be used to predict how changing each reaction condition will impact the polymerization time required to achieve the desired conversion.

As already mentioned in the introduction, star teroligomers consist of polymer chains covalently linked to one core resulting in reduced hydrodynamic radii compared to linear polymer coils, so standard GPC does not deliver reliable values for molecular weights without corresponding calibration. Thus GPC measurements were performed with a multi-angle light scattering (MALS) detector to obtain absolute molecular weights (Figure 3).

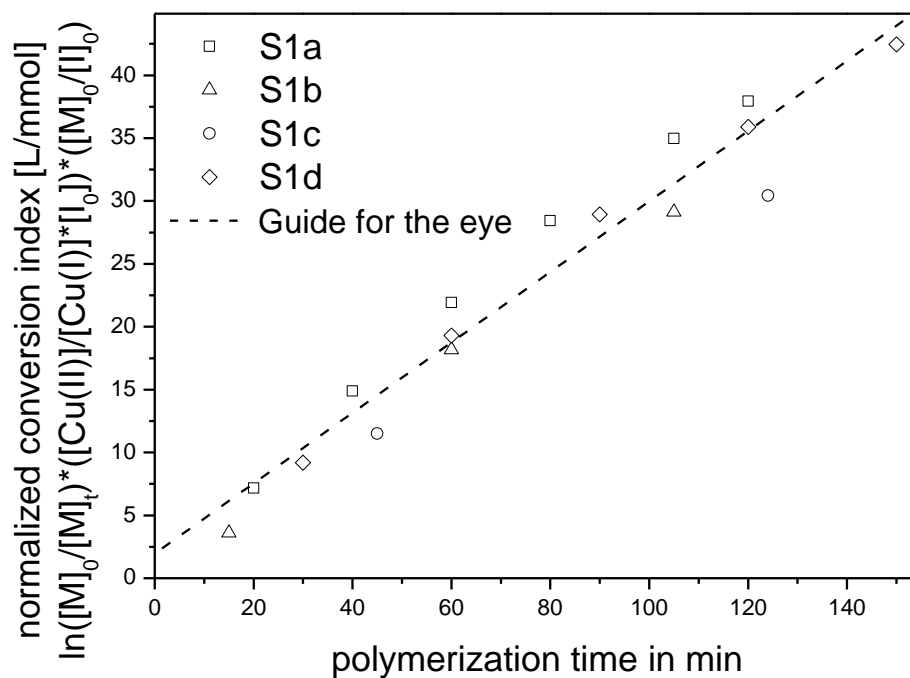


**Figure 2:** Plot of the normalized conversion index versus polymerization time for **S1a** (□), **S1b** (△), **S1c** (○), **S1d** (◇).

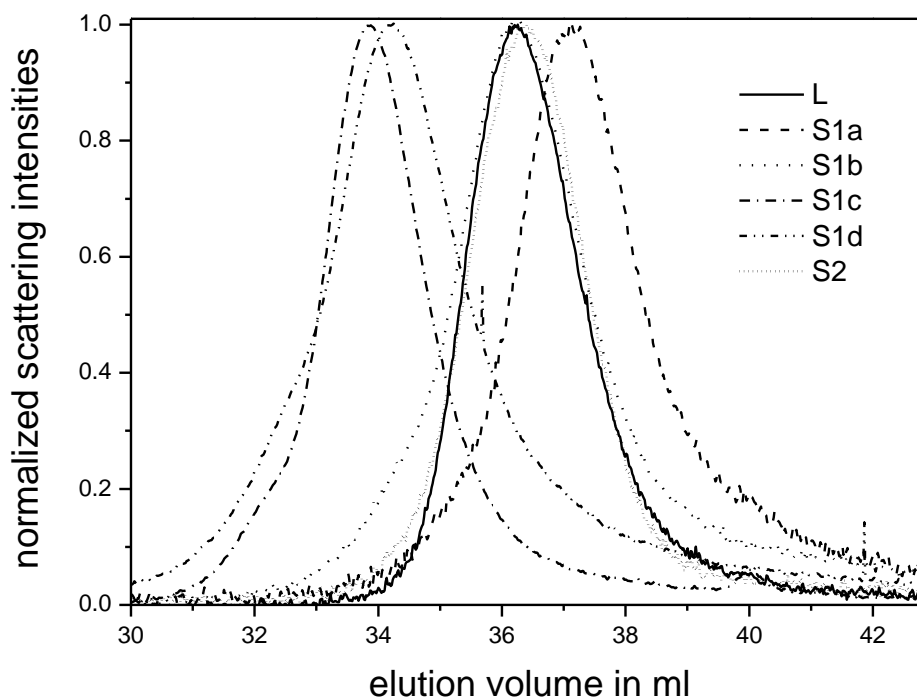


**Figure 3:** Normalized scattering intensity of GPC traces of **L**, **S1a**, **S1b**, **S1c**, **S1d** and **S2** measured with THF as the eluent and a multi-angle light scattering detector. Slight recombinations are visible by shoulders for the star-shaped teroligomers **S1c** (dash dot) and **S1d** (dash dot dot) due to the fact, that the scattering detector is disproportionally sensitive to the molecular size (intensity  $\sim$  diameter<sup>6</sup>).

As already indicated by the first order kinetics and observed for all star-shaped teroligomer narrow monomodal distributions were detected. All traces have a symmetrical shape and show no signs of tailing indicating a quantitative initiation and a controlled character. The shift to a lower elution volume corresponds to an increase in molecular weight and hence, an increasing arm length for the star teroligomers series **S1a- S1d** with an average of 5.3 arms. These traces are comparable in quality (shape and distribution) to their linear counterpart indicating equally good control. The scattering detector is disproportionately sensitive (Intensity  $\sim$  diameter<sup>6</sup>)<sup>38</sup> to changes in molecular size. Hence, recombination shoulders result in a disproportionately strong signal with MALS detection as can be seen for sample **S1c** (dash dot) and **S1d** (dash dot dot). As a result the GPC analysis shows negligible coupling up to 50% conversion. The reason for this rather unusual high conversion may be explained by the dilution of 5:1 excess anisole to monomer and especially by the steric hindrance of the bulky monomers suppressing termination reactions. According to evaluation of reaction kinetics and the fact that sterical hindrance of the bulky monomers suppresses termination reactions, the arm length has no influence on the extension of the coupling reactions. In summary, this series of star-shaped oligomers successfully demonstrates the strength of this synthetic route at preparing well-defined copolymers of diverse arm length but of the same monomer composition.

Using the normalized conversion index (Equation 2), two different star-shaped teroligomers (**S1a**, **S2**) and the linear oligomer (**L**) were prepared with an overall target  $DP_n$  of 40. This yielded three materials comprised of the same monomer compositions but different architectures. The resulting materials demonstrate the opportunity for fundamental studies. Series similar to this would allow detailed investigations of the impact of architecture to material properties in low molecular weight systems. The synthesis work demonstrates the reproducible reaction pathway and precise prediction capability for complex copolymers with different architecture.

The chemical nature and the resulting initiating efficiency,  $f$ , of initiators **S1a** ( $f = 5.3$ ), **S2** ( $f = 2.4$ ), and **L** ( $f = 1$ ) directly influence the slope of the normalized conversion index versus time, but show an almost perfect linear dependency (Figure 4).

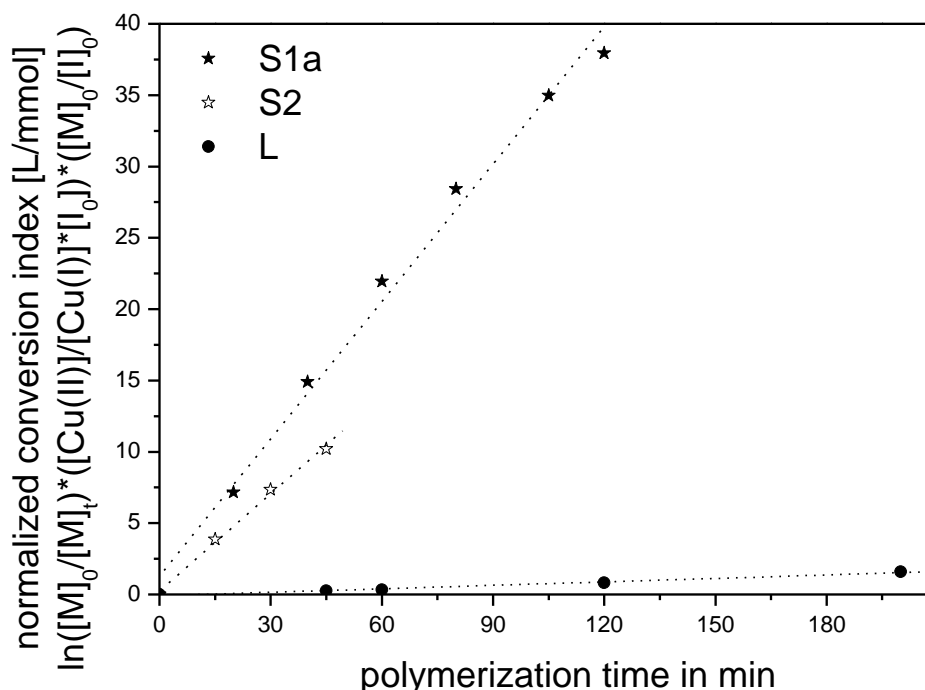


**Figure 4:** Plot of normalized conversion index versus time for **S1a** (★), **S2** (☆), **L** (●). The different slopes originate from the different investigated initiators.

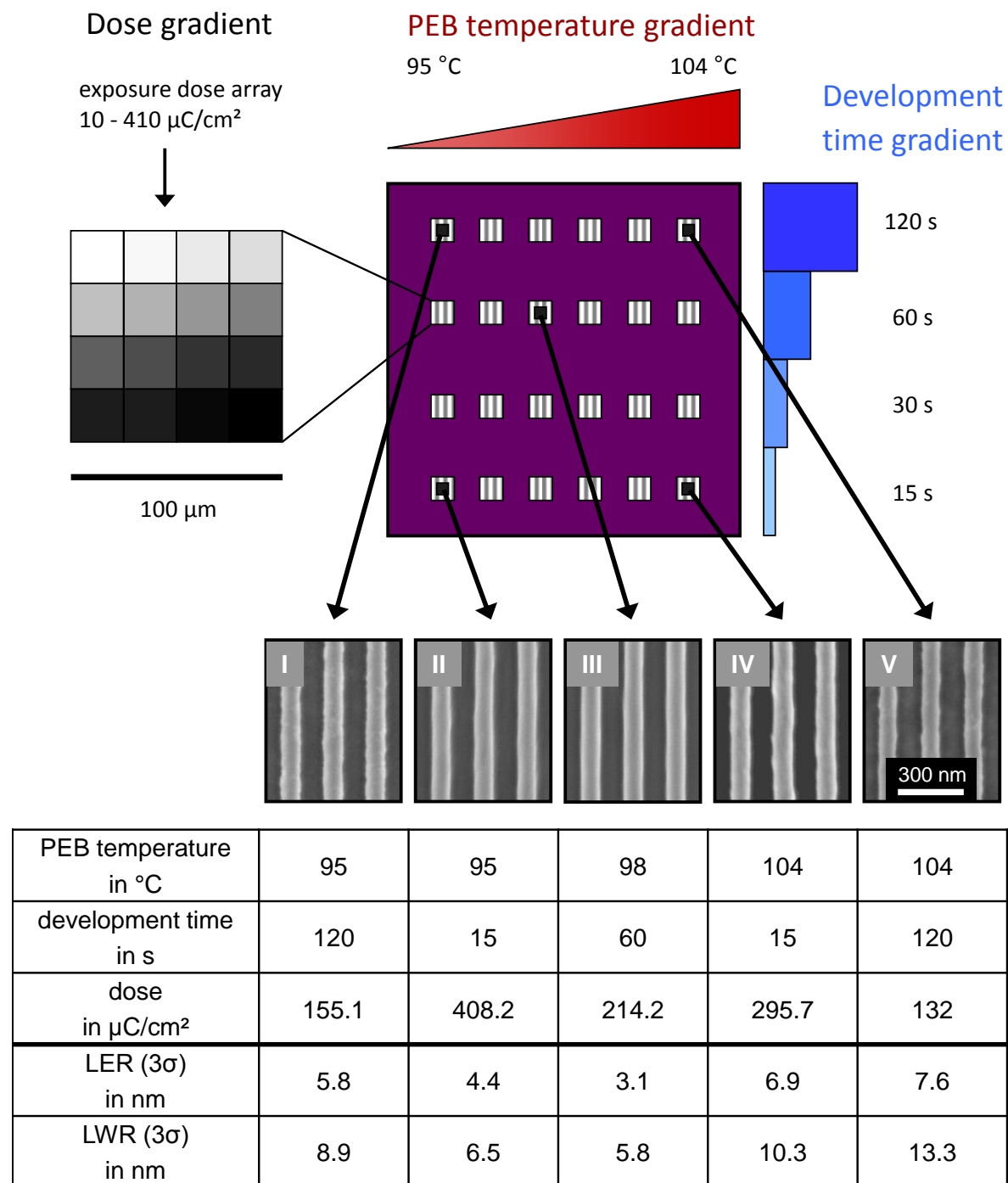
In Figure 4 the plot of the normalized conversion index and the represented linear connection show impressively the independency of  $[I]_0/[Cu^I]_0$  and  $[Cu^I]_0/[Cu^{II}]_0$  ratios, but corresponding synthesis requires a various polymerization time obvious by the different slopes. This allows the systematical investigation of **S1a**, **S2** and **L** synthesized under different reaction conditions.

In order to achieve the highest level of precision, the individual conversion rate had to be determined for each initiator. Dilution and catalyst ratios can then be altered accordingly to achieve a polymerization of sufficient duration to take multiple  $^1\text{H-NMR}$  aliquots. As a consequence the investigated ATRP reaction follows the same kinetic and allows this systematic investigation of star polymers of different arm numbers and a linear model polymer.

### Lithographic application

The literature known linear teroligomer synthesized from the monomers GBLMA, MAMA and HAMA is a high performance resist material and has recently been the focus of other research.<sup>39,40</sup> In addition, Hadziioannou et al. published the first lithographic investigations on hyperbranched terpolymers of these monomers at the same copolymer

composition.<sup>26</sup> All of the synthesized resists with this specific monomer formulation had a targeted molecular weight of about 21 kg/mol. The patterning process of the hyperbranched polymer yielded a line edge roughness (LER) ( $3\sigma$ ) of ~6 nm and a line width roughness (LWR) ( $3\sigma$ ) of ~10 nm. Here, the well-defined star **S1d** in contrast to the non-controlled hyperbranched polymer is investigated for a proof of principle of utilizing the star architecture for lithographic patterning. The star teroligomer **S1d** is synthesized according to the above optimized formulation and has a comparable  $M_w$  of 23 kg/mol to the published hyperbranched resist material. The optimization of the lithographic variables (post exposure bake temperature, development time and exposure dose) for the new star resist were investigated with a combinatorial library: triphenylsulfonium perfluoro-1-butanoylsulfonate, a photoacid generator, was added to the star resist. This mixture was dissolved in propylene glycol monomethyl ether acetate and spin-cast. The post apply bake was done at 125 °C for 150 s on a hotplate to remove residual solvent and a film thickness of 90 nm was obtained. Electron beam lithography, a direct write technique, was used to generate an acid from the photo acid generator simulating a high resolution photolithography scanner. The exposed area consisted of a dose gradient (10 - 410  $\mu\text{C}/\text{cm}^2$ ), exposing 100 nm line/space pattern on an area of (100  $\mu\text{m}$ )<sup>2</sup>. A subsequent thermal treatment for 30 s (post exposure bake; PEB), performed with a temperature gradient from 95 °C to 104 °C, activated the acid catalyzed deprotection of the polymer component methyl adamantyl methacrylate releasing the polar carboxyl groups responsible for the development contrast. A development time gradient was achieved by dipping the resist film stepwise in a base developer (0.26 N tetramethylammonium hydroxide; TMAH) for (15, 30, 60, and 120) s to dissolve the exposed areas. By applying the three gradients in different directions to the same substrate a ternary combinatorial library schematically shown in Scheme 3 was prepared. Selected SEM images of line/space patterns and their corresponding LER and LWR values are depicted in Scheme 3 representing the 576 unique combinations of the aforementioned three variables.



**Scheme 3:** The upper figure shows a schematic illustration of the ternary combinatorial library consisting of the PEB temperature gradient, the development time step gradient, and the e-beam dose gradient. The table exhibits patterns from the four corners of the combinatorial library (I, II, IV, V) and the optimized pattern (III). The respective conditions (PEB temperature, development time, and dose) of these patterns and the calculated LER and LWR are listed.

The combinatorial investigation demonstrates the strong interdependence of resist processing variables. The optimized patterns were observed at a PEB temperature of 98 °C, a development time of 60 s, and an e-beam dose of 214.2  $\mu\text{C}/\text{cm}^2$  resulting in an excellent LER value of 3.1 nm and LWR of 5.9 nm. The patterns with a PEB temperature outside the observed optimum temperature exhibit visible increases of LER and LWR (image I and V). The investigated development time step gradient demonstrates the clear contrast of the star resist **S1d**. Here, the trend is observed that a short development time (image II and IV) results in clearer lines than those achieved after overdeveloping at 120s (image I and V). The electron beam dose exposure gradient shows the strong influence of this variable and its dependence on the other lithographic variables. Underexposure and overexposure were detected by sharp increases in LER and LWR values and by resist stripping. In conclusion, the combinatorial investigation results in an efficient optimization for the overall lithographic process variables in one library and demonstrates the high potential of the star resist as an architectural candidate for low roughness resists.

## Conclusions

This work greatly expands both the precision of star-shaped oligomers synthesis and the capability to study the impact of arm number and arm length in the star-shaped oligomer regime for a wide range of materials and properties. Four star teroligomers with average arm lengths of 7, 10, 19, and 20 monomer units and a linear model oligomer were synthesized with an identical monomer composition by changing the ratios of  $[\text{M}]_0/[\text{I}]_0$  and  $[\text{Cu}^{\text{I}}]_0/[\text{Cu}^{\text{II}}]_0$ . In addition, a technique for preparing multifunctional initiators with reduced functionality was introduced. High precision, star-shaped teroligomers initiated from the same core but with different numbers of arms were successfully synthesized. The achieved narrow and symmetrical molecular weight distributions with low polydispersity indices (PDIs < 1.1) were achieved even at conversion up to  $X_p=50\%$ . The potential of utilizing the well-defined star architecture for lithographic purposes was demonstrated by a combinatorial approach achieving a novel high resolution positive resist with LER of 3.1 nm and LWR of 5.8 nm.

**Acknowledgement**

This work was supported by the Semiconductor Research Corporation's Global Research Collaboration (GRC) Program [Tasks 1675.002 and 1677.001] and the German Research Foundation (Deutsche Forschungsgemeinschaft), Collaborative Research Center (Sonderforschungsbereich) 481, project A6. D.C.F. was supported by a GRC and Applied Materials fellowship. Research was performed in part at the University of Bayreuth, Macromolecular Chemistry I, the Bayreuth Institute of Macromolecular Research, and the Cornell Center for Materials Research, which is supported by NSF [Grant DMR 0520404] part of the NSF Materials Research Science and Engineering Center program. In addition we thank EUV technology for the roughness evaluation software SuMMIT™.

## References

- 1 K. Matyjaszewski and N. V. Tsarevsky, *Nature Chem.*, 2009, **1**, 276-288.
- 2 C. N. Likos and H. M. Harreis, *Condens. Matter Phys.*, 2002, **29**, 173-200.
- 3 C. N. Likos, *Soft Mater.*, 2006, **2**, 478-498.
- 4 C. N. Likos, H. Löwen, M. Watzlawek, B. Abbas, O. Jucknischke, J. Allgaier and D. Richter, *Phys. Rev. Lett.*, 1998, **80**, (20), 4450-4453.
- 5 M. Sawamoto, S. Kanaoka, T. Omura and T. Higashimura, *Polym. Prepr.*, 1992, **33**, 148-149.
- 6 R. J. Sutherland, and R. B. Rhodes, *Dispersant viscosity index improvers*, 1994, **US5360564**.
- 7 H. J. Spinelli, *Silicone containing acrylic star polymers*, 1991, **US5019628**.
- 8 R. J. Hunter, *Foundations of Colloid Science, Vol. 1*. Oxford University Press: New York, 1986.
- 9 G. Grest, L. J. Fetters and J. S. Huang, *Adv. Chem. Phys.*, 1996, **94**, 67-163.
- 10 H.-P. Hsu, W. Nadler and P. Grassberger, *Macromolecules*, 2004, **37**, 4658-4663.
- 11 C. von Ferber and Y. Holovatch, *Condens. Matter Phys.*, 2002, **29**, 117-136.
- 12 J. Dzubiella and A. Jusufi, *Condens. Matter Phys.*, 2002, **30**, 285-305.
- 13 J. Bohrisch, C. D. Eisenbach, W. Jaeger, H. Mori, A. H. E. Müller, M. Rehahn, C. Schaller, S. Traser and P. Wittmeyer, *Adv. Polym. Sci.*, 2004, **165**, 1-41.
- 14 F. Ganazzoli, *Condens. Matter Phys.*, 2002, **5**, 37-71.
- 15 F. A. Plamper, H. Becker, M. Lanzendöfer, M. Patel, A. Wittemann, M. Ballauff, A. H. E. Müller, *Macromol. Chem. Phys.*, 2005, **206**, 1813-1825.
- 16 W. B. Liechty, D. R. Kryscio, B. V. Slaughter, and N. A. Peppas, *Annu. Rev. Chem. Biomol. Eng.*, 2010, **1**, 149-173.
- 17 J. H. Adair, T. Li, T. Kido, K. Havey, J. Moon, J. Mecholsky, A. Morrone, D. R. Talham, M. H. Ludwig and L. Wang, *Mater. Sci. Eng., R*, 1998, **23**, 1-242.
- 18 G. F. Matz, A. L. Melby, S.-R. T. Chen, and N. F. Vozza, *Low molecular weight water soluble polymer composition and method of use*, 2001, **WO 2001006999**.
- 19 L. M. De Leon-Rodriguez, A. Lubag, D. G. Udugamasooriya, B. Proneth, R. A. Brekken, X. Sun, T. Kodadek and A. Dean Sherry, *J. Am. Chem. Soc.*, 2010, **132**, 12829-12831.
- 20 D. P. Sanders, *Chem. Rev.*, 2010, **110**, 321-360.
- 21 M. Yoshiiwa, H. Kageyama, F. Wakasa, M. Takai, K. Gamo and Y. Shirota, *Appl. Phys. Lett.*, 1996, **69**, 2605.

- 22 D. Yang, S. W. Chang and C. K. Ober, *J. Mater. Chem.*, 2006, **16**, 1693-1696.
- 23 A. D. Silva and C. K. Ober, *J. Mater. Chem.*, 2008, **18**, 1903-1910.
- 24 J. Dai, S. W. Chang, A. Hamad, D. Yang, N. Felix and C. K. Ober, *Chem. Mater.*, 2006, **18**, 3404,3411.
- 25 G. G. Barclay, M. A. King, Z. Mao, C. Szmanda, D. Benoit, E. Malmstrom, H. Ito and C. J. Hawker, *Polym. Prepr.*, 1999, **40**, 438-439.
- 26 C. L. Chochos, E. Ismailova, C. Brochon, N. Leclerc, R. Tiron, C. Sourd, P. Bandelier, J. Foucher, H. Ridaoui, A. Dirani, O. Soppera, D. Perret, C. Brault, C. A. Serra and G. Hadziioannou, *Adv. Mater.*, 2009, **21**, 1121-1125.
- 27 D. Baskaran, A. H. Mueller and K. Matyjaszewski, *Controlled and Living Polymerizations: From Mechanisms to Applications*, Wiley-VCH Verlag, Weinheim, Germany, **2010**.
- 28 W. A. Braunecker and K. Matyjaszewski, *Prog. Polym. Sci.*, 2007, **32**, 93-146.
- 29 K. Matyjaszewski, *ACS Symposium Series Vol. 1023*, **2009**.
- 30 M. Zhang and A. H. E. Mueller, *J. Polym. Sci., Part A: Polym. Chem.*, 2005, **33**, 759-785.
- 31 D. M. Haddleton, R. Edmonds, A. M. Heming, E. J. Kelly and D. Kukulj, *New J. Chem.*, 1999, **23**, 477-479.
- 32 G. Odian, *Principles of Polymerization*, John Wiley & Sons, Inc.: Hoboken, New Jersey, **2004**.
- 33 D. Rein, P. Rempp and P. J. Lutz, *Makromol. Chem. Macromol. Symp.*, 1993, **67**, 237-249.
- 34 F. A. Plamper, H. Becker, M. Lanzendöfer, M. Patel, A. Wittemann, M. Ballauff, and A. H. E. Müller, *Macromol. Chem. Phys.*, 2005, **206**, 1813-1825.
- 35 W. Tang and K. Matyjaszewski, *Macromol. Theory Simul.* 2008, **17**, 359-375.
- 36 A. Goto, T. Fukuda, *Prog. Polym. Sci.*, 2004, **29**, 329-385.
- 37 K. Matyjaszewski and J. Xia, *Chem. Rev.*, 2001, **101**, 2921-2990.
- 38 H. Holthoff, S. U. Egelhaaf, M. Borkovec, P. Schurtenberger, H. Sticher, *Langmuir* 1996, **12**, 5541-5549.
- 39 H. Momose, A. Yasuda, A. Ueda, T. Iseki, K. Ute, T. Nishimura, R. Nakagawa and T. Kitayama, *Proc. SPIE-Int. Soc. Opt. Eng.*, 2007, **6519**, 65192F.
- 40 K. Furukawa, S. Seki, T. Kozawa and S. Tagawa, *Proc. SPIE-Int. Soc. Opt. Eng.*, 2008, **6923**, 692334-1.



## 4.4 Tailored Star Block Copolymer Architecture for High Performance Chemically Amplified Resists

By *Florian Wieberger, Christian Neuber, Christopher K. Ober, and Hans-Werner Schmidt\**

[\*] Prof. H.-W. Schmidt, F. Wieberger, Dr. C. Neuber  
Makromolekulare Chemie I

Bayreuther Institut für Makromolekülforschung (BIMF) and Bayreuther Zentrum für Kolloide und Grenzflächen (BZKG)

Universität Bayreuth

95440 Bayreuth, Germany

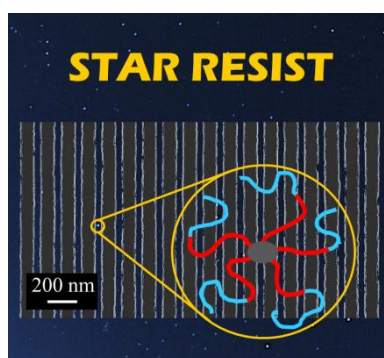
E-mail: hans-werner.schmidt@uni-bayreuth.de

Prof. C. K. Ober

Department of Materials Science and Engineering

Cornell University

Ithaca, NY 14853, USA



Keywords: tailored molecular architectures, star block copolymers, atom-transfer radical polymerization; electron-beam lithography, resist sensitivity

This paper is published in  
*Advanced Materials* **2012**, *24*, 5939-5944.

The material performance of polymers is primarily given by their chemical nature but can be tuned by the polymer architecture.[1,2] Tailored macromolecular architectures have been developed for targeted advanced applications and are the focus of many research activities.[3] Typically polymer architecture is controlled by a bottom-up approach, thus chain growth topology is defined by both an initiating molecule and the monomers used. In this context the availability of a number initiator structures with different numbers of initiating sites suited for a variety of monomers is especially valuable for controlled radical polymerization techniques. Due to the availability of suitable reagents and the possibility of defined molecular assembly of monomers, tailored polymers and architectures have become more sophisticated in recent years.[4] Besides random, gradient, and block copolymers, which simply differ in composition, graft copolymers or brushes, stars, (hyper)branched polymers or networks have been extensively investigated. Established and versatile methods for the synthesis of such tailored macromolecules include controlled radical polymerization techniques and the simple to use atom transfer radical polymerization (ATRP) in particular.[5] A large number of polymer designs have been developed using primarily ATRP or its combination with other techniques. Recent examples show a wide range of hyperbranched polymers[6] or polymer brushes[7] as well as different types of dendrimer-like[8] and miktoarm star polymers,[9] star-linear block polymers[10] and star block copolymers.[11] As an example of star block copolymers, the combination of two different synthesis routes have been demonstrated. One strategy starts with the synthesis of a macroinitiator via a “core-first” polymerization from a star-shaped initiator[12] while in the second route the “core” is formed by an “arms-first” approach linking linear homopolymers (arms).[13] In both cases the resulting macroinitiator was used for a subsequent second polymerization to achieve the star block copolymer architecture.

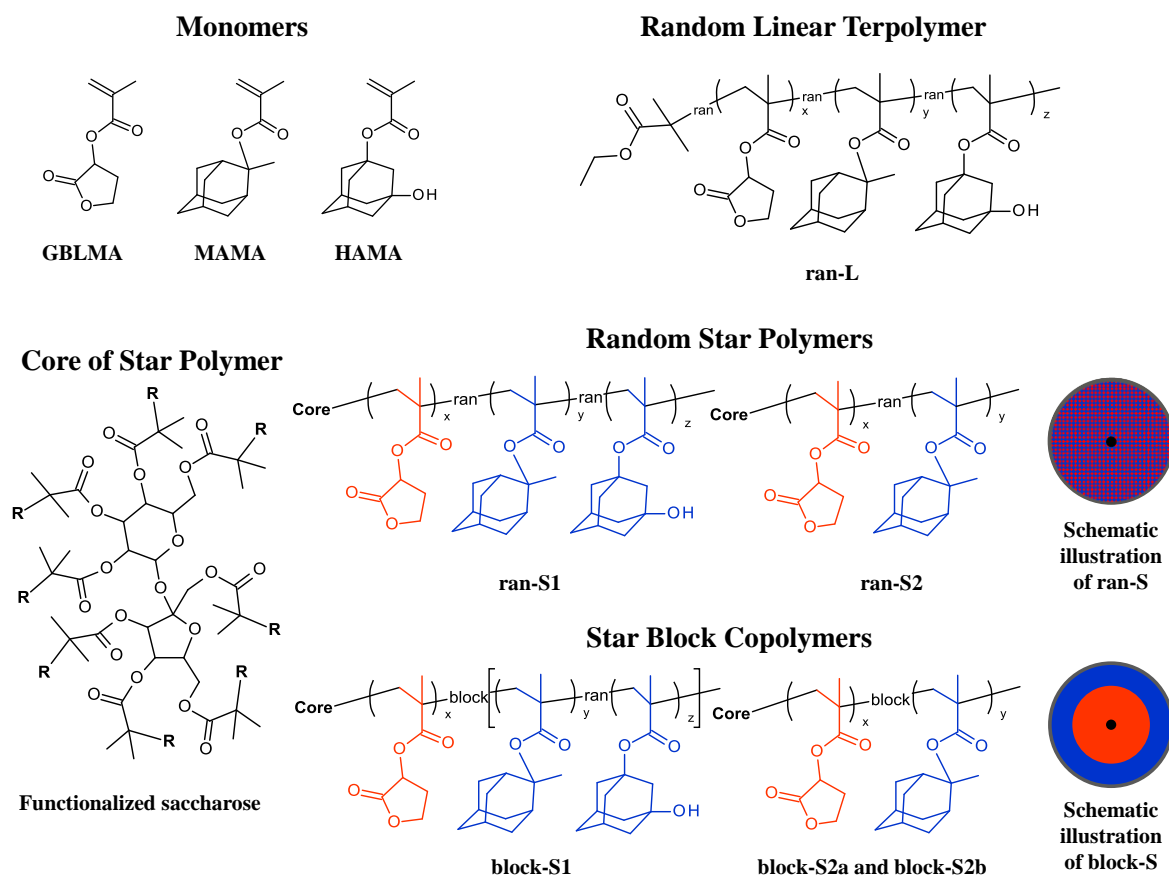
Tailored polymer architectures with their unique properties were developed concerning possible applications in various research fields and must fulfill particular requirements. The properties defined by the given architecture are important for their successful introduction in topics like drug delivery,[14] biomedical applications,[15] microelectronic materials,[16] organic devices,[17] coatings,[18] or lithographic patterning.[19] The first polymers mainly used for commercial applications as photoresist were a linear poly(vinylcinnamate) and cresol-formaldehyde type polymers (Novolac) but they soon revealed limits in resolution. The development of new polymers serving as resists has continued to progress to keep in step with further developments of patterning tools and other requirements.[20] The current trend in

polymeric resists is based on random terpolymers with tailored monomer compositions as chemically amplified resist materials.[21] Recent investigations of this class of polymer resists have reported the advantages of controlling macromolecular topology. Terpolymers with a hyperbranched architecture[22] as well as star topology[23,24] were reported as resists of high potential and with improved performance.

Based on these results we present for the first time star block copolymers for use as high performance resist materials. In addition to their controlled spherical shape these copolymers offer well defined monomer incorporation and placement due to their shell-like structure. The tailored star block copolymers were synthesized utilizing the core-first ATRP route by the full conversion of a first monomer and in-situ polymerization of additional added monomer resulting in narrow dispersity (PDI  $< 1.2$ ). Their application for lithographic patterning was efficiently optimized by a combinatorial investigation[25] and the new high performance star resist material features an impressive improvement in sensitivity and solubility in contrast to randomly distributed star polymers or a reference linear terpolymer.

The chemical structures of the used monomers and of the random linear terpolymer, as well as of the core[26] of the star polymer and the corresponding arms of the random star copolymers and also of the star block copolymers are shown in **Scheme 1**. Current industrially used high performance polymer photoresists for 193 nm lithography consist of  $\alpha$ -gamma butyrolactone methacrylate (GBLMA) as lactone monomer, methyl adamantyl methacrylate (MAMA) as acid-labile leaving monomer, and hydroxyl adamantyl methacrylate (HAMA) as polar monomer and are used not only for 193 nm lithography but also for extreme ultraviolet (EUV; 13.4 nm) and electron beam lithography.[21] Thus we selected these monomers for the synthesis of our reference linear terpolymer ran-L (composed of GBLMA/ MAMA/ HAMA) as well as the random star copolymers ran-S1 (GBLMA/ MAMA/ HAMA) and ran-S2 (GBLMA/ MAMA) while the monomer ratio follows the published hyperbranched polymer resist monomer composition.[27] Based on a star molecular architecture we demonstrate further progress by synthesizing the tailored star block copolymers block-S1 (GBLMA/ MAMA/ HAMA) and block-S2a and block-S2b (GBLMA/ MAMA) using the ATRP technique via full conversion of monomers for the first block and subsequent in-situ polymerization of subsequently added monomers to achieve target conversions. To increase the development contrast the monomer HAMA is eliminated for

block-S2 polymers and replaced with monomer GBLMA (block-S2a) or with monomer MAMA (block-S2b).



**Scheme 1.** Chemical structures of used monomers GBLMA, MAMA, HAMA, the core for the star polymers (functionalized saccharose), and synthesized reference linear terpolymer (ran-L), random star copolymers (ran-S1, ran S2) and tailored star block copolymers (block-S1, block-S2a, and block-S2b) are shown. The schematic illustration of ran-S represents the random monomer distribution (blue and red squares) within the polymer arms, while the schematic illustration of block-S illustrates the core-shell-like structure of the block copolymer arms.

Monomer feed and the polymer composition analyzed by  $^1\text{H-NMR}$  are listed in **Table 1**. The detection of monomer consumption is possible as the characteristic  $^1\text{H-NMR}$  peaks of vinyl protons of each monomer differ: 6.39 ppm for GBLMA, 6.27 ppm for MAMA, and 6.22 ppm for HAMA (Supporting Information, Figure S1). The theoretically calculated molecular weights are listed in Table 1. Absolute molecular weights and polydispersity indices were characterized by GPC utilizing a multi-angle light scattering detector and the refractive index increment  $dn/dc$ . The targeted molecular weights of the star polymer are in good agreement to the theoretical values. Assuming that the molecular size of a linear polymer is more expanded in comparison to a more compact star polymer the target molecular

weight of the ran-L was set one third lower. For all polymers a monomodal distribution with a symmetrical shape was detected (Figure S2) and all polymers showed a narrow molecular weight distribution with PDIs below 1.2 indicating their controlled character.

**Table 1.** Monomer feed compositions, corresponding molecular weights, polydispersity indices, and polymer compositions of synthesized linear and star polymers.

Samples	Monomer Feed Composition (in molar equivalent)			Targeted $M_n^{[a]}$ [kg mol <sup>-1</sup> ]	$M_n, \text{MALS}$ [kg mol <sup>-1</sup> ]	PDI <sup>[b]</sup>	Polymer composition (in %) <sup>[c]</sup> GBLMA / MAMA / HAMA
	GBLMA	MAMA	HAMA				
ran-L	40	40	20	13.5	15.5	1.10	46.8 / 29.6 / 23.7
ran-S1	40	40	20	22.4	23.9	1.05	48.5 / 30.0 / 21.5
ran-S2	50	50	-	23.7	25.8	1.02	62.4 / 37.6 / -
block-S1	30 <sup>[d]</sup>	50 <sup>[e]</sup>	20 <sup>[e]</sup>	25.6	30.8	1.18	54.4 / 28.1 / 17.5
block-S2a	50 <sup>[d]</sup>	50 <sup>[e]</sup>	-	26.3	30.0	1.17	69.0 / 31.0 / -
block-S2b	33 <sup>[d]</sup>	67 <sup>[e]</sup>	-	27.8	32.3	1.19	53.2 / 46.8 / -

[a] Theoretical calculated molecular weight. [b] polydispersity index measured by MALS detection.

[c] Determined by <sup>1</sup>H-NMR. [d] Conversion of GBLMA close to 100 %. [e] Addition of new monomer after full conversion of GBLMA.

As the star block copolymers have a core-shell-like structure – the hydrophilic lactone monomer units are incorporated into the inner shell and the more hydrophobic adamantyl monomer units in the outer shell – the surface of films prepared from the star block copolymers and random star copolymers should differ in polarity. Therefore the tailoring given by architecture is in addition supported by water contact angle measurement for all reported polymers (Table S1; Figure S3). The measurements yielded contact angles of around 70° for films spin-coated of ran-L and the ran-S1 describing a more polar surface. In contrast the contact angle of nearly 81° was measured for the more nonpolar ran-S2 film. This is due to the fact that the polar hydroxyl group of the monomer HAMA is missing in ran-S2 and thus the surface has higher hydrophobicity. The same effect of hydrophobicity change of the film surface was observed for the star block copolymers. Here the film surface of the block-S1 shows a contact angle close to 77° and the film surfaces of spin-coated block-S2a and block-S2b feature higher contact angles of about 90°. The results correspond to the higher amount of incorporated polar monomer HAMA positioned in the outer shell of block-S1 and to the HAMA free block-S2a and block-S2b with outer shells formed only by the nonpolar monomer MAMA.

Furthermore the dissolution behavior of the synthesized polymers should be influenced by molecular architecture. Therefore films of each polymer with added photoacid generator (PAG) were spin-coated on quartz crystals, flood exposed for PAG activation, and annealed in a post exposure bake (PEB) to catalyze the deprotection of MAMA. A solubility change is expected for the deprotected and thus more polar resist materials developable in an aqueous tetramethylammonium hydroxide (TMAH) solution. For the systematic investigation of the development contrast clarifying the solubility difference between protected and deprotected resist the quartz crystal microbalance (QCM) technique was used for characterization.[28] Therefore unexposed and exposed films of all investigated materials spin-coated on quartz crystals were clamped in the holder and immersed in the developer solution. The resulting traces of film thickness variation, calculated from the detected QCM frequencies, are shown in **Figure 1a**. All non-exposed films (★) show no significant change in film thickness over a period of five minutes demonstrating their complete insolubility in the applied developer solution. The solubility change of the film is produced by the elimination of 2-methylideneadamantane (only possible for MAMA units) resulting in polar methacrylic acid groups bonded to the star. The outer shell of block-S1 (○) consists of both MAMA and of HAMA units which cannot be deprotected; thus only an insufficient polarity change can be generated and the film swells to a film thickness increase of 20 %. The exposed reference film of ran-L (△) and the film of ran-S1 (□) show a distinct swelling character over 40 s and 63 s, respectively, followed by their complete dissolution. However, ran-S2 (△), block-S2a (▽), and block-S2b (◇) show a barely measureable fast swelling followed again by complete dissolution: while dissolution takes 60 s for ran-S2, the films of block-S2a and block-S2b are completely dissolved within the first five seconds. Here the outer shell consists only of MAMA units and thus the polarity change is well controlled. Based on these promising dissolution investigations the polymers were exposed to different doses to investigate their sensitivity. Again films of each polymer and PAG mixture were spin-coated on silicon substrates under equal conditions. The films were exposed to an electron beam dose gradient of 25 increasing doses, annealed for PEB and developed in TMAH. The resulting patterns were measured in regard to dose dependent achieved film thickness loss using a stylus profiler. The measured film thicknesses confirm the results given by the QCM investigations (see Figure 1b). The film of block-S1 (○) showed at the highest dose of  $397 \mu\text{C cm}^{-2}$  only a 20 % loss in film thickness. As indicated by QCM measurements, ran-L and ran-S1 need the longest development time period and require relatively high doses to clear ( $160 \mu\text{C cm}^{-2}$  for

ran-L ( $\triangle$ ) /  $92 \mu\text{C cm}^{-2}$  for ran-S1 ( $\square$ )). However, the nearly identical characters of ran-S2, block-S2a, and block-S2b of the QCM measurements disclose differences in their sensitivity. Ran-S2 ( $\triangle$ ) needs only the dose of  $77 \mu\text{C cm}^{-2}$  to clear and requires therefore a higher dose than its star block copolymer counterparts: block-S2a ( $\nabla$ ) requires the clearing dose of  $31 \mu\text{C cm}^{-2}$  and block-S2b ( $\diamond$ ) of only  $21 \mu\text{C cm}^{-2}$ , respectively. This powerful sensitivity increase up to eight times of the star block copolymers in comparison to reference linear polymer ran-L demonstrates the advantageous and progress in tailoring the molecular architecture by following the star block copolymers concept.

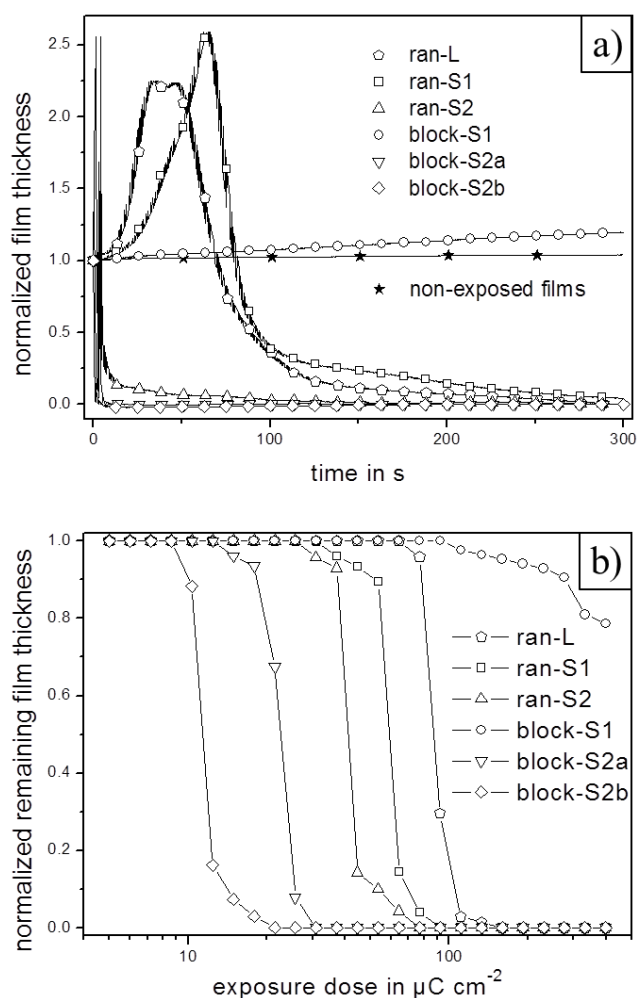
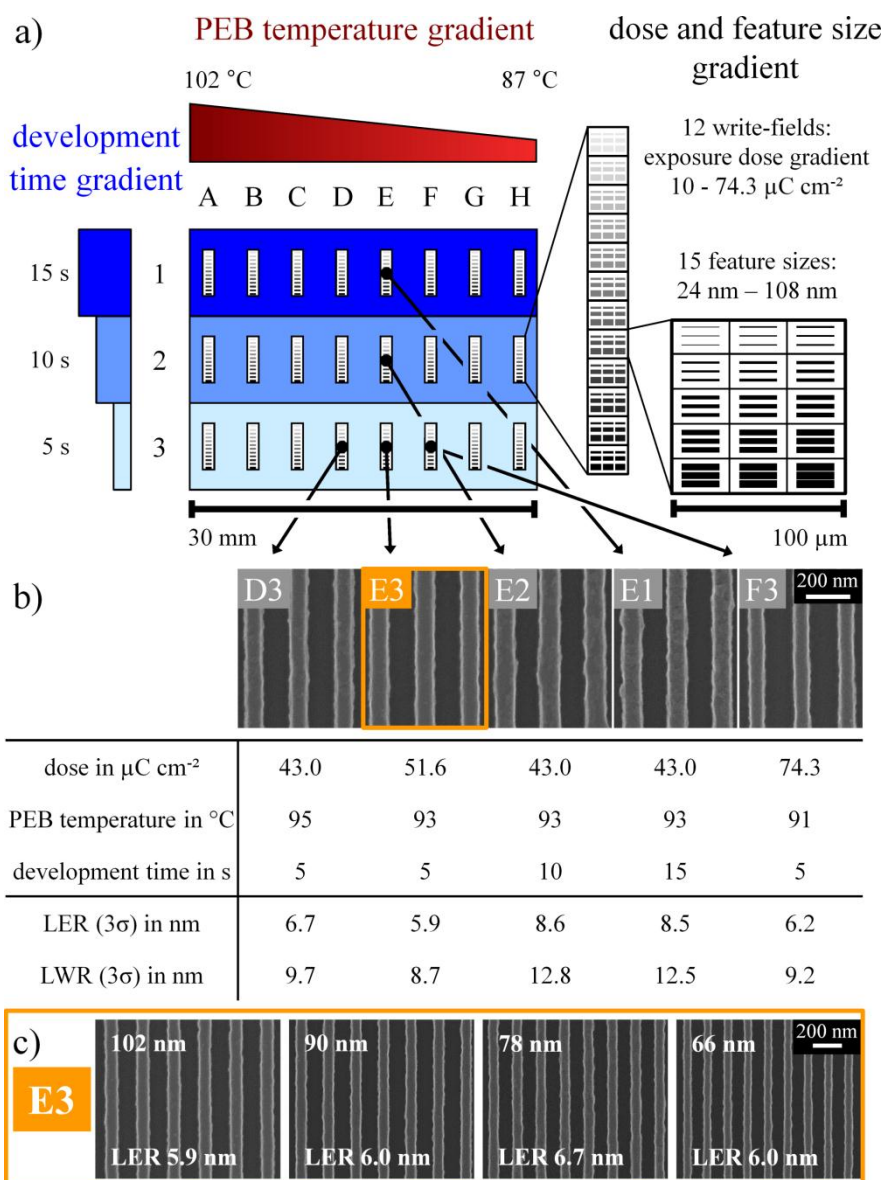


**Figure 1.** a) Quartz crystal microbalance measurements of non-exposed and flood exposed polymer resist films. All non-exposed films ( $\star$ ) exhibit no significant change in film thickness while the flood exposed films just swell (block-S1  $\circ$ ), swell and subsequently dissolve (ran-L  $\triangle$  / ran-S1  $\square$ ), or rapidly swell and dissolve within seconds (ran-S2  $\triangle$  / block-S2a  $\nabla$  / block-S2b  $\diamond$ ).

b) Sensitivity curves of investigated polymer resist films utilizing electron beam exposure. Block-S1 ( $\circ$ ) was developed partly even at the highest dose while the other polymers show high development contrasts. The most sensitive polymer is block-S2b ( $\diamond$ ) exhibited a clearing dose of  $21.5 \mu\text{C cm}^{-2}$ .

Based on these encouraging results the most promising polymer block-S2b was used for lithographic patterning investigations. For the multi-step lithographic patterning process consisting of numerous strongly interacting variables a combinatorial approach was used to demonstrate the potential of this new resist material. Utilizing a 20 kV electron beam tool an exposure dose as well as feature size gradient were combined with a PEB temperature gradient and a development time gradient to create a ternary combinatorial library (**Scheme 2a**). This library allows the reliable optimization of applied variables in one experiment. Scanning electron microscopy (SEM) images of selected patterns, the corresponding line edge roughness (LER: deviation of feature edge from ideal shape), line width roughness (LWR: deviation of line width) as well as the process conditions are tabulated in Scheme 2b. The optimized pattern was observed in sector E3 with the dose of  $51.6 \mu\text{C cm}^{-2}$ , the PEB temperature of  $93 \text{ }^\circ\text{C}$ , the short development time of 5 s, and showed the LER of 5.9 nm and the LWR of 8.7 nm. The patterns with the identical development time but some higher PEB temperature of  $95 \text{ }^\circ\text{C}$  (D3) needed a lower dose of  $43.0 \mu\text{C cm}^{-2}$ , but drops in performance reported by the LER of 6.7 nm and the LWR of 9.7 nm. A similar behavior was observed at the lower PEB temperature of  $91 \text{ }^\circ\text{C}$  in sector F3 but requiring the higher dose of  $74.3 \mu\text{C cm}^{-2}$ . This dose/PEB temperature correlation is controlled by the thermally activated acid catalyzed deprotection of MAMA: at a higher dose, lower PEB temperature (and vice versa) is required to yield the same deprotection rate. For longer development periods of 10 s and 15 s at the optimized PEB temperature of  $93 \text{ }^\circ\text{C}$  LER and LWR values exceed 8 nm and 12 nm for sectors E2 and E1, respectively. In Scheme 2c the feature size gradient in sector E3 with observed 1:1 line/space patterns from 102 nm to 66 nm are shown. All patterns show clear lines with similar LER values of about 6 nm. To demonstrate the potential of the star block copolymer block-S2b as new tailored high performance resist candidate a further combinatorial library was also prepared utilizing the reference linear terpolymer ran-L. The optimized sector was observed at a four times higher dose of  $202.7 \mu\text{C cm}^{-2}$ , applying the same PEB temperature of  $93 \text{ }^\circ\text{C}$ , and the clear higher development time of 30 s in comparison to the optimized sector of block-S2b. In the optimized sector of the reference linear terpolymer ran-L 1:1 line/space patterns from 102 nm to 66 nm were identified with LER values of about 7 nm to 8 nm (Figure S4). As a result, the significantly higher sensitivity with the consistent LER values of 6 nm for block-S2b offers the star block copolymers as new generation of resist materials.



**Scheme 1.** a) Schematic illustration of the investigated ternary combinatorial library consisting of an exposure dose and feature size gradient combined with a PEB temperature gradient and a development gradient.

b) Selected SEM images of the ternary combinatorial library demonstrate the influences of the applied variable gradients. In addition, corresponding exposure doses, PEB temperatures, and development times as well as analyzed LER and LWR values are added.

c) Selected SEM images of electron beam written feature size gradient in sector E3 and corresponding LER values demonstrate the high potential of star block copolymer block-S2b.

In summary we have successfully demonstrated that tailoring the molecular architecture towards a star block copolymer provides a significant improvement in realizing a new generation of high-sensitivity and high performance resist materials. The synthesis of the tailored star block copolymers proceeded for the first time *in-situ* via a core-first ATRP route as well as under controlled conditions with PDIs below 1.2. The new star block copolymers

demonstrated their excellent solubility contrast in the exposed state and their up to eight times increased sensitivity in comparison to the reference linear polymer. The most sensitive star block copolymer was investigated in a combinatorial library for its lithographic performance. In the optimized sector, well-defined 1:1 line/space patterns down to 66 nm with LER values of about 6 nm were achieved utilizing a 20 kV electron-beam tool. As future high resolution resists for even smaller feature widths will be limited by molecular size, further investigations concerning star block copolymers with reduced molecular weight and reduced monomer block composition will provide opportunities for further improvement of patterning performance.

### *Experimental*

The ternary library consists of a temperature gradient perpendicular to a development time gradient, which represents the variable gradients of the binary library, while an electron beam exposure dose gradient is applied in very small areas matrix-like to this binary library. A film was spin cast on a silicon wafer out of a 2.5 wt.% solution of block-S2b and the photoacid generator triphenylsulfonium perfluoro-1-butanefluoroborate 19/1 (w/w) in cyclohexanone/cyclohexane 3/2 (v/v). Subsequently the film was annealed under vacuum for the post apply bake (PAB) at 125 °C for 2.5 min resulting in a film thickness of 80 nm. Then the substrate was cut to a quadrat with an edge length of about 30 mm under Argon-atmosphere to avoid base contamination which causes T-top formation.

As the first applied variable of the combinatorial library the electron beam exposure dose and feature size gradient was processed in 288 write-fields structured matrix-like applied with a Zeiss LEO 1530 equipped with a Raith Elphy Plus utilizing an acceleration voltage of 20 kV. This matrix consists of three rows times eight columns of sectors, each containing 12 write-fields representing the exposure dose gradient from 10 – 74.3  $\mu\text{C cm}^{-2}$ , while in a single write-field – 100  $\mu\text{m} \times 100 \mu\text{m}$  in size – the feature size variation in steps of 6 nm from 24 – to 108 nm is given. Each sector has a length of 2 mm and a width of 100  $\mu\text{m}$ ; between each column the gap was 3.5 mm and 10 mm between each row, respectively. Subsequently the post exposure bake (PEB) was applied – parallel to the rows of the exposed matrix – by a temperature gradient from 87 °C to 102 °C for 30 s. This temperature gradient was prepared on an aluminum plate with ice-water as cooling source on one end and a hot plate adjusted to 220 °C as heating source on the opposite resulting in a slope of 0.6 °C  $\text{mm}^{-1}$ . The

development time step gradient was applied alongside the columns of the exposed matrix for 5, 10, 15 s in a 0.26 N tetramethylammonium hydroxide solution. Therefor the substrate was subdivided into three segments whereas each segment contains one row of write-fields.

The developed film was sputtered with 1.3 nm platinum and investigated in a scanning electron microscope (SEM) Zeiss LEO 1530. The observed SEM images of the line/space patterns were evaluated for line edge and line width roughness by the software SuMMIT<sup>TM</sup> from EUV technology.

### *Acknowledgements*

The authors gratefully acknowledge the assistance of Marietta Böhm in terms of GPC/MALS measurements. This work was supported by the Semiconductor Research Corporation's Global Research Collaboration (GRC) Program [Tasks 1675.002] and the Deutsche Forschungsgemeinschaft, SFB 481 [Project No. A6]. In addition we thank EUV technology for the roughness evaluation software SuMMIT<sup>TM</sup>. Supporting Information is available online from Wiley InterScience or from the author.

## Supporting Information

<b><u>Table of Contents</u></b>	<b><u>Page</u></b>
Materials	<b>S1</b>
Synthesis of random linear terpolymer and random star polymers (Table S1)	<b>S2</b>
Synthesis of star block copolymers (Table S2)	<b>S3</b>
Selected <sup>1</sup> H-NMR spectrum (300 MHz) of the monomers (Figure S1)	<b>S4</b>
GPC traces of polymers (Figure S2)	<b>S5</b>
Water contact angle measurements (Table S3)	<b>S5</b>
Water contact angle measurements (Figure S3)	<b>S6</b>
Dissolution investigations	<b>S6</b>
Sensitivity investigations	<b>S7</b>
Ternary library of reference linear terpolymer ran-L (Figure S4)	<b>S7</b>

*Materials*

The eight site ATRP initiator 2,3,4,6,1',3',4',6'-octa-O-(2-bromoisobutyryl)-saccharose was kindly provided from Felix Plamper, Macromolecular Chemistry II, University of Bayreuth, Germany. Methyl adamantyl methacrylate (MAMA) and hydroxyl adamantyl methacrylate (HAMA) were purchased from Idemitsu Chemicals and  $\alpha$ -gamma butyrolactone methacrylate (GBLMA) from Kuraray. MAMA and GBLMA were passed through a basic alumina column to remove the inhibitor, HAMA was used as received. All other chemicals were purchased from Aldrich and were used as received.

*Synthesis of random linear terpolymer and random star polymers*

A mixture of GBLMA, MAMA, HAMA, CuCl, CuCl<sub>2</sub>, ethyl 2-bromoisobutyrate and anisole (16 mL) in the case of random linear terpolymer **ran-L** (see **Table S1**) or a mixture of GBLMA, MAMA, HAMA, CuCl, CuCl<sub>2</sub>, 2,3,4,6,1',3',4',6'-octa-O-(2-bromoisobutyryl)-saccharose and anisole (16 mL) in the case of random star polymer **ran-S1** or a mixture of GBLMA, MAMA, CuCl, CuCl<sub>2</sub>, 2,3,4,6,1',3',4',6'-octa-O-(2-bromoisobutyryl)-saccharose and anisole (16 mL) in the case of random star polymer **ran-S2** was stirred in a screw cap vial with a rubber septum at 65 °C and degassed with nitrogen for 30 min. The ligand N,N,N',N'',N'''-pentamethyldiethylenetriamine (PMDETA) (equimolar to CuCl and CuCl<sub>2</sub>) was dissolved in 4 mL anisole and degassed for 30 min, too. The ligand's solution was added to the monomers' solution with a degassed syringe at time t = 0. Throughout the reaction aliquots were taken to follow the conversion of the monomers with <sup>1</sup>H-NMR in CDCl<sub>3</sub>. The polymerization was ended at a conversion of 55 %/34 %/55 % (GBLMA/MAMA/HAMA) for **ran-L**, of 61 %/37 %/55 % for **ran-S1**, and of 71 %/43 %/- for **ran-S2**. The reaction was cooled down with liquid nitrogen, diluted in THF and passed through a silica column to remove the copper catalysts. The solution was concentrated and precipitated in cold methanol. The polymer was collected via filtration, dried, freeze-dried in 1,4-dioxane yielding a white powder. The molecular weights, polydispersity indices and polymer compositions are shown in Table 1, GPC traces are shown in Figure S1.

**Table S1.** Amounts of reagents for synthesis of random linear terpolymer ran-L and random star polymers ran-S1 and ran-S2.

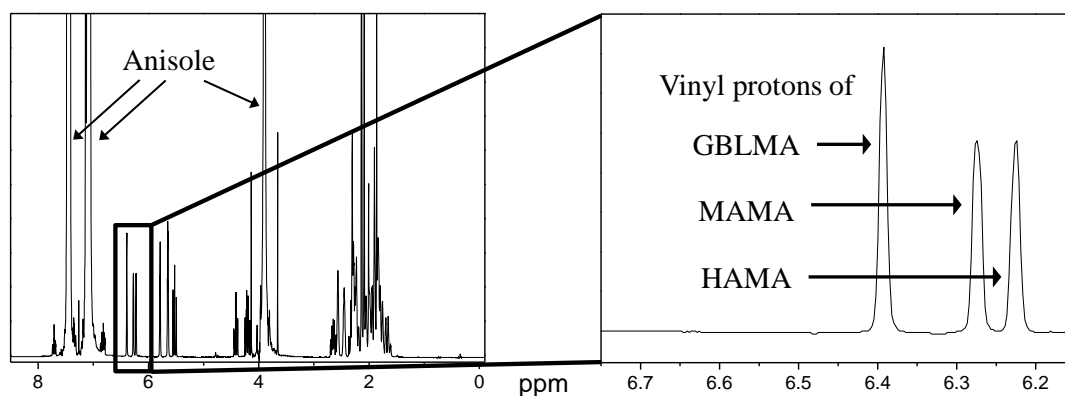
	Initiator	GBLMA	MAMA	HAMA	CuCl	CuCl <sub>2</sub>
<b>ran-L</b>	34.52 mg (0.18 mmol)	1.69 g (9.91 mmol)	2.32 g (9.91 mmol)	1.17 g (4.96 mmol)	8.76 mg (0.09 mmol)	11.90 mg (0.09 mmol)
<b>ran-S1</b>	198.79 mg (0.13 mmol)	1.76 g (10.37 mmol)	2.43 g (10.37 mmol)	1.22 g (5.18 mmol)	34.25 mg (0.35 mmol)	92.85 mg (0.69 mmol)
<b>ran-S2</b>	94.58 mg (0.06 mmol)	1.05 g (6.16 mmol)	1.44 g (6.16 mmol)	-	16.30 mg (0.16 mmol)	44.18 mg (0.33 mmol)

*Synthesis of star block copolymers*

A mixture of GBLMA, CuCl, CuCl<sub>2</sub>, 2,3,4,6,1',3',4',6'-octa-O-(2-bromoisobutyryl)-saccharose and anisole (16 mL) in the case of star block copolymer **block-S1** (see **Table S2**) or a mixture of GBLMA, CuCl, 2,3,4,6,1',3',4',6'-octa-O-(2-bromoisobutyryl)-saccharose and anisole (16 mL) in the case of star block copolymer **block-S2a** or a mixture of GBLMA, CuCl, 2,3,4,6,1',3',4',6'-octa-O-(2-bromoisobutyryl)-saccharose and anisole (15 mL) in the case of star block copolymer **block-S2b** was stirred in a screw cap vial with a rubber septum at 65 °C and degassed with nitrogen for 30 min. The ligand N,N,N',N'',N''-pentamethyldiethylenetriamine (PMDETA) (equimolar to CuCl and CuCl<sub>2</sub>) was dissolved in 3 mL anisole and degassed for 30 min, too. The ligand's solution was added to the monomers' solution with a degassed syringe at time called this time  $t_1 = 0$ . Throughout the reaction aliquots were taken to follow the conversion of  $\alpha$ -gamma butyrolactone with <sup>1</sup>H-NMR in CDCl<sub>3</sub>. Meanwhile a mixture of MAMA and HAMA in the case of star block copolymer **block-S1** or MAMA in the case of star block copolymer **block-S2a** or **block-S2b** was dissolved in 5 mL anisole and degassed for 30 min. After fully conversion of  $\alpha$ -gamma butyrolactone the adamantyl monomer's solution was added to the reaction solution with a degassed syringe at time called  $t_2 = 0$ . Subsequently an aliquot was removed from the reaction solution to follow the conversion of the added monomers with <sup>1</sup>H-NMR in CDCl<sub>3</sub>. The polymerization was ended at a conversion of 31 %/47 % (MAMA/HAMA) for **block-S1**, of 45 %/- for **block-S2a**, and of 44 %/- for **block-S2b**. The reaction was rapidly cooled down with liquid nitrogen, diluted in THF and passed through a silica column to remove the copper catalysts. Then the solution was concentrated and precipitated in cold methanol. The polymer was collected via filtration, dried, freeze-dried in 1,4-dioxane yielding a white powder. The molecular weights, polydispersity indices and polymer compositions are shown in Table 1, the GPC traces are shown in Figure S2.

**Table S2.** Amounts of reagents for synthesis of star block copolymers block-S1 and block-S2a/b.

	Initiator	GBLMA	MAMA	HAMA	CuCl	CuCl <sub>2</sub>
<b>block-S1</b>	198.79 mg (0.13 mmol)	1.46 g (8.55 mmol)	3.34 g (14.25 mmol)	1.35 g (5.70 mmol)	34.25 mg (0.35 mmol)	92.85 mg (0.69 mmol)
<b>block-S2a</b>	141.87 mg (0.09 mmol)	1.42 g (8.32 mmol)	1.95 g (8.32 mmol)	-	80.56 mg (0.81 mmol)	-
<b>block-S2b</b>	198.62 mg (0.13 mmol)	1.54 g (9.06 mmol)	4.25 g (18.12 mmol)	-	112.60 mg (1.14 mmol)	-

**Figure S1** <sup>1</sup>H-NMR spectrum (Bruker Avance 300) of the monomers GBLMA/MAMA/HAMA in an anisole solution in CDCl<sub>3</sub> show the different shifted vinyl protons of GBLMA (6.39 ppm), MAMA (6.27 ppm), and HAMA (6.22 ppm).

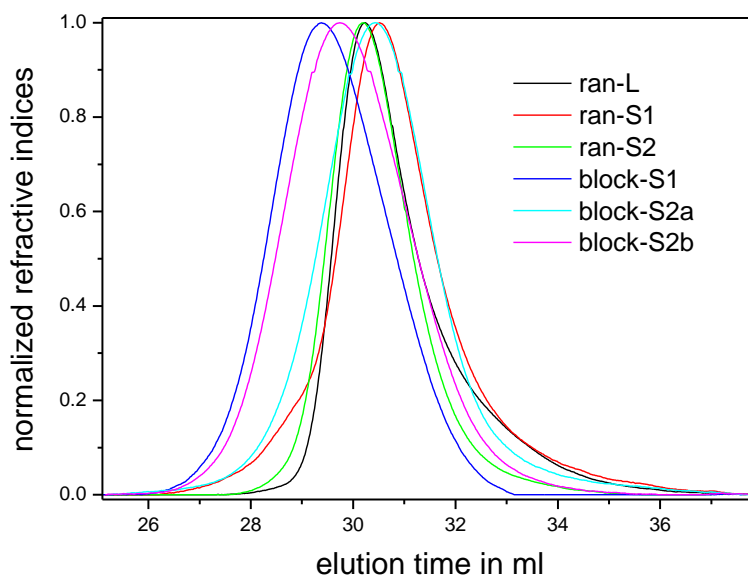


**Figure S2.** GPC traces of linear terpolymer (ran-L), random star polymers (ran-S1, ran S2) and star block copolymers (block-S1, block-S2a, block-S2b).

#### *Water contact angle measurements*

Solutions of 2.5 wt.% of each polymer in cyclohexanone/cyclohexane 3/2 (v/v) were prepared and spin cast on silicon wafer and annealed to a subsequent post apply bake (PAB) at 125 °C for 60 s achieving film thicknesses of about 80 nm. Water contact angle measurements were investigated by a DataPhysica OCA using deionized water.

**Table S3.** Water contact angle measurements on films made of linear terpolymer (ran-L), random star polymers (ran-S1, ran S2) and star block copolymers (block-S1, block-S2a, block-S2b) and the average of five runs.

run	ran-L	ran-S1	ran-S2	block-S1	block-S2a	block-S2b
1	71.0°	66.4°	79.3°	76.8°	89.4°	89.1°
2	71.5°	67.1°	80.4°	75.6°	90.5°	90.1°
3	72.0°	67.1°	81.6°	77.1°	90.2°	89.3°
4	71.5°	68.3°	80.7°	77.6°	89.0°	89.4°
5	71.6°	67.8°	81.0°	77.1°	88.8°	90.1°
average (1 $\sigma$ )	71.5 $\pm$ 0.4°	67.3 $\pm$ 0.7°	80.6 $\pm$ 0.9°	76.8 $\pm$ 0.8°	89.6 $\pm$ 0.7°	89.6 $\pm$ 0.5°

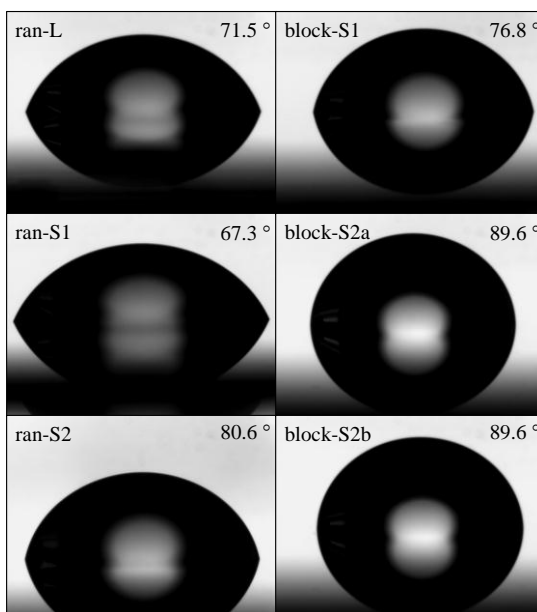


**Figure S3.** Pictures of water droplets on spin cast polymer film surfaces (linear terpolymer (ran-L), random star polymers (ran-S1, ran S2) and star block copolymers (block-S1, block-S2a, block-S2b)) and their corresponding measured contact angles.

### *Dissolution investigations*

The quartz crystal microbalance (QCM) measurements (remote oscillator and controller card: Inficon) were performed with a solvent-proof QC-holder (Maxtec CHC-100). The measurements were controlled by adapted LabView software and the data density was four points per second. The QCs (5 MHz) were spin cast with solutions of 2.5 wt.% (each polymer plus added photoacid generator triphenylsulfonium perfluoro-1-butanesulfonate 19/1 (w/w)) in cyclohexanone/cyclohexane 3/2 (v/v), subsequently annealed for PAB at 125 °C for 60 s achieving film thicknesses of about 80 nm. In doing so two of each polymer films were prepared and one of this pair was flood exposed to UV light (248 nm; Fusion UV Systems: F300S) and then applied to the post exposure bake at 95 °C for 30 s. The QCs were successively mounted in the QC-holder and immersed into the 0.26 N tetramethylammonium hydroxide development solutions for five minutes to collect the frequency rate.

### *Sensitivity investigations*

The silicon wafer were spin cast with solutions of 2.5 wt.% (each polymer plus added photoacid generator triphenylsulfonium perfluoro-1-butanesulfonate 19/1 (w/w)) in cyclohexanone/cyclohexane 3/2 (v/v) subsequently annealed for PAB at 125 °C for 60 s yielding film thicknesses of about 80 nm. Each wafer was exposed to a dose gradient ranging from 5 to 397.5  $\mu\text{C cm}^{-2}$  – one dose in an area of 20  $\mu\text{m}$  x 100  $\mu\text{m}$  – applied with a Zeiss LEO 1530 equipped with a Raith Elphy Plus utilizing an acceleration voltage of 20 kV. After a post exposure bake (95 °C; 30 s) the wafer were developed (30 s; 0.26 N TMAH). The yielded profile heights of each different exposed area were measured and reported in respect to the film thickness by a stylus profiler (Veeco Dektak 150).

### *Ternary library of reference linear terpolymer ran-L*

The ternary library consists of a temperature gradient perpendicular to a development time gradient, which represents the variable gradients of the binary library, while an electron beam exposure dose gradient is applied in very small areas matrix-like to this binary library. A film was spin cast on a silicon wafer out of a 2.5 wt.% solution of ran-L and the photoacid generator triphenylsulfonium perfluoro-1-butanesulfonate 19/1 (w/w) in cyclohexanone/cyclohexane 3/2 (v/v). Subsequently the film was annealed under vacuum for the post apply bake (PAB) at 125 °C for 2.5 min resulting in a film thickness of 80 nm. Then the substrate was cut to a quadrat with an edge length of about 30 mm under Argon-atmosphere.

As first applied variable of the combinatorial library the electron beam exposure dose and feature size gradient was processed in 120 write-fields structured matrix-like applied with a Zeiss LEO 1530 equipped with a Raith Elphy Plus utilizing an acceleration voltage of 20 kV. This matrix consists of three rows times four columns of sectors, each containing 10 write-fields representing the exposure dose gradient from 100 – 288.7  $\mu\text{C cm}^{-2}$ , while in a single write-field – 100  $\mu\text{m}$  x 100  $\mu\text{m}$  in size – the feature size variation in steps of 6 nm from 42 – to 108 nm is given. Each sector has a length of 2 mm and a width of 100  $\mu\text{m}$ ; between each column the gap was 9 mm and 15 mm between each row respectively. Subsequently the post exposure bake (PEB) was applied by a temperature step gradient. The substrate was cut along the rows into three pieces; one of the pieces was annealed at a temperature of 93, 95, and 97 °C, respectively, for 30 s. The development time step gradient was applied alongside

the columns of the exposed matrix for 5, 15, 30, 60 s in a 0.26 N tetramethylammonium hydroxide solution. Therefor each substrate piece was subdivided into four segments whereas each segment contains one row of write-fields.

The developed film was sputtered with 1.3 nm platinum and investigated in a scanning electron microscope (SEM) Zeiss 1530. The observed SEM images of the line/space patterns were evaluated for line edge and line width roughness by the software SuMMIT<sup>TM</sup> from EUV technology and the optimized patterns are shown in Figure S4.

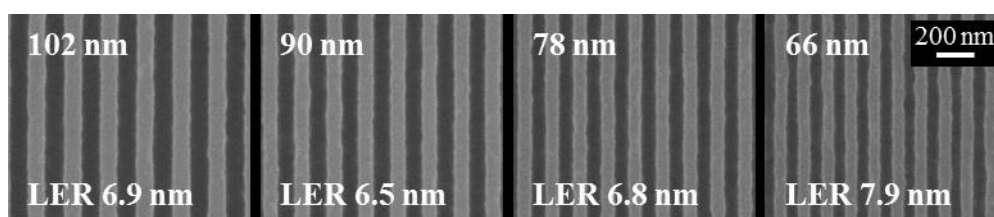


**Figure S4:** Selected SEM images of e-beam written feature size gradient in optimized sector and corresponding LER values of reference linear terpolymer ran-L.

*Literature*

- \_[1] B. I. Voit, A. Lederer, *Chem. Rev.* **2009**, *109*, 5924.
- \_[2] X. Zhu, Y. Zhou, D. Yan, *J. Polym. Sci. B Polym. Phys.* **2011**, *49*, 1277.
- \_[3] A. H. E. Müller, K. Matyjaszewski, *Controlled and living polymerizations: Methods and materials*, Wiley-VCH, Weinheim **2009**.
- \_[4] A. Gregory, M. H. Stenzel, *Prog. Polym. Sci.* **2012**, *37*, 38.
- \_[5] T. E. Patten, K. Matyjaszewski, *Adv. Mater.* **1998**, *10*, 901.
- \_[6] C. Gao, D. Yan, *Prog. Polym. Sci.* **2004**, *29*, 183.
- \_[7] R. Barbey, L. Lavanant, D. Paripovic, N. Schüwer, C. Sugnaux, S. Tugulu, H.-A. Klok, *Chem. Rev.* **2009**, *109*, 5437.
- \_[8] A. Sunder, R. Haag, R. Mülhaupt, H. Frey, *Adv. Mater.* **2000**, *12*, 235.
- \_[9] H. Gao, K. Matyjaszewski, *Prog. Polym. Sci.* **2009**, *34*, 317.
- \_[10] A. Hirao, M. Hayashi, S. Loykulant, K. Sugiyama, S. Ryu, N. Haraguchi, A. Matsuo, T. Higashihara, *Prog. Polym. Sci.* **2005**, *30*, 111.
- \_[11] K. Matyjaszewski, *Polym. Int.* **2003**, *52*, 1559.
- \_[12] J. L. Hedrick, M. Trollsås, C. J. Hawker, B. Atthoff, H. Claesson, A. Heise, R. D. Miller, D. Mecerreyes, R. Jérôme, P. Dubois, *Macromolecules* **1998**, *31*, 8691.
- \_[13] V. Y. Lee, K. Havenstrite, M. Tjio, M. McNeil, H. M. Blau, R. D. Miller, J. Sly, *Adv. Mater.* **2011**, *23*, 4509.
- \_[14] R. Haag, *Angew. Chem. Int. Ed.* **2004**, *43*, 278.
- \_[15] C. C. Lee, J. A. MacKay, J. M. J. Fréchet, F. C. Szoka, *Nat. Biotechnol.* **2005**, *23*, 1517.
- \_[16] J. L. Hedrick, T. Magbitang, E. F. Connor, T. Glauser, W. Volksen, C. J. Hawker, V. Y. Lee, R. D. Miller, *Chem. Eur. J.* **2002**, *8*, 3308.
- \_[17] J. Schmidt, J. Weber, J. D. Epping, M. Antonietti, A. Thomas, *Adv. Mater.* **2009**, *21*, 702.
- \_[18] K. Matyjaszewski, J. Spanswick, *Mater. Today* **2005**, *8*, 26.

- \_[19] H. E. Meijer, *Processing of polymers*, Wiley-VCH, Weinheim **1997**.
- \_[20] J. H. Bruning, *Proc. SPIE*, **2007**, 6520, 04.
- \_[21] D. P. Sanders, *Chem. Rev.* **2010**, 110, 321.
- \_[22] C. L. Chochos, E. Ismailova, C. Brochon, N. Leclerc, R. Tiron, C. Sourd, P. Bandelier, J. Foucher, H. Ridaoui, A. Dirani, O. Soppera, D. Perret, C. Brault, C. A. Serra, G. Hadziioannou, *Adv. Mater.* **2009**, 21, 1121.
- \_[23] J. Iwashita, T. Mimura, T. Hirayama, T. Iwai, in *Proc. SPIE*, **2009**, 7273, 30.
- \_[24] F. Wieberger, D. C. Forman, C. Neuber, A. H. Gröschel, M. Böhm, A. H. E. Müller, H.-W. Schmidt, C. K. Ober, *J. Mater. Chem.* **2011**, 22, 73.
- \_[25] W.-A. C. Bauer, C. Neuber, C. K. Ober, H.-W. Schmidt, *Adv. Mater.* **2011**, 23, 5404.
- \_[26] F. A. Plamper, H. Becker, M. Lanzendörfer, M. Patel, A. Wittemann, M. Ballauff, A. H. E. Müller, *Macromol. Chem. Phys* **2005**, 206, 1813.
- \_[27] W. Hinsberg, G. Wallraff, C. Larson, B. Davis, V. Deline, S. Raoux, D. Miller, F. Houle, J. Hoffnagle, M. Sanchez, C. Rettner, L. Sundberg, D. Medeiros, R. Dammel, W. Conley, *Proc. SPIE* **2004**, 5376, 21.
- \_[28] A. de Silva, L. K. Sundberg, H. Ito, R. Sooriyakumaran, R. D. Allen, C. K. Ober, *Chem. Mater* **2008**, 20, 7292.



## 5 Publication list

### Publications and manuscripts of this thesis

1. F. Wieberger, T. Kolb, C. Neuber, C. K. Ober, and H.-W. Schmidt  
“*Combinatorial techniques to efficiently investigate and optimize thin film nanopatterning*”  
Submitted to *Molecules*
2. F. Wieberger, D. C. Forman, C. Neuber, A. H. Gröschel, M. Böhm, A. H. E. Müller, H.-W. Schmidt and C. K. Ober  
“*Tailored Star-Shaped Statistical Teroligomers via ATRP for Lithographic Applications*”  
*Journal of Materials Chemistry* **2012**, 22, 73-79
3. F. Wieberger, C. Neuber, C. K. Ober, and H.-W. Schmidt  
“*Tailored Star Block Copolymer Architecture for High Performance Chemically Amplified Resists*”  
*Advanced Materials* **2012**, 24, 5939-5944.

### Additional publications

1. F. Schacher, T. Rudolph, F. Wieberger, M. Ulbricht, and A. H. E. Müller  
“*Double Stimuli-Responsive Ultrafiltration Membranes from Polystyrene-block-poly(N,N-dimethylaminoethyl methacrylate) Diblock Copolymers*”  
*ACS Applied Materials & Interfaces* **2009**, 1(7), 1492-1503
2. F. Wieberger, D. C. Forman, M. Skarba, C. Schneider, C. K. Ober, M. Ballauff, A. H. E. Müller, and H.-W. Schmidt  
“*Report on Star Resists in Solution and on Surfaces*”  
*Semiconductor Research Corporation Deliverable Report* **2009**, P051494

## Publication list

3. F. Wieberger, D. C. Forman, M. Skarba, A. Küst, A. Gröschel, S. Ganzleben, M. Ballauff, A. H. E. Müller, C. K. Ober, and H.-W. Schmidt  
*“Report on Fundamental Investigations on Dissolution Control of STAR Polymer Resists“*  
*Semiconductor Research Corporation Deliverable Report 2009*, P053658
4. F. Wieberger, A. Gröschel, D. C. Forman, C. K. Ober, A. H. E. Müller, and H.-W. Schmidt  
*“New Tailored STAR Polymer Resist for Improved LER“*  
*Semiconductor Research Corporation Deliverable Report 2010*, P058826
5. D. Forman, F. Wieberger, A. Gröschel, A. Müller, H.-W. Schmidt, and C. K. Ober  
*“Comparison of Star and Linear ArF Resists“*  
*Proceedings of SPIE 2010*, 7639 (Advances in Resist Materials and Processing Technology XXVII), 76390P/1-76390P/8.
6. F. Wieberger, D. Forman, C. Neuber, M. Skarba, C. K. Ober, and H.-W. Schmidt  
*“Dissolution Control by a Doped Developer“*  
*Proceedings for TECHCON 2010*, P056538
7. A. H. Gröschel, P. D. Petrov, T. I. Löbling, M. Müllner, F. Wieberger, and A. H. E. Müller  
*“Janus Micelles are Effective Non-Covalent Dispersants for Multi-walled Carbon Nanotubes”*  
Submitted to *Angewandte Chemie*

## Conference talks

1. *“Investigation on Resolution and Development Processes - Control of Dissolution through Macromolecular Architecture and Control of Ionic Interaction”* SRC Annual Review Presentation Task 1675.002 **2009**, Amherst MA, USA, 20. – 21. October 2009
2. *“Dissolution Control by a Doped Developer”* TECHCON **2010**, Austin TX, USA, 13. – 14. September 2010
3. *“New tailored STAR polymer resist for improved LER”* SRC Annual Review Presentation Task 1675.002 **2010**, Amherst MA, USA, 09. – 10. November 2010

## Poster presentations

1. F. Wieberger, W.-A. Bauer, C. Neuber, C. K. Ober and H.-W. Schmidt  
*“Combinatorial Optimization of a Molecular Glass Resist for Electron Beam Lithography”* Frontiers in Polymer Science 2009, Mainz, Germany, 07. – 09. June 2009
2. F. Wieberger, W.-A. Bauer, C. Neuber, C. K. Ober and H.-W. Schmidt  
*“Combinatorial Optimization of a Molecular Glass Resist for Electron Beam Lithography”* Bayreuther Polymer Symposium (BPS) 2009, Bayreuth, Germany  
13. – 15. September 2009
3. F. Wieberger, D. C. Forman, M. Skarba, A. Gröschel, A. Küst, S. Ganzleben, C. K. Ober, M. Ballauff, A. H. E. Müller, and H.-W. Schmidt  
*“Investigation on Resolution and Development Processes - Control of Dissolution through Macromolecular Architecture and Control of Ionic Interaction”* SRC Annual Review Presentation Task 1675.002 **2009**, Amherst MA, USA, 20. – 21. October 2009

## Publication list

4. F. Wieberger, D. C. Forman, A. Gröschel, C. K. Ober, A. H. E. Müller, and H.-W. Schmidt  
*“Dissolution Control by a Doped Developer”* TECHCON **2010**, Austin TX, USA, 13. – 14. September 2010
  
5. F. Wieberger, T. Kolb, C. Neuber, D. Forman, M. Krysak, C. K. Ober, and H.-W. Schmidt  
*“Combinatorial Techniques for the Optimization of photo-patternable Materials”*  
Polymers in Biomedicine and Electronics - Biannual Meeting of the GDCh-Division of "Macromolecular Chemistry" and Polydays **2010**, Berlin, Germany 03. – 05. October 2010

## Danksagung

Zum Entstehen dieser Doktorarbeit haben viele Personen beitragen und ihnen gilt mein allerherzlichster Dank.

Allen voran danke ich meinem Doktorvater Herrn Prof. Dr. Hans-Werner Schmidt vom Lehrstuhl Makromolekulare Chemie I für die interessante und anwendungsbezogene Themenstellung, für den äußerst gut ausgestatteten Arbeitsplatz, für die Möglichkeit und das Vertrauen eigene Ideen und Herangehensweisen zu verwirklichen und für die vielen wissenschaftlichen Diskussionen mit ihm, von welchen ich selbst auch noch zukünftig profitieren werde.

Besonderer Dank gilt auch Herrn Dr. Christian Neuber, der mir immer hilfsbereit mit Rat und Tat zur Seite stand und mein erster Ansprechpartner in meiner Doktorarbeit war, aber auch schon in meinem Hauptpraktikum und in meiner Diplomarbeit. Bedanken möchte ich mich für seine konstruktive Kritik, sowie die erfrischenden und gewinnbringenden Diskussionen mit ihm. Zudem hat er unermüdlich und tatkräftig meine Manuskripte korrekturgelesen. Es freut mich sehr, dass ich in Christian einen Freund und Mentor gefunden habe.

Einen nicht unwesentlichen Beitrag an dieser Arbeit hat mein Laborkollege Herr Tristan Kolb. Das Thema, an dem wir beide in unserer Diplomarbeit und Doktorarbeit arbeiteten, schweißte uns zum *Litho-Team* zusammen. Die erfolgreiche Zusammenarbeit lässt sich zurückführen auf die gewinnbringende Zusammenlegung unserer unterschiedlichen Sicht- und Herangehensweisen. Ich danke ihm für die hilfreichen Diskussionen sowie seine stete Hilfsbereitschaft nicht nur zu üblichen Arbeitszeiten.

Des Weiteren möchte ich mich bei meinen ehemaligen Kooperationspartnern Herrn Prof. Dr. Christopher Kemper Ober, Herrn Dr. Drew C. Forman und Frau Marie Krysak bedanken. Aus den freundlichen und regen Diskussionen, der Zusammenarbeit und den Auslandsaufenthalten konnte ich sehr viel profitieren und für meine Zukunft lernen.

Herzlich danken möchte ich allen meinen Kollegen und Kolleginnen vom Lehrstuhl Makromolekulare Chemie I, die neben den zahlreichen wissenschaftlichen Diskussionen über die Jahre gute Freunde geworden sind und auch für die gute Atmosphäre, die ich an diesen Lehrstuhl so geschätzt habe und noch immer tue. Besonders Frau Doris Hanft danke ich für die Unterstützung bei der nicht immer leichten Betreuung der HPLC-Anlage und dem ganzen

## Danksagung

GPC-Team, die auch kurzfristigen Messungen ermöglichten. Ebenso gilt mein Dank Frau Petra Weiss, welche mir in so manchen bürokratischen Angelegenheiten geholfen hat.

Dem Lehrstuhl Makromolekulare Chemie II gilt auch mein Dank, allen voran Herrn André Gröschel und Herrn Andreas Hanisch für ihre stete Diskussionsbereitschaft sowie die vielen GPC-Messungen. Ebenfalls möchte ich Frau Marietta Böhm danken, die sowohl GPC- als auch MALS-Messungen für mich auch sehr kurzfristig durchgeführte.

Das Gefühl jederzeit am Lehrstuhl MC II willkommen zu sein hat mich sehr gefreut.

Für die finanzielle Unterstützung sowie die Auslandsaufenthalte möchte ich mich bei der Deutschen Forschungsgemeinschaft und „Semiconductor Research Corporation“ bedanken.

Auch möchte ich mich bedanken bei allen die mir über die Jahre Freunde geworden sind und meine Studienzeit so abwechslungsreich gemacht haben, alle aufzuzählen würde den Rahmen gehörig sprengen. Es freut mich auch sehr, dass der Kontakt zu einigen, die mir während meines Studiums gute Freunde geworden, aber mittlerweile in Deutschland weit verstreut sind, nicht abgebrochen ist und hoffentlich nie abbrechen wird. In dieser Zeit wurde auch die Chemiker-Spaß-Gesellschaft e.V. gegründet und ich es freut mich, dass ich bei der Gründung dabei sein durfte. Was der engagierte Verein seit seiner Gründung geleistet hat ist bemerkenswert.

Zu guter Letzt danke ich meiner gesamten Familie überaus für die immerwährende Unterstützung und das entgegengebrachte Verständnis und Vertrauen während des Studiums aber besonders in den letzten Monaten dieser Arbeit.

Danke!

## **Erklärung**

Hiermit erkläre ich, dass ich die vorliegende Arbeit selbstständig verfasst und keine weiteren als die von mir angegebenen Quellen und Hilfsmittel benutzt habe.

Ferner erkläre ich, dass ich weder anderweitig mit oder ohne Erfolg versucht habe eine Dissertation einzureichen noch mich einer Doktorprüfung zu unterziehen.

Bayreuth, den 09.Mai 2012

---

Florian Wieberger

